The copyright of this thesis vests in the author. No quotation from it or information derived from it is to be published without full acknowledgement of the source. The thesis is to be used for private study or non-commercial research purposes only.

Published by the University of Cape Town (UCT) in terms of the non-exclusive license granted to UCT by the author.

University of Cape Town

University of Cape Town

Dynamic-systems analysis of self-excitation associated with a capacitor-coupled substation (CCS) – induction machine system

University of Cape Town

Kevin Reeves

January 2006

ACKNOWLEDGEMENTS

I would like to thank:

Prof. Gaunt, for his supervision and willingness to help me at any time

Prof. Braae, for all of his good ideas, help with control

Irene, for always being there to help and encourage me

Andrew, for always being willing to 'throw ideas around' with me and for proof-reading

Chris Wozniak, for sharing his invaluable knowledge with me

Antonio, for listening to my ideas

My family, for their love

God, for giving me this privilege

University of Cape Town

DECLARATION

I, Kevin Alan Reeves declare that I know the meaning of plagiarism and declare that all the work in the document, save for that which is properly acknowledged, is my own.

signature removed

Kevin Alan Reeves

27 May 2006

University of Cape Town

TERMS OF REFERENCE

1. Study the literature relevant to capacitor-coupled substation (CCS) technology and sub-synchronous resonance (SSR) that arises as a result of using a CCS to supply power to an induction motor (IM), as is the case at the Meru Substation. Study data from industrial applications where similar problems have been experienced, in particular those associated with the Meru substation.

2. Based on data collected and analysed, develop a hypothesis pertaining to the most likely cause of CCS-IM SSR. The hypothesis will become the 'compass' to guide the path that research and modelling should take.

3. Study literature connected with the prevention and compensation of the possible causes of SSR. Both passive and active compensation techniques should be investigated. The latter is referred to as FACTS (Flexible Alternating Current Transmission Systems) compensation techniques, which form the basis of current injection techniques.

4. Model SSR, using various computer packages and mathematical tools. Use this model to investigate compensation techniques.

5. Build a physical, laboratory model that replicates the problem associated with the Meru Substation and the Petronet Induction Motor Load.

6. Generalize the results of the investigation to any single- or three-phase CCS supplying any load and the stabilization thereof.

University of Cape Town

EXECUTIVE SUMMARY

Background

A CCS (Capacitor Coupled Substation) is an inexpensive way of distributing power to communities that live near to high voltage power lines but do not benefit from their presence [1].

Eskom installed a CCS at Meru, which was to deliver power to a 1.35 MVA [30] induction-motor, owned by Petronet. However, at low motor speeds (~60% of operating speed) severe sub-synchronous resonance (SSR), in the form of voltage and current oscillations was experienced [16]. SSR was not experienced when the CCS was used to supply power to a resistive load [16]. The possible return on investment is 1:14, provided a solution to the instability problem is found. [16]

The purpose of this thesis is therefore to establish the cause of SSR at the Meru-Petronet system, and other similar systems, and investigate various compensation techniques.

Procedure used

A literature study was conducted as the first step in determining the cause of SSR. Literature regarding CCSs, induction machines and SSR associated with those systems was studied. Technical reports and studies relating to the Meru-Petronet system were also examined.

The assumption that the voltage source was ideal was made to allow the core focus of the thesis to be on SSR, which was previously understudied with respect to CCS-IM systems.

Based on the findings of the literature study, it was found that the most likely cause of SSR was either ferroresonance or self-excitation [18], both of which lead to SSR. However, after studying these in more detail, self-excitation was revealed to be the more plausible cause of SSR.

University of Cape Town

A dynamic model, in the form of a transfer function, representing the CCS – induction motor system was then developed. The model was an extension of that developed by Wagner [23], and was obtained in a similar manner to that used by Limebeer et al. [35]. The model was used to analyse self-excitation, and its compensation when associated with CCS - induction motor systems.

Main findings

The Meru system used a ferroresonance-filter. Typical over-voltages and current spikes associated with ferroresonance were not observed at Meru or in laboratory models. In conjunction with literature studied this led to the conclusion that ferroresonance was not the cause of SSR, and that the problem was most likely due to self-excitation.

The dynamic model was validated by showing it to behave in the same way as the mathematical models of Wagner [23] and Limebeer et al. [35].

Three CCS-induction machine systems were then compared against the dynamic model predictions: a UCT laboratory model, a laboratory model made at Stellenbosch University, and finally the Meru-Petronet system. Results showed that self-excitation was indeed associated with all three of these systems. However, accurate equivalent circuit parameters were required to make resonant frequency predictions. These were unavailable for the Petronet induction motor, limiting its use in the model validation process. Resonant frequency predictions were reasonably accurate for the other two systems; inaccuracies being attributed to incorrect system parameters and model incompleteness.

The dynamic model was very useful in evaluating self-excitation compensation techniques, whose effects were clearly visible on Root-Locus plots. It was found that the transfer function, which represented the induction-motor series-capacitor system, was uncontrollable, with respect to preventing self-excitation. This was because the system-poles moved towards the open-loop pole positions in steady state. Open-loop pole positions are not affected by the addition of a controller. Therefore, to prevent self-

University of Cape Town

excitation, either the CCS-induction machine system must be modified, using shunt-resistors [2, 23], for example; or controlled using an active-filter (FACTS device), such as a current injector. These prevention techniques are required to supply energy to the CCS-IM system during the rotor speed range where it is susceptible to SSR. Therefore, a relatively simple starting sequence could be used to start motors that are required to run at close to rated speed. However, in the case where a VSD is used to control the rotor to a speed falling in the region where self-excitation is likely to occur, such a starting sequence would prove ineffective.

The effect of compensating inductance used to nullify the capacitive effect of the CCS was questioned. The compensating inductance makes the CCS an ideal source at supply frequency, but eliminates the ability of a CCS to improve the power factor of the larger grid network, by using its capacitive nature to cancel some of the inductiveness normally associated with a grid network [4]. With compensation, shunt resistors will consume ~50% of the power supplied to a CCS in order to damp self-excitation, but without compensation, damping resistors will use less than 16% of that power.

Conclusions

Based on the data collected, the following conclusions are made:

- The possible return on investment is 1:14, provided a solution to the instability problem is found. [16]
- A transfer function analysis of the CCS-IM system provided quick and valuable insight about system stability.
- A CCS-IM system is ultimately controlled by open-loop pole positions, making it uncontrollable by means of a passive controller, such as a passive filter.
- To prevent self-excitation, either the system configuration needs to be adjusted, or controlled actively using FACTS devices.
- It must also be noted that damping or current injection is only required to pull a CCS-IM system past the region in which SSR is likely to occur.

University of Cape Town

- Compensating inductance in a CCS cancels the capacitive effects of the CCS, making the CCS an ideal source at supply frequency.
- An un-compensated CCS will improve the power factor of the overall grid, assuming that the grid is slightly inductive.
- Compensating inductance significantly increases the power that is consumed by shunt resistors in order to damp self-excitation.
- The dynamic model did not take into account the influence of the differences between induction machines, such as the various types of induction machine rotors, and assumed that the voltage source was ideal, which resulted in slight model inaccuracies. However, such differences did not have a significant effect the underlying structure of the model.
- The Meru CCS was tested successfully [16] with resistive loads.
- With accurate equivalent circuit parameters, motor information, and possibly small model adjustments, the CCS-IM model can be used to predict the frequency at which SSR will occur and determine the size of the current injector or shunt resistance required to prevent SSR resulting form self-excitation, for systems such as Meru-Petronet setup.

Recommendations

Based on the conclusions that have been made, the following recommendations and future work is proposed:

- The dynamics of the CCS-IM transfer function model are controlled by open-loop pole positions. This means that a passive controller, such as a passive filter is not an adequate solution to CCS-IM SSR.
- To prevent self-excitation, either the system configuration must be adjusted or FACTS devices must be used to prevent it actively.
- Because damping or current injection is only required to pull a CCS-IM system past the region in which SSR is likely to occur, such a system should be designed, in terms of its power rating, with this in mind; especially when considering

University of Cape Town

motors that are controlled to operate predominantly within the region that SSR is likely to occur.

- It is advisable not to use CCS technology to supply power to induction motors until self-excitation problems have been resolved. However, the technology can presently be used to supply power to remote communities that use predominantly resistive loads.

Future work

- Adapt the dynamic model to cater for the differences in induction machines, and take into account the effect of supply voltage on resonant frequency predictions.
- Measure the equivalent circuit parameters of the Petronet induction motor, and adjust the model accordingly. So that the CCS-IM model can be used to predict SSR experienced by the Meru-Petronet System. Then, the system can be designed so that either the resonating region falls outside of the operating region of the motor, or resonance information can be used in the sizing of a current injector or damping resistor.
- Investigate the suitability of using no inductive compensation. In this way, much less power will be consumed by shunt-resistors if they are used to prevent self-excitation; and the overall grid-power-factor will be improved by the capacitive effect of the CCS, assuming the larger network has a slightly inductive nature. The lifetime cost of each method must be studied in order to complete the comparison.

University of Cape Town

TABLE OF CONTENTS

University of Cape Town

University of Cape Town

University of Cape Town

University of Cape Town

List of illustrations

Table of Figures

University of Cape Town

University of Cape Town

University of Cape Town

List of Tables

University of Cape Town

GLOSSARY

ADC:	Analogue to Digital Converter
CCS:	Capacitor Coupled Substation
DAC:	Digital to Analogue Converter
DSP:	Digital Signal Processor
FACTS:	Flexible Alternating Current Transmission Systems
IM:	Induction Motor
mmf:	Magneto motive force
PWM:	Pulse Width Modulation
SSR:	Sub-Synchronous Resonance
VSD:	Variable Speed Drive
UCT:	The University of Cape Town

University of Cape Town

NOMENCLATURE

a:	N_1/N_2 = turns ratio
B:	friction and windage constant
C_1:	capacitor of a CCS closest to the incoming voltage (F)
C_2:	capacitor of a CCS which is connected to neutral (F)
C_{thev}:	per-phase Thevenin Equivalent Capacitance (H)
f:	frequency of supply voltage (Hz)
f_{nat}:	natural frequency of an induction motor (Hz)
f_{res}	resonant frequency of system (Hz)
J:	inertia (kgm^2)
L_{com}:	compensating inductance of a CCS circuit (H)
L_1 or Ls	per-phase stator inductance (H)
L_2 or Lr	per-phase rotor inductance (H)
M:	mutual inductance (H)
n:	rotor speed (rpm)
n_s:	synchronous speed (rpm)
p:	number of poles in an induction machine
R'_2 or Rr:	per-phase rotor resistance (Ω) = a^2R_2
R_1 or Rs:	per-phase stator winding resistance (Ω)
R_c:	per-phase stator core loss resistance (Ω)
R_{thev}:	per-phase Thevenin Equivalent Resistance (Ω)
q:	slip (no units). For Chapter 4 only. In all other instances, s = slip
s:	slip (no units). except in chapter 4, where it s = $\frac{\partial}{\partial t}$ and q=slip
T_{elec}:	electrical torque produced by an induction machine (Nm)
T_{load}:	torque demanded by the load (Nm)
V_1:	per-phase terminal voltage (V)
V_{thev}:	per-phase Thevenin Equivalent terminal voltage (V)
ω_m:	mechanical speed of the rotating shaft (rad/s)

University of Cape Town

ω_s:	synchronous speed (rad/s)
X'_2 or Xr	per-phase rotor reactance (Ω) = a^2X_2
X_1 or Xs:	per-phase stator reactance (Ω)
X_m:	per-phase stator magnetizing reactance (Ω)
X_{thev}:	per-phase Thevenin Equivalent Reactance (Ω)
Z_1:	input impedance of an induction machine (Ω)

University of Cape Town

1 INTRODUCTION

1.1 Subject of this report

This report concerns an investigation into sub-synchronous resonance (SSR) associated with Capacitor Coupled Substations (CCS) particularly those that arise when used to supply induction motors (IM). Various compensation techniques are also discussed.

1.2 Purpose of this thesis

A CCS offers a low cost alternative to a conventional, inductor-transformer. Although series-capacitor applications have been used since the 1940s [23], [2] CCS technology still has its problems.

When a CCS is used to supply power to induction motors, particularly large induction motors that have a high inertia [29], SSR is sometimes experienced. It is the purpose of this thesis to determine the causes of this SSR. This will result in a clear understanding of the problem, creating a path to its solution.

A solution can only be proposed once the causes of SSR have been identified and understood.

1.3 Background to the investigation

A CCS was installed at Meru, South Africa, in 2002/3. The main purpose of the CCS was to supply a 1.35MVA [30] variable speed induction motor (IM) that was to be used by Petronet for a pump. It was found that at low motor speeds (~60% of operating speed) severe voltage and current oscillations were experienced [16]. When powered by a traditional sub-station, such oscillations were not observed. Other loads were successfully tested with the Meru CCS.

It is highly likely that the SSR experienced was because of an interaction between the CCS and induction motor, as no oscillations occurred when the Petronet induction motor was supplied from a conventional substation.

University of Cape Town

1.4 Need for Capacitor Coupled Substations (CCS)

Firstly, it must be noted that the 'traditional transformer' referred to here is an inductive transformer, consisting of a primary and secondary winding. The main advantage of the CCS over the traditional transformer is that it is generally cheaper [14]. Typically, capacitors are cheaper than inductors because of the expensive copper windings used to construct inductors that are not present in capacitors. Further savings are achieved using innovative CCS methods, such as the use of the lightning conductor, in overhead power lines, as one of the capacitors in the CCS [3]. A CCS is economically advantageous because of the way in which can it increase the transmission capacity of a power line by reducing the inductance of a grid [4], due to the capacitive nature of a CCS.

The cost factor makes CCSs ideal for supplying power to communities in remote areas [5], particularly those that are situated near to high voltage overhead power lines [1], but do not benefit from them. A sketch of a single-phase CCS distribution system is shown in Figure 1. It can be seen that the CCS takes in a high voltage and divides that voltage to a lower voltage, which is used to supply a variety of loads.

University of Cape Town

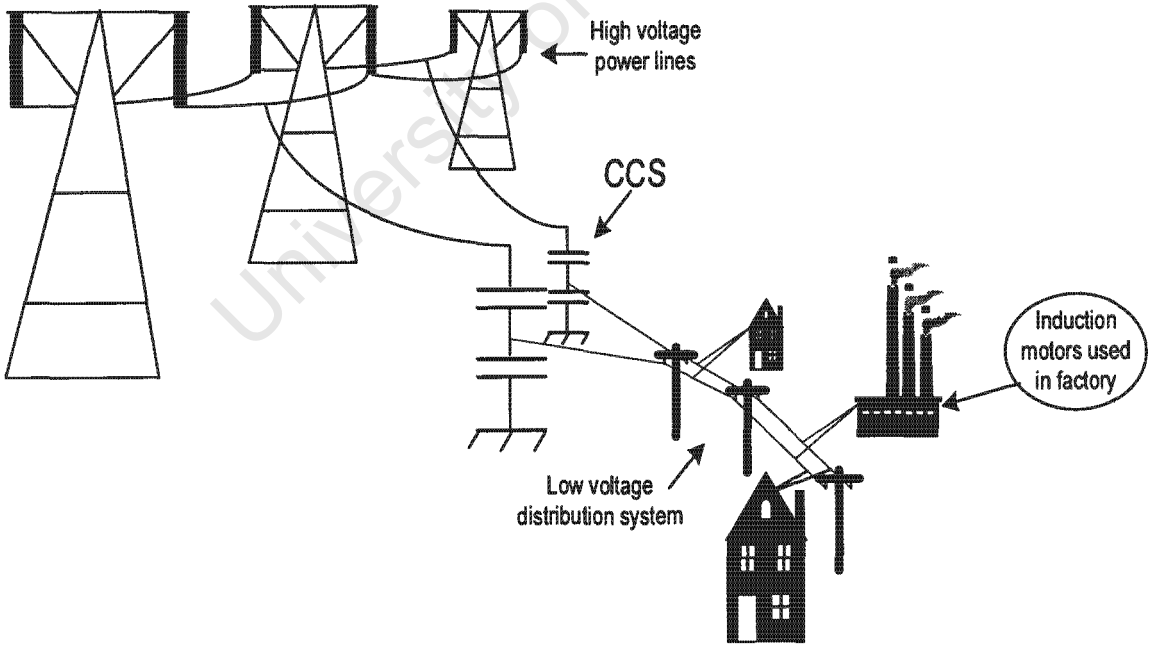

Figure 1: A single-phase CCS supply system pictorially described

1.5 Limitations of development

There were no significant limitations to development. The worst being the absence of accurate parameters for the Petronet induction motor, as Petronet was unwilling to allow their motor to be used for experiments. As a result, the Meru-Petronet system could not be used to validate the control-systems model developed.

The assumption that the voltage source was ideal must also be noted. Although this may lead to slight inaccuracies in results, the underlying structure of models developed and key concepts examined would not be affected. The reason for this assumption was allow a greater emphasis to be placed on an analysis of the phenomenon of SSR, which was previously understudied with respect to a CCS-IM system.

1.6 Plan of development

As stated in the terms of reference, the direction that research will take shall be based on an initial hypothesis. Following that, research and simulation/ modelling-paths will be developed.

Chapter 1 has laid down the foundation of this dissertation. The aims of research have been stated, as well as the history of CCS-IM (Capacitor Coupled Substation – Induction Motor) systems that lead to a need for such research.

Chapter 2 is a literature study of the CCS, the induction motor and of SSR associated with a CCS-IM scenario. Technical reports that have been submitted documenting the SSR phenomenon will be given special attention in this section.
Based on the findings of chapter two, a hypothesis as to the cause of CCS-IM sub-synchronous resonance (SSR) will be made. The course of the dissertation, from then on, will then be to validate, refine or reject that hypothesis.

University of Cape Town

Chapter 3 is a literature study into the hypothesised causes of SSR, namely ferroresonance and self-excitation. Literature regarding various control-system tools will also be studied in this section.
After studying this literature, the hypothesis will be refined, narrowing the focus of research.

In **Chapter 4,** various dynamic models are constructed. These will be used to predict the resonant frequencies of the CCS-IM system. Because of the valuable insight provided by the control-model, possible solutions are proposed.

Chapter 5 explains simulations performed using Matlab® and Simulink®.

In **Chapter 6,** a laboratory model is constructed. An instrument capable of recording relevant parameters will also be developed.

Chapter 7 ties together predicted simulated and actual results. The different solutions are also discussed.

Following this is a discussion of those results and possible solutions to SSR in **chapter 8**.

Finally, conclusions and recommendations are made in **chapters 9 and 10** respectively.

University of Cape Town

2 LITERATURE SURVEY

In order to be in a position to make a significant contribution to the stability of the CCS-induction motor system (CCS-IM), it was first required that the author become familiar with the relevant apparatus and concepts involved.

It is important to note that the study conducted here was not a "power system stability" analysis as described by J. de Cock [10]. He described this as the analysis of a system of generators, connected via busses to many different loads. He conducted various tests such as load flow, short circuit and dynamic tests. Based on the results of these tests, the stability of a power system can be determined. In this thesis, the author assumes that interaction between generators supplying power and other busses connected to the Meru-CCS are not the cause of the sub-synchronous resonance experienced.

The purpose of this section was to study the following literature:

- Capacitor Coupled Substation (CCS),
- Induction motor,
- Literature relating to SSR experienced in a CCS-IM scenario; including technical reports documenting instances of SSR.

Once this data was collected, a hypothesis explaining the major causes of CCS-IM SSR was proposed.

University of Cape Town

2.1 CCS Literature Study

2.1.1 The CCS

A CCS is a capacitor-divider, and can be used instead of a conventional transformer to divide voltage. A CCS is analogous to a resistor potential divider, except more suitable for power consumption reasons.

An inductor and a capacitor are both energy storage elements. The energy stored in a capacitor is proportional to the square of the voltage across it, whereas an inductor's energy is proportional to the square of the current flowing through it. ($E_{inductor}= ½LI^2$ and $E_{capacitor}= ½CV^2$ where E is in Joules.) The voltage across a capacitor is proportional to the integral of the current flowing into it (2.1). The voltage across an inductor is proportional to the derivative of the current flowing through it (2.2).

$$V_{Cap} = \frac{1}{C}\int I\partial t \tag{2.1}$$

$$V_{Ind} = L\frac{\partial I}{\partial t} \tag{2.2}$$

Due to the mathematically opposite nature of a capacitor and an inductor, as shown in equations (2.1), (2.2) and the energy relationship described in the preceding paragraph, when these devices are connected in series or parallel, energy can oscillate between them.

Circuit Diagram of the CCS:

Shown here is a conceptual circuit diagram of a CCS, showing the open circuit model only.

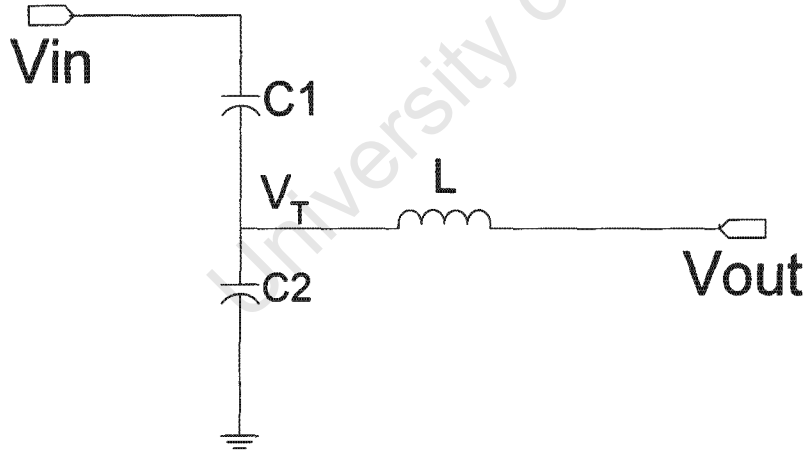

Figure 2: Circuit diagram of a CCS

Where the tap voltage, V_T, is determined as follows:

$$V_T = V_{in}\frac{C1}{C1+C2} \tag{2.3}$$

University of Cape Town

It can be more convenient to analyse the Thevenin Equivalent Circuit of the open circuit CCS:

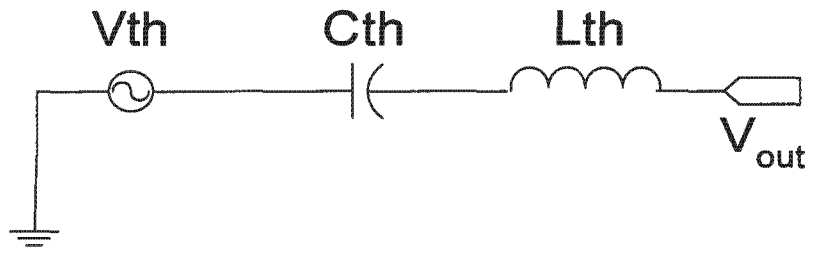

Figure 3: Thevenin Equivalent circuit of a CCS

Where: V_{thev} = Thevenin Equivalent Voltage,

C_{thev} = Thevenin Equivalent Capacitance.

$$V_{thev} = \frac{C1}{C1+C2} V_{in} \tag{2.4}$$

$$C_{thev} = C1+C2 \tag{2.5}$$

The inductor is added to compensate for the capacitive effect of the Thevenin impedance, C_{thev}, at the supply frequency [6]. In practice, the inductor does not exactly cancel the capacitor's effects as it includes some resistance, but it makes the CCS close to an ideal source at supply frequency, meaning that the source impedance is close to zero at that frequency.

When $X_L = X_{C\ thev}$, then $jwL = \frac{-1}{jwC_{thev}}$

$$\therefore\ LC_{thev}\omega^2 = 1 \tag{2.6}$$

Equation (2.6) shows how to calculate the inductance needed to compensate for the capacitive effects of the CCS, for a specific ω value.

2.1.2 The passive filter (tank circuit)

A passive (band pass) filter can be included to damp resonations at frequencies other than the operating frequency of the supply. This filter was initially used by the Canadian

University of Cape Town

power company, Hydro-Quebéc to prevent ferroresonance. The same filter was used in the Meru CCS.

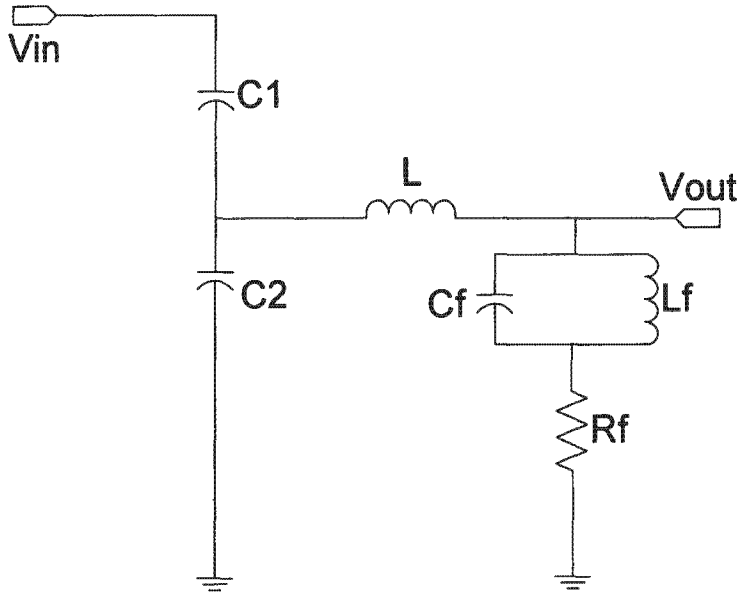

Figure 4: CCS with passive filter

The values used in the Meru filter can be found in the appendix 'A'.

2.2 Induction motors

Induction motors are the most widely used motors in industry, constituting eighty percent of the total number of motors used [7]. The Petronet motor is an induction machine driven by a variable speed drive (VSD). The machines that were used during the testing stage of the CCS were induction machines, started direct on-line. A literature study of induction motors was conducted for this reason.

2.2.1 Induction motor theory

Most of the material in this section was gathered from a textbook written by P.C. Sen: "Principles of Electric Machines and Power Electronics" [8].

Induction machines are also referred to as asynchronous machines. For a transfer of energy to take place from either electrical energy to mechanical energy, or visa- versa; the electrical speed of the rotor must differ from the electrical speed of the stator. That is,

University of Cape Town

the rotor's speed must be different from the synchronous speed, therefore the term 'asynchronous machine'.

A typical induction machine consists of a rotor rotating inside a stator (see Figure 5). The stator is normally made of laminations of high-grade sheet steel, in these laminations there are slots in which windings are placed. The rotor of an induction motor is most commonly one of two types: squirrel cage or wound rotor. Squirrel cage rotors consist of a cage of bars that are electrically shorted at both ends (see Figure 6). The wound rotor configuration is the same as that of the squirrel cage arrangement except that instead of shorting the bars at each end, these are connected via slip rings.

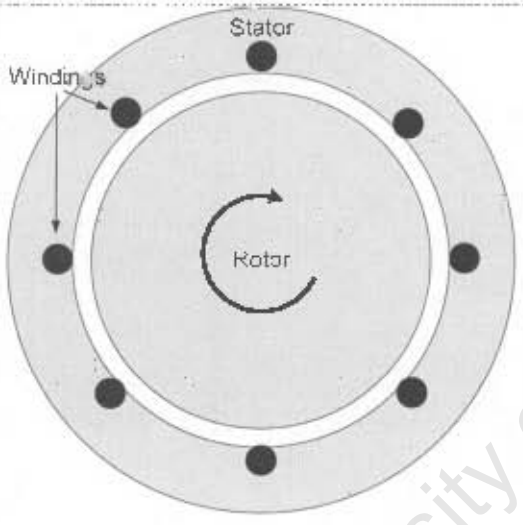

Figure 5: Cross-section of an induction motor

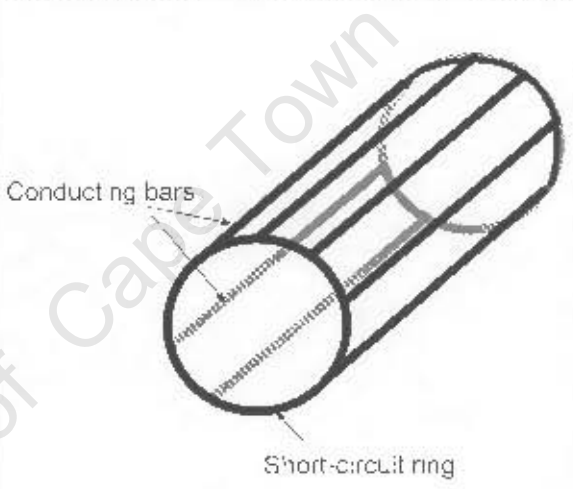

Figure 6: Squirrel cage configuration

University of Cape Town

When a current flows through the windings of the stator, a magnetic field is produced. Faraday stated that when this magnetic field cuts the conducting bars of the rotor, an induced a voltage is set up within it [8]. A resulting current, and therefore magnetic field, will exist in the rotor. Interaction between the magnetic field of the stator and the rotor sets up a torque in the machine. If the magnetic field of the stator and the rotor were rotating at the same speed then there would not be an induced voltage established in the rotor. With no induced voltage, the rotor would have no magnetic field, and therefore it would be impossible for a torque to be generated in the machine.

The difference between the rotor speed and the rotating field of the stator is called the slip. Slip is an important term that will form a vital part of this study later.

$$s = \frac{n_s - n}{n_s} \tag{2.7}$$

Where: s = slip (no units)

n_s = synchronous speed (rpm)

n = rotor speed (rpm)

Synchronous speed is given by:

$$n_s = \frac{120f}{p} \tag{2.8}$$

Where: f = supply voltage frequency (Hz)

p = number of poles in the machine (no units)

University of Cape Town

2.2.2 Equivalent circuit of an induction motor

Although simple, and not strictly a dynamic model, the following equivalent circuit can be used to model the machine.

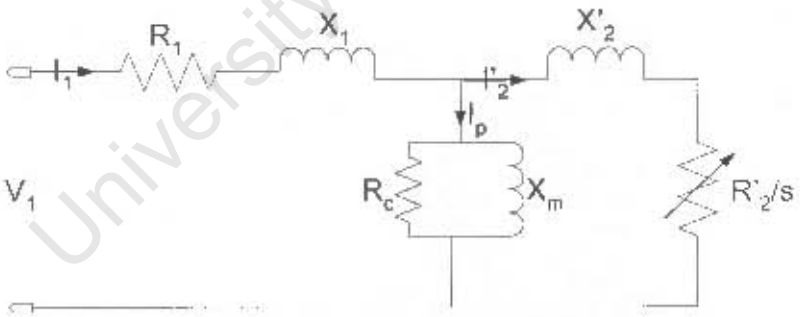

Figure 7: Equivalent circuit of the induction motor [8]

Where: V_1 – per-phase terminal voltage (V)

R_1 = per-phase stator winding resistance (Ω)

L_1 = per-phase stator inductance (H) $X_1 = 2\pi f L_1$

f = frequency of supply voltage (Hz)

L_m = per-phase stator magnetizing inductance (H) $X_m = 2\pi f L_m$

R_c = per-phase stator core loss resistance (Ω)

a = N_1/N_2 = turns ratio

L_2 = per-phase rotor inductance (H) $X'_2 = a^2 X_2 = a^2 2\pi f L_2$

R_2 = per-phase rotor resistance (Ω) $R'_2 = a^2 R_2$

From the equivalent circuit, the following equations are derived.

The power developed in the rotor circuit is:

$$P_{rotor} = I_2^2 R_2 \tag{2.9}$$

The power developed across the air gap is:

$$P_{ag} = I_2^2 \frac{R_2}{s} \tag{2.10}$$

Thus, the remaining power will be the mechanical power:

$$P_{mech} = I_2^2 \frac{1-s}{s} R_2 \tag{2.11}$$

The resistance $\frac{1-s}{s} R_2$ represents the total mechanical load, including rotational losses [7].

It is recommended by the IEEE that R_c be omitted from the equivalent circuit diagram, and instead the core losses (due to R_c) should be lumped together with the friction and windage losses [8]. This has little effect on the accuracy of the equivalent circuit. At start up, friction and windage losses are large, and the core losses are small. However, at rated speed, friction and windage losses are small, whereas core losses are large. The resulting sum of friction and windage plus core losses is almost constant at all rotor speeds, therefore justifying the removal of R_c from the equivalent circuit diagram. By ignoring R_c, the Thevenin Equivalent Circuit will be:

University of Cape Town

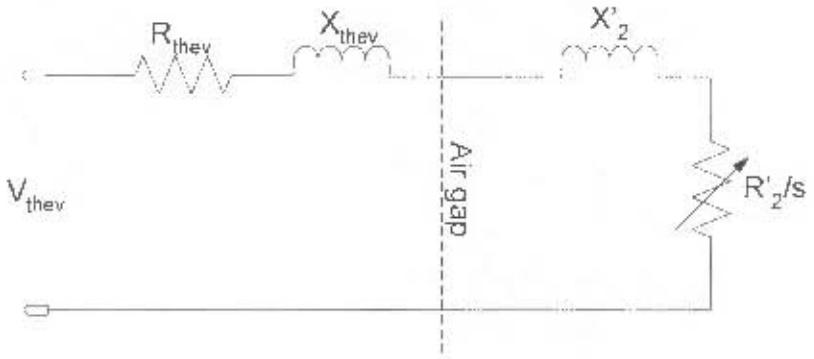

Figure 8: IEEE Thevenin Equivalent Circuit of an induction machine [8]

V_{thev} = Per-phase Thevenin Equivalent terminal voltage

R_{thev} = Per-phase Thevenin Equivalent Resistance

X_{thev} = Per-phase Thevenin Equivalent Reactance

Where:

$$V_{thev} = \frac{X_m}{\sqrt{R_1^2 + (X_1 + X_m)^2}} V_1 \tag{2.12}$$

$$Z_{thev} = R_{thev} + X_{thev} \tag{2.13}$$

$$Z_{thev} = \frac{jX_m(R_1 + jX_1)}{R_1 + j(X_1 + X_m)} \tag{2.14}$$

$$P_{mech} = T_{mech}\omega_{mech} \tag{2.15}$$

So,

$$T_{mech(per-phase)} = \frac{1}{\omega_{syn}} \frac{V_{thev}^2}{(R_{thev} + R'_2/s)^2 + (X_{thev} + X'_2)^2} \frac{R'_2}{s} \tag{2.16}$$

Note that this is the per-phase torque, so the total torque is 3 times this.

Using equation (2.16), and typical 3kW machine parameters (as determined by laboratory tests - see appendix 'A'), the following torque-speed plot is obtained:

University of Cape Town

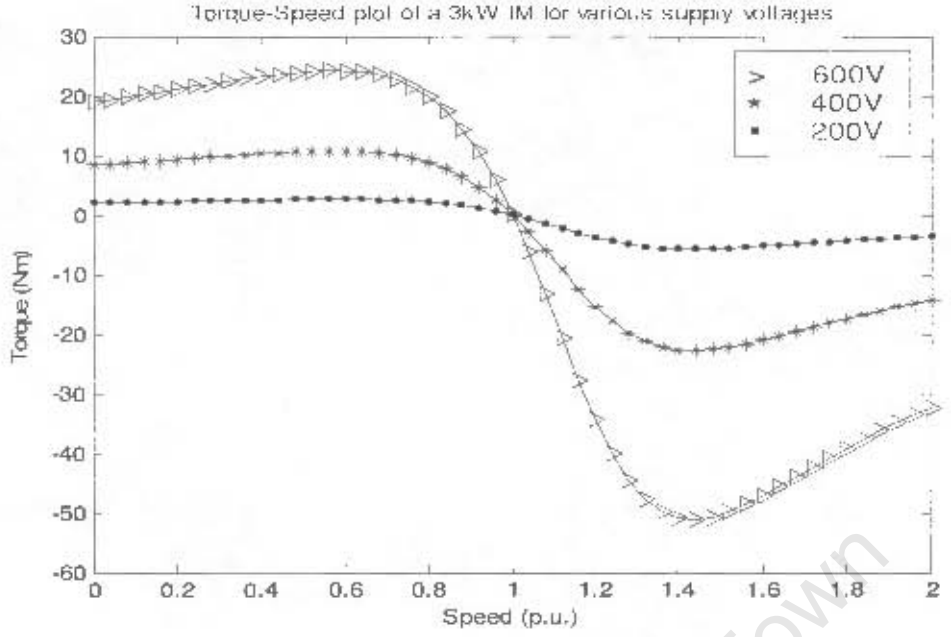

Figure 9: Torque-speed profile of a 3kW induction motor for various supply voltages

From this graph (Figure 9), parameters such as starting torque and maximum torque can be determined. Torque is proportional to the square of the supply voltage, as per equation (2.16). The input impedance (Z_1) of an induction motor as determined from Figure 7, is:

$$Z_1 = R_1 + jX_1 + \frac{jX_m(R'_2/s + jX'_2)}{R'_2/s + j(X_m + X'_2)} \tag{2.17}$$

Thus, the stator/ input current is;

$$I_1 = \frac{V_1}{Z_1} \tag{2.18}$$

When the machine is running close to steady state, slip(s) is small, so the term $\frac{R_2}{s}$ is large. However at start-up s = 1, thus $\frac{R_2}{s}$ is much smaller, and therefore, the current (I_1) is larger. Typically, the starting current is 5 to 8 times rated current [8].

The power factor of the machine is given by:

$$PF = \cos(\theta_1) \tag{2.19}$$

University of Cape Town

θ_1 = phase angle of stator current, $1_1 = \frac{\mathrm{Re}(Z_1)}{\mathrm{Im}(Z_1)}$

The way in which an induction motor converts electrical energy to mechanical energy is illustrated conveniently with a power flow diagram [8]:

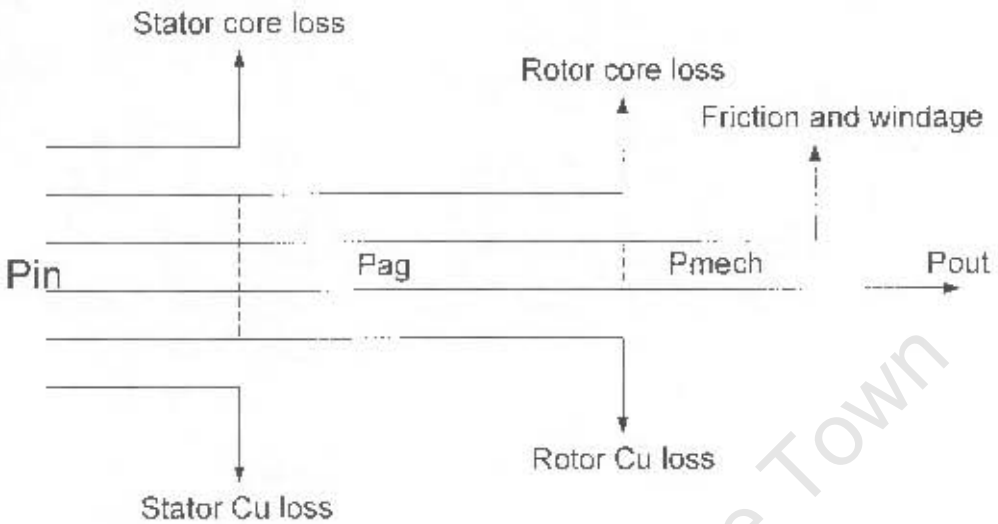

Figure 10: Power flow diagram [8]

In other words, $P_{out} = P_{in} - P_{losses}$.

All the power quantities represented above are real. Only real power is of interest in Figure 10, as only real power can be converted into mechanical energy. This means that the stator and rotor core losses shown above are simply due to hysteresis and eddy current losses in the laminations of the respective cores.

University of Cape Town

2.2.3 Dynamic torque-tracking of an induction motor

Under normal operating conditions, when a voltage is applied to an induction motor, it will speed up until the electrical torque that it is generating is equal to the load torque plus losses [9].

$$T_{elec} = T_{load} + J\frac{\partial}{\partial t}(\omega_r) + B\omega_r \quad (2.20)$$

[10]

Where: J = inertia (kgm^2)

B = friction and windage constant

ω_r = rotor speed (rad/s)

Friction and windage refers to the power losses that result from such items as the induction motor fan and bearing friction. Also included in friction and windage losses are the core losses, as per section 2.2.2.

Therefore, the torque transfer function is:

$$\text{Transfer function} = \frac{\omega_r(s)}{T_{elec}(s) - T_{load}(s)} = \frac{1}{Js + B} \tag{2.21}$$

This can be represented in block-diagram format as:

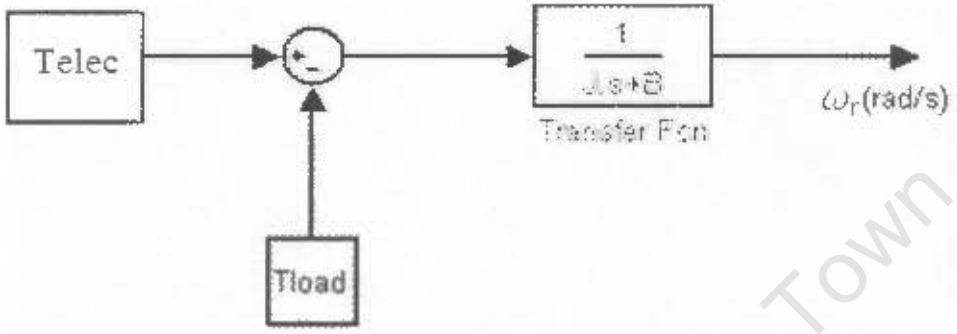

Figure 11: Torque characteristic of an induction machine [9]

So, when the induction motor experiences a change in torque its time constant, T, is given by T=J/B, and it will take 4T to settle to within a 2% of its steady-state value. Hence, after roughly $4*\frac{J}{B}$ seconds the IM will settle at a new torque [11]. This is a rough estimate, as torque variation is only linear if the change in speed is small (~5% of synchronous speed – refer to Figure 9).

2.2.4 Inertia [9]

The inertia of an induction machine is often required, as it was in section 2.2.3. The inertia of the rotating elements of an induction motor can be calculated. By treating the rotor as a solid, rotating disk (as shown in Figure 12) its inertia is:

$$J = ½\ mr^2 \tag{2-1}$$

m = the mass of the rotor, which was calculated using the formula:

mass = volume×density . The rotor consists of a mild steel core of density ~7650kg/m^3.

University of Cape Town

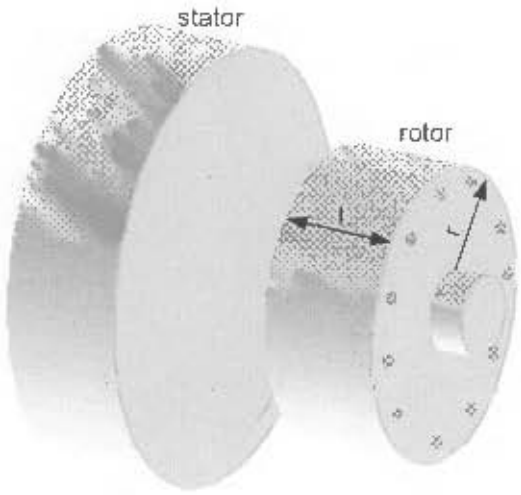

Figure 12: Components of an induction motor

For the Petronet 1.35MVA IM, the rotor radius, r, and length, L, were estimated to be:

$$r = 0.4\text{m}$$

$$L = 0.8\text{m}$$

Therefore, the mass of the rotor is:

$$M_{rotor} \simeq 0.8 \times \pi \times 0.4^2 \times 7650 = 3076kg \qquad (2.22)$$

The total mass of the Petronet motor (rotor+stator) is 5600kg (see appendix 'A'). If the rotor accounts for half of the mass of the motor then the estimate (2.22) is reasonable.

Therefore, the inertia of the rotor is:

$$J_{rotor} = \tfrac{1}{2} \times 3076 \times 0.4^2 = 246kgm^2$$

2.2.5 Friction and windage

If the friction and windage losses are assumed to be between 1% and 5% of the rated power of an induction motor; then, because power is proportional to torque, between 1% and 5% of the rated torque will therefore be used by friction and windage losses.

University of Cape Town

So, for example, if the rated torque of a pump is 300Nm at the rated speed of the motor, and it is estimated that friction and windage losses are 5%, then using the torque equation:

$$T_{elec} = T_{load} + J\frac{\partial}{\partial t}w_r + Bw_r \tag{2.23}$$

5% of the torque to be lost to friction and windage:

$B\omega = 15.0 \quad \omega = 314 rad/s$

$\therefore B = 0.05$

Therefore, B = 0.05 Nms/rad

2.2.6 Variable Speed Drives

A variable speed drive (VSD) is a device that controls the speed of an induction motor. It was necessary to investigate these devices as one was used to control the speed of the Petronet IM, and therefore could possibly be the cause of SSR.

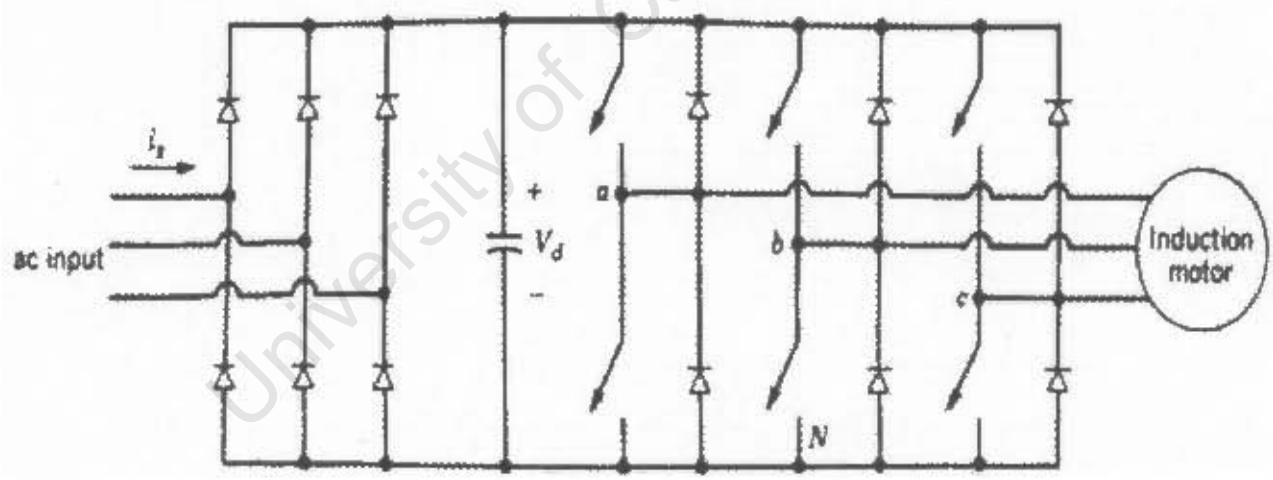

Figure 13: Variable Speed Drive [12]

Apart from very-high power applications where cycloconverters are used, variable speed drives use inverters with a dc input [12]. Typically, a VSD works by first rectifying the supply voltage using a full-bridge rectifier and a smoothing capacitor, which acts as a filter. The resulting DC voltage is used to supply solid-state switches (IGBTs or mosfets) (see Figure 13) which switch in such a way as to produce a PWM (Pulse Width

University of Cape Town

Modulation) waveform as shown in Figure 14 that is used to drive an induction motor. Amplitude of the output voltage is controlled by varying the duty-cycle (on-off) periods of the PWM waveform [7]. To increase the amplitude of the output waveform, the on-time is made longer, compared to the off time, and visa-versa. Frequency can simply be varied by increasing or decreasing the period of the fundamental PWM waveform.

The speed of the IM is proportional to the frequency of the supply. In order to maintain rated torque for all speeds, the air-gap flux (Φ_{ag}) must be kept constant. This is achieved by varying the amplitude of the supply voltage in proportion to its frequency [12].

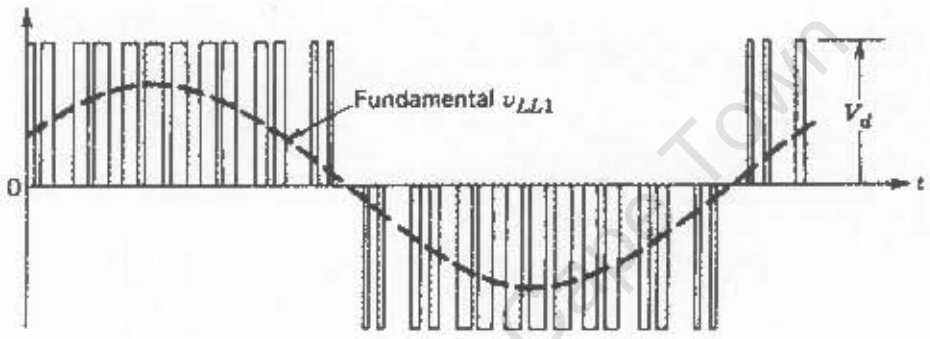

Figure 14: Variable Speed Drive switching pattern [12]

There are three main types of inverter-variable-speed-drives [12]:

1. Pulse-width-modulated voltage source inverter (PWM-VSI) with a diode rectifier
2. Square-wave voltage source inverter (square-wave VSI) with a thyristor rectifier
3. Current source inverter (CSI) with a thyristor inverter

The main difference between these inverters is the CSI and VSI type. With the VSI, a dc voltage is used as a source, whereas with the CSI a dc current source is used.

2.2.7 Harmonics in induction motors

Harmonics in an induction motor are mainly due to space and time harmonics [8], but can also occur as a result of other interferences, such as self-excitation or ferroresonance.

University of Cape Town

Space harmonics:

These arise from the fact that phase windings in a machine are distributed over a finite number of slots. The effects of this on the magneto-motive-force (mmf) of the machine are shown:

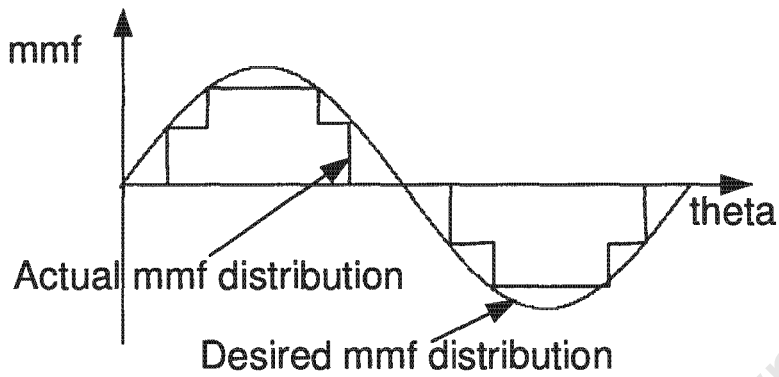

Figure 15: Actual phase mmf distribution in an induction motor

Because the mmf is not distributed in a sinusoidal pattern, by Fourier's theorem, harmonics will therefore be present. In addition, space harmonics can occur at sub-synchronous frequencies [8, pp 277]. These harmonics affect the stability of both the supply and the performance of the IM. However, such effects are usually minimal.

Time harmonics:

Time harmonics exist because of solid-state mechanisms, such as variable speed drives, that are used to control the voltage and frequency of induction motors. Because these mechanisms are essentially switching the input voltage in a non-sinusoidal fashion, harmonic currents exist. Time harmonics occur at super-synchronous frequencies [8, pp 272]. Time harmonics cause the induction motor to experience a torque ripple, which in turn affects its rotor speed. It can be shown however, that if the inertia of the machine is large then speed ripple will be negligible.

$$\text{Amplitude of speed rippple} = k\frac{\text{amplitude of torque ripple}}{\text{ripple frequency} \times \text{inertia}} \qquad (2.24)$$

Equation (2.24) shows that the larger the inertia of the motor, the smaller the speed ripple will be [8].

University of Cape Town

2.2.8 Crawling

It is important to mention crawling here, as this can also lead to sub-synchronous resonance (SSR).

Crawling arises as a result of the unusual relationship between the slots in an induction machine. This relationship can result in large sub-synchronous harmonics at about one-seventh of synchronous speed. The harmonics result in a torque dip (in the IM), which may cause "the motor to 'hang' or 'crawl' at low speeds." [13]

Typical resonating frequencies associated with crawling are at about 14% of the fundamental frequency. The oscillations that are under investigation have been observed within the 60% of the fundamental frequency [16]. Therefore, it is not likely that crawling is the cause of the SSR under investigation.

2.2.9 Dynamic model of an Induction Motor

In some cases, it is advantageous to use a more complex model of an induction motor. For the purpose of this investigation, a dynamic model of an induction motor was not deemed necessary. Instead, the equivalent circuit (of section 2.2.2) was adjusted to represent the dynamics characteristic with SSR, then transfer function equations were developed for that circuit.

University of Cape Town

2.3 Literature relating to SSR experienced in a CCS-IM scenario

Summaries of reports that have already been conducted concerning the Meru-Petronet problem shall be discussed. The title of each report is made the heading of each of the following subsections, shown in inverted commas. A paper that is not related to the Meru-Petronet system shall first be summarised, this paper is of interest, as it documents the success of a CCS system.

2.3.1 "Capacitor divider substation"

This paper was written by Bolduc, Bouchard and Beaulieu [14] to document the success of the CCS technology that was implemented in Canada by Hydro-Quebéc. Findings made can be summarised:

- The development of a passive damper-filter (patented by Hydro-Quebéc) solves ferroresonance problems, making a 1.5-2MW CCS possible.
- A CCS will be beneficial to a transmission line, as it will reduce system losses by cancelling some of the reactive current.
- A CCS at Rivièr Ste Anne has been operational, with positive results, since August 1994.

The remainder of the reports investigated in this section (section 2.3) were directly associated with the Meru-Petronet system.

2.3.2 "Evaluation of a 275kV TO 22kV Capacitor Coupled Substation"

A brief summary of the findings of this report, which was compiled by Schilder and Mathebula [16] is as follows:

- SSR was only observed when the Meru CCS was used. "Normal operating conditions exist when the Petronet load is powered from the Ruston rural 22kV supply."
- "It is believed that the CCS is cheaper at smaller power levels from 1.5 to 5MVA, than conventional transformers." In addition, a CCS has lower maintenance costs.
- The use of a non-saturating air cored reactor and a damping filter enables ferroresonance to be avoided.
- "Severe flicker was experienced when running the (Petronet) motor at 60% of full speed (from the Meru-CCS)" with strong 40Hz and 60Hz components observed in the voltage FFT.
- Significantly less flicker was observed at speeds greater than 89% of full speed, with weak 48Hz and 52Hz components observed in the voltage FFT.
- "The shunt filter at Meru is not the cause of the CCS/Petronet instability."

University of Cape Town

- "It seems that a resistive load may be run successfully off Meru, provided that no or only very small motors are run from the CCS." However, SSR was also experienced when smaller motors were run from the Meru substation.
- "The following separate procedures were carried out to stabilise the CCS/motor load combination in the laboratory, with no or very little success:
    a) A parallel resistive load (up to 3 times the motor load power), which has no effect.
    b) A series resistor, which has the negative effect of reducing voltage regulation.
    c) A shunt filter, which has no effect.
    d) Detuning the series circuit (reducing the capacitance to half the inductance), which reduces the voltage regulation. (This was based on the fact that series capacitive compensation of transmission lines should never exceed 50%.)"
- "A resistor in parallel with the series capacitor stabilises all Mini Cap-Tap and motor load combinations, provided that this resistor value is less than or equal to the magnitude of the capacitive reactance at the fundamental frequency.
    - This does not provide the solution, since the resistor adds loading to the capacitive divider and results in unacceptably low voltages at the output."
- The component values of the Meru CCS were measured and found to be accurate.
- "The CCS was designed and built at a cost of about R10 million, and, the total budget for this project is only R700k. The possible return on investment is 1:14, provided a solution to the instability problem is found. Eskom will benefit a lot in future should the CCS technology be made successful."
- "Indications are that smaller (100 kVA to 170 kVA) capacitive coupled substations (CCS) have been built and used successfully in Canada, Mexico and South America."

University of Cape Town

2.3.3 "Captap series resonance compensation"

A brief summary of the findings of this report, which was compiled by Beukes, Lategan and Molepo [18] is as follows:

- Various methods of solving resonance problems associated with CCS technology were investigated.
- Ferroresonance was initially attributed to the cause of resonance.
- CCS technology works well, and "the only problem currently experienced with this technology is instability with motor loads."
- A CCS laboratory model was built.
- "It was shown that the captap system suffers from induction machine self-excitation problems and not from ferroresonance as initially suspected."
- At 10kW power level, "the best way of solving the problem is by using a back-to-back converter between the source and the load."
- The authors concluded that "passive compensation is not a viable solution," because of high power losses and poor voltage regulation.

2.3.4 "Analysis of Simulation Studies for the Eskom 275/22kV Capacitor Coupled Substation – CCS"

Braae, Folly, and Gaunt [30] prepared a report regarding the Meru-Petronet system for Eskom using control tools such as:

- transfer function analysis,
- block diagram algebra and
- Root-Locus plots.

Results showed that "Sub-synchronous modes were found at about 30Hz in the Matlab, dynamic analysis and laboratory model, which corresponds with the reported field measurements."

University of Cape Town

It was concluded, "Dynamic analysis, based on lumped parameter models and block diagram algebra, indicates that the CCS gives rise to two oscillatory modes, one super-synchronous and the other sub-synchronous. Both represent damped transients."

It was also found by these authors that "Variations in the CCS component values indicate that the dynamic behaviour of the CCS is critically dependent on the resistance in the band pass filter (tank circuit)."

The way the tank circuit (see sect. 2.1.2) affects CCS stability was also investigated, in particular variations in tank circuit resistance:

Tank circuit resistance	Effect	
Increase	"Reduces duration of transients noted in the no-load situation."	"Sharpens the filtering at the synchronous frequency."
Decrease	"Emphasises the oscillatory nature of the CCS dynamics."	"Reduces the filtering at the synchronous frequency."

Also stated in the report:
"The linear model indicates that the dynamics of the load will impact on the modes of the overall CCS system, particularly for low reactance, high power loads when oscillatory modes with longer transient decay times become evident."

Summary

This report showed that

- Two oscillatory modes exist, the lower being at ~30Hz.
- Resistance of the tank circuit plays a critical role in CCS-instability.
- Dynamics of the load will affect the stability of the overall CCS system.

University of Cape Town

2.3.5 "Harmonic penetration from capacitor coupled sub-stations"

Nene and Naidoo [15] prepared a report regarding the Meru-Petronet system for Eskom. The following findings were made:

Frequency domain simulations of the Meru-Petronet system showed that "two resonant points (31.7Hz and 77.9Hz) occur when Petronet is supplied from the CCS. These increase during high loading conditions to about 33Hz and 86Hz respectively. [15]"

A simulation of when the Petronet load was supplied from the Ruston 22kV busbar via a conventional (inductive) substation, "No resonance or current modulation occurs;" although, 76% total-harmonic-distortion was observed in the current waveform. However, this distortion was attributed to the sizing of the Ruston transformer and the thickness of the cable supplying the Pertonet load from the Ruston substation.

2.4 Hypothesis regarding the cause of SSR

The purpose of this section is two-fold. It acts as both a examination area for the development of a hypothesis that will guide the course of research here forth, and as a summary of this chapter.
Based on data that has been collected in chapter 2, focusing on the analysis of the possible causes of SSR mentioned in section 2.3, the following is noted:

1. SSR is not experienced when an induction motor is connected to a conventional distribution sub-station. The following evidence confirms this:
    - Typical induction motor datasheets give no indication of such oscillations. Because CCSs are not commonplace, it must be assumed that manufacturers test their induction motors using power obtained from a conventional substation.
    - The Petronet Induction Machine did not show signs of SSR when connected to a conventional substation, but did when connected to the Meru CCS [16].

University of Cape Town

It is therefore highly likely that SSR is caused by some form of interaction between the CCS and IM. This means that there is little need to research SSR that may be caused by either the IM or CCS in isolation. For example, harmonics as a result of the design of a particular rotor [8] in an induction machine.

2. From the research report conducted by Johan Beukes for Eskom [18], and warnings of possible SSR mentioned by Bolduc et al. [14], (section 2.3) the following causes of SSR emerge as the most likely source of the CCS-IM problem:
    - Ferroresonance and
    - Self-excitation.

The following hypothesis is therefore made:

SSR associated with a CCS-IM setup arises because of an interaction between the CCS and IM. The most likely cause of this resonance is either ferroresonance or self-excitation.

The course of the dissertation here-forth will be to validate, refine, or disprove, this hypothesis. For this reason, the following chapter is a literature study into ferroresonance and self-excitation. After which, a dynamic-systems mathematical model will be developed using a control systems methods. Simulations and laboratory models will then be constructed to test the model, and therefore the hypothesis.

University of Cape Town

3 EXAMINATION OF FERRORESONANCE AND SELF-EXCITATION

In this section, the phenomena of ferroresonance and self-excitation are investigated, and various solutions to these problems discussed.

Various dynamic-systems analysis tools, such as Root-Locus and state-space methods, shall be introduced at the end of this chapter, as these tools will be required in subsequent chapters.

SSR associated with CCS systems are not limited to induction machines. Hunting may also be experienced when synchronous machines are driven from a CCS [2]. Hunting is an "unstable state in which a machine output, system frequency, etc. runs alternatively too fast and too slow." [17] The focus of this study was CCS – induction machine SSR. After studying this literature, the hypothesis proposed at the end of chapter 2 shall be refined.

University of Cape Town

3.1 Ferroresonance

An explanation of ferroresonance will now follow based mainly on literature form Beukes et al. [18].

Ferroresonance is most likely to occur in the distribution transformers that are connected to a CCS. It can also occur in induction machines that are connected to the CCS as these also include inductors that are susceptible to saturation. Ferroresonance results in dangerous current spikes and over-voltages that can damage equipment [21].

In the past, a capacitive divider in series with an inductor (such as a transformer) was never used to supply power because of the problem of ferroresonance. Above a certain voltage, the magnetizing inductance of the inductor saturates. Saturation occurs as the ferromagnetic core of the inductor reaches its magnetic limit. This effect causes a non-

linear rise in current at the peak of the supply voltage waveform, as shown in Figure 16. In turn, the current increase causes the capacitor to build up charge, which forms the initial conditions for the next cycle. This process can lead to super synchronous and/or sub synchronous resonance [17]. Ferroresonance and can lead to the failure of distribution transformers [19] and other inductive loads. Signs of ferroresonance include "violent wave distortion, abnormally large magnetizing currents, and fluctuations in voltage." [23]

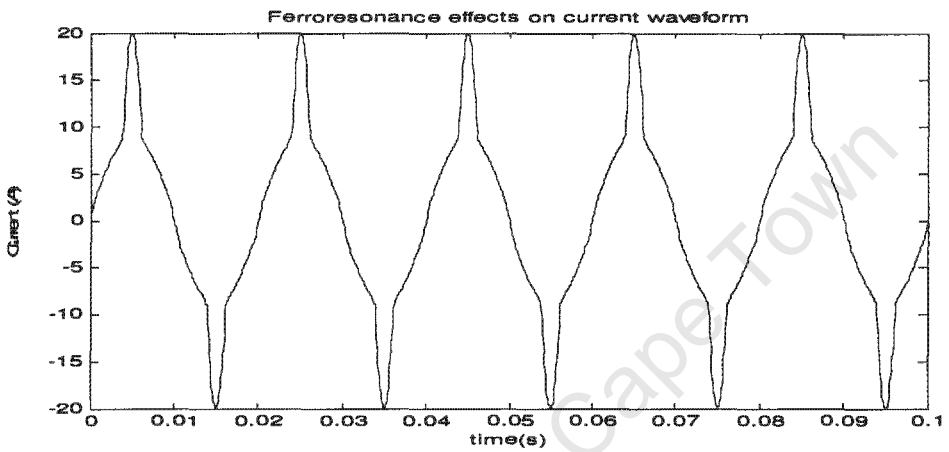

Figure 16: Voltage waveform resulting from ferroresonance

University of Cape Town

3.1.1 Explanation of ferroresonance

Ferroresonance can be explained by simplifying the Thevenin Equivalent circuit of a CCS as follows:

- Making the load purely inductive and,
- lumping both the inductance of the load and the inductance used to compensate for the Thevenin Equivalent capacitance together [18].

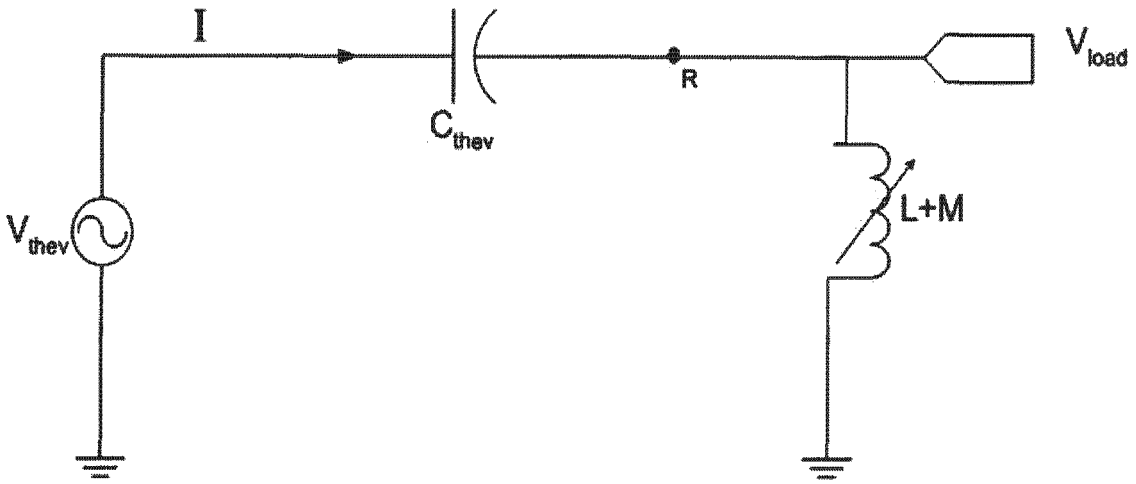

Figure 17: Circuit used to analyse ferroresonance [18]

Note that the mutual inductance (M) of the inductor (of inductance 'L') is also included. This makes the inductor a non-linear device because its inductance changes as the ferromagnetic core saturates.

From Figure 17, it can be seen that V_{load} is:

$$V_{load} = V_{thev} + \frac{I}{\omega C_{thev}} \tag{3.1}$$

and also

$$V_{load} = I\omega(L+M) \tag{3.2}$$

These equations are plotted on the graph of Figure 18. The system operating point, under no-load conditions, can be at one of the three intersections of these curves. Assuming that the load is inductive, then the current will lag the voltage by 90°. The stability of these points can be illustrated by applying a load change, ΔI [18]. The reduced current at operating point '1' will cause the capacitor voltage to reduce, moving the system towards operating point '1a'. The reduced voltage will in turn cause the inductor current to reduce, resulting in the operating point moving to point '1b', and then to point 1c. It can be seen that the system will eventually settle at operating point 2.

University of Cape Town

Similarly, if a load change, ΔI, is applied at point '2' then the operating point will move to point '2a', and then to point '2b'. The nature of the system will result in it settling at point '2'. Therefore operating point '2' is stable.

If, however a load change is applied that pushes the system past the knee point of the inductive curve, then the system will not return to operating point '2', as illustrated by applying a load change to operating point '3'. This moves the operating point towards 3a, then to '3b'. It can be seen that the system voltages and currents quickly become excessive, resulting in ferroresonance.

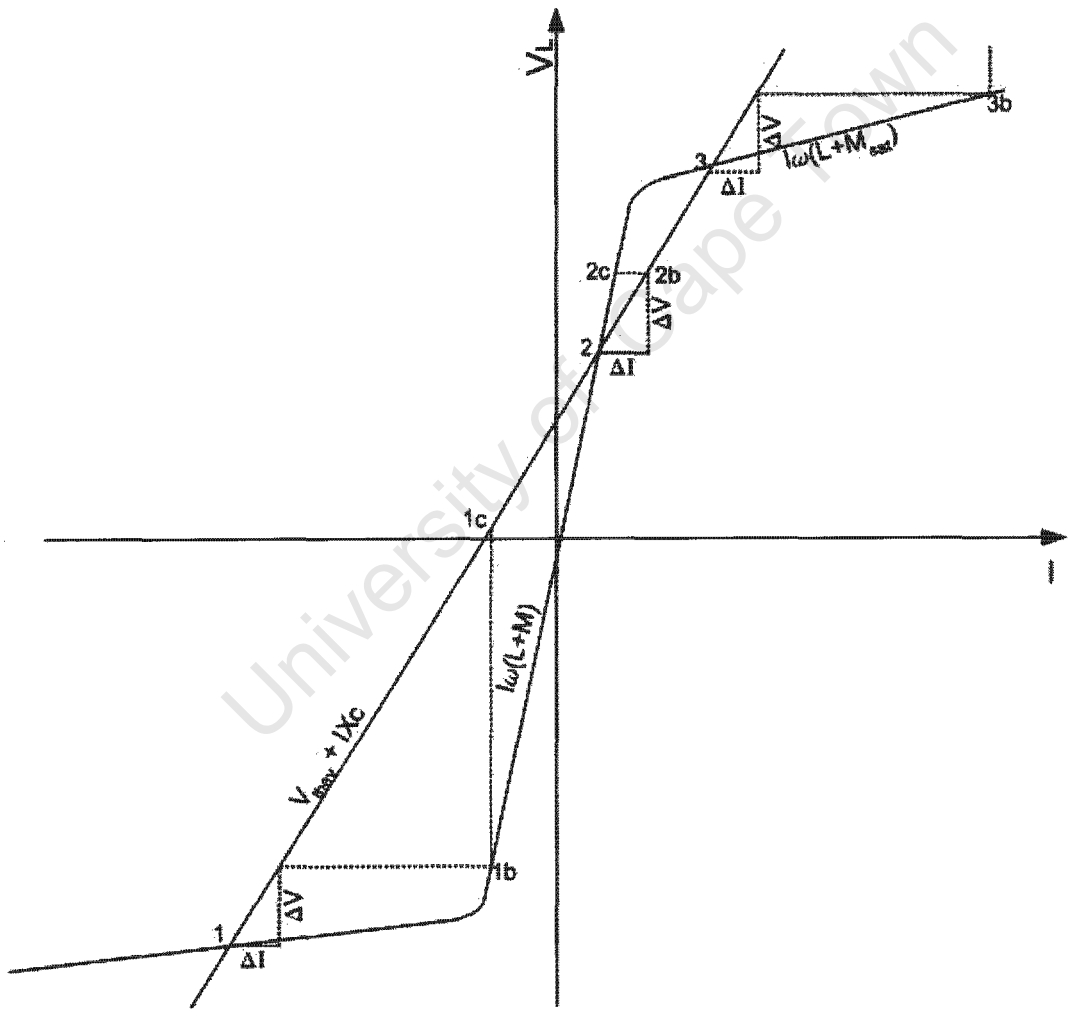

Figure 18: Ferroresonance graphical explanation [18]

University of Cape Town

3.1.2 Prevention of ferroresonance

Methods of preventing ferroresonance consist of modifying either the inductance curve [$I\omega(L+M_{sat})$] or the capacitance curve [$V_{thev} + IXc$] of Figure 18 so that the knee (point at which the magnetising inductance saturates) of the inductance curve is further away from operating point '2'. This enables the system react to a greater load change before becoming unstable, and hence reducing the possibility of ferroresonance. Two methods are illustrated in Figure 19: decreasing Xc and inserting increasing amounts of series resistance R at point 'R' in Figure 17.

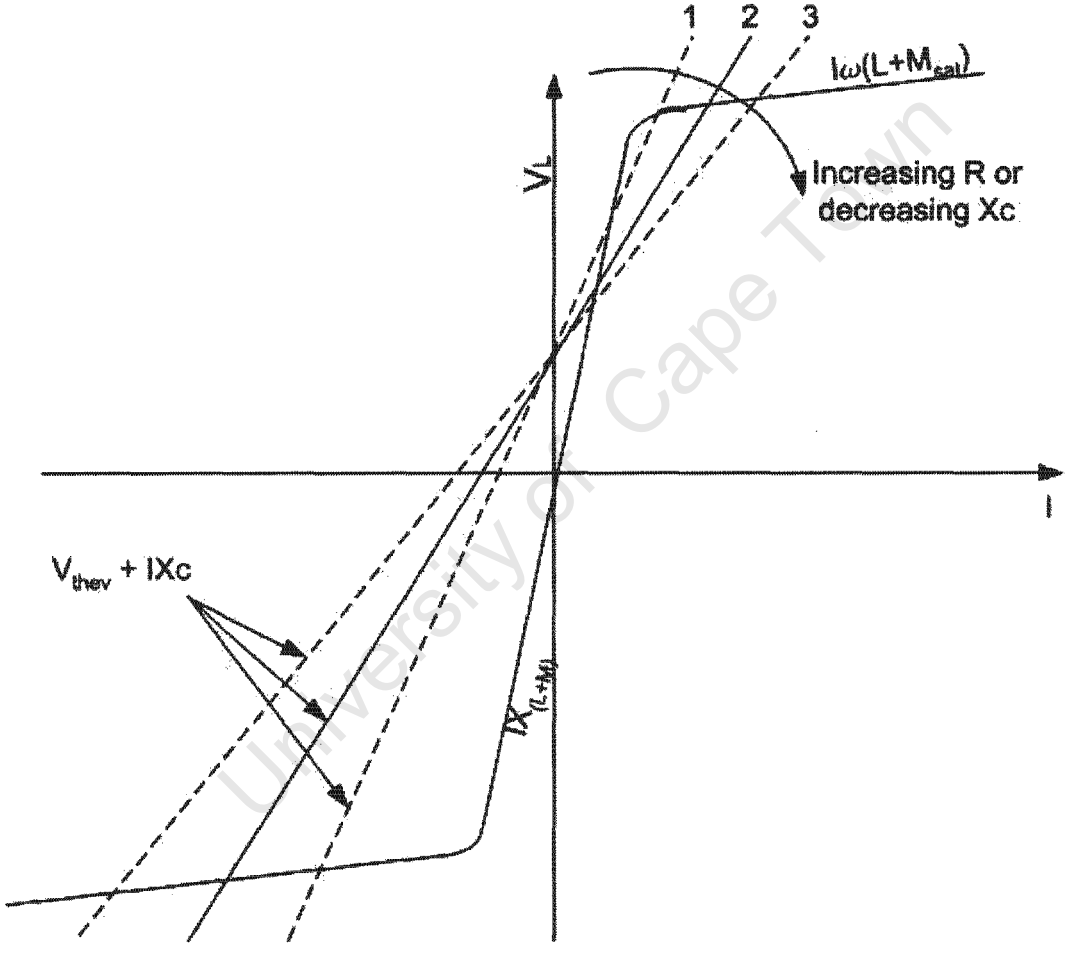

Figure 19: Effect of changing the value of Xc and R [18]

Decreasing X_c, where $X_c=\left(1/\omega C_{thev}\right)$:

One way to reduce the possibility of ferroresonance is by changing the Thevenin Equivalent Capacitance of the CCS (Figure 19). Decreasing X_c moves line 2 to position

3. At position 3 "the normal operating point is moved further away from the knee of the inductance curve and the system is more stable [18]," as illustrated by Figure 19.

Increasing R:

Similarly, if series resistance (R_{series}) is introduced at point 'R' into Figure 17, the inductance curve would be less steep as illustrated by the modified inductance voltage:

$V_{ind} = V_{thev} + \frac{1}{\omega C} - IR_{series}$, where V_{ind} is the voltage across the inductor (V_{load}).

Thus, the normal operating point would once again be moved further away from the knee of the inductance curve, making the system more stable, as illustrated by Figure 19.

Prevention of ferroresonance using a RLC Filter [20]:

The circuit diagram of a RLC filter, also known as a 'tank circuit' or 'passive filter' is shown in Figure 4.

A Bode plot of the impedance of the RLC filter gives insight as to its behaviour. The parameters of the Meru passive filter (see appendix 'A') result in the Bode plot of Figure 20.

It can be seen that this is a band-pass filter. At 50Hz, the filter has high impedance, and therefore 50Hz signals are not attenuated. However, the impedance of the filter rapidly decreases, moving away from 50Hz. Therefore, those signals other than 50Hz will be attenuated. This can be used to suppress ferroresonance as well as harmonic transients [20]. "The use of a surge arrestor in the capacitive substation could further improve the damping of transient over-voltages." [20] Hence, a passive circuit in conjunction with surge arrestors would make an even better ferroresonance damping system than any of the two components would in isolation.

University of Cape Town

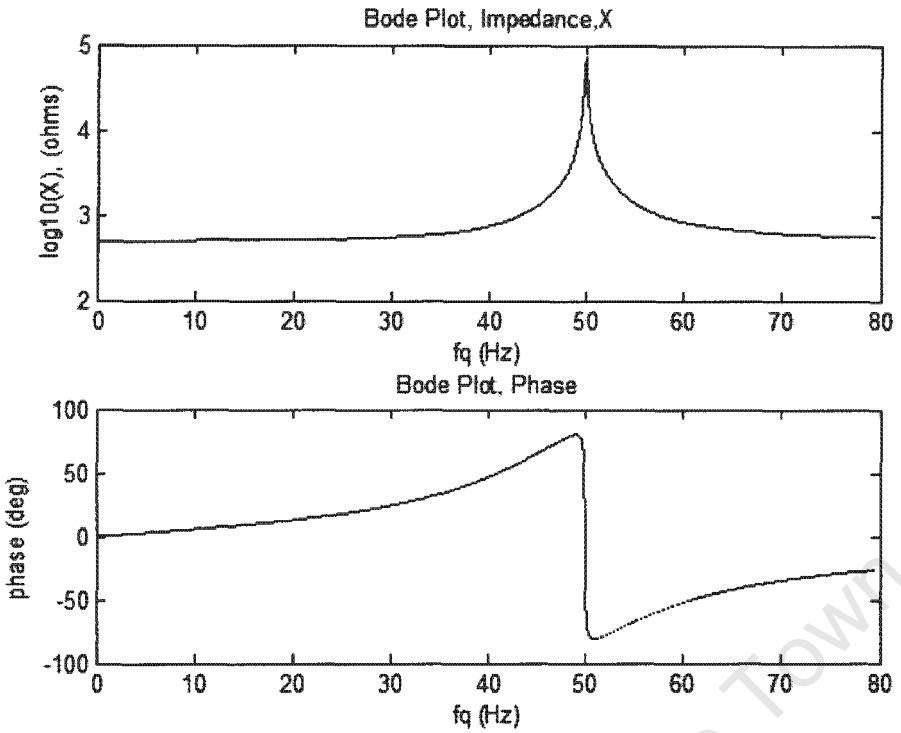

Figure 20: Bode plot of the passive filter at the Meru Sub-station

Prevention of ferroresonance using power electronic devices:

Dangerous current spikes and over-voltages due to ferroresonance can be damped using power electronic devices. "A damping resistor is switched to the secondary side of the system transformer, when necessary [21]."

Summary:

Both passive and active ferroresonance suppression techniques have been discussed here, showing the relative ease with which ferroresonance can be prevented. Ferroresonance is a well-known phenomenon, and was the suspected cause of Meru-Petronet oscillations [18]. However, resonance still occurs at Meru with the ferroresonance filter in place, showing that either the ferroresonance filter did not work, or there was another cause of the SSR. Bolduc et al. [14] showed the success of using such a filter to damp ferroresonance. Tests were done on the actual filter at Meru, confirming that the correct parameter values were installed, and showing that the filter was in good working order [16]. It therefore

University of Cape Town

appears that ferroresonance is not the cause of the SSR under investigation. This fact is confirmed by the absence of current spikes during testing [16]. "The severe distortion commonly associated with ferroresonance is not visible in any of the measured current waveforms (from the Meru sub-station)." [22 pp.33].

3.2 Self-excitation

In 1941, C.F. Wagner [23] showed that under certain 'conditions, an induction machine connected in series with a capacitor experienced sub-synchronous resonance (SSR). He attributed the cause of this SSR to self-excitation, and showed that an induction motor that experiences SSR will not run up to its operating speed. Wagner's work shall be examined in this section.

3.2.1 Analysis of self-excitation based on Wagner's 1941 paper [23]

Currents can flow in a circuit in two ways: because of an external voltage being applied to the circuit, or in accordance with the natural frequency of the circuit. Normally, currents associated with the natural frequency will eventually die down due to resistance of the circuit, but in cases where there is little resistance to damp oscillations, they can become excessive. This may well be the case when an induction motor is connected in series with a capacitor.

When an induction motor is connected in series with a capacitor, a current is set up because of the external voltage applied to the circuit (natural circuit). Another current can exist due to the natural frequency (f) of the circuit (resonant circuit), shown in Figure 21.

Note, the core loss (R_c) has been omitted from this circuit, rather to be included with friction and windage losses [8]. Also, note that where there is a voltage source in the natural circuit, there is simply a line of zero impedance in the resonant circuit, because the source impedance is assumed to be zero. The resonant circuit is operating at its resonant frequency, shown by 'f_{res}' in Figure 21.

University of Cape Town

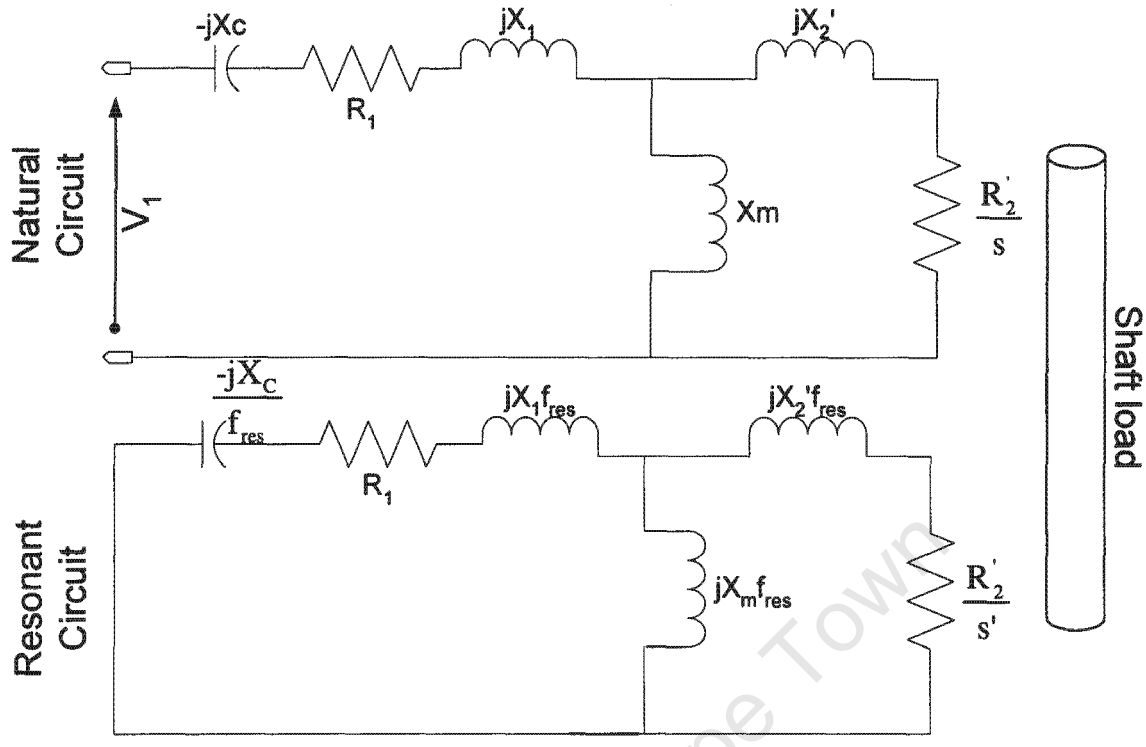

Figure 21: Natural and resonant circuits of an induction motor [23]

University of Cape Town

Because we are concerned with SSR, the resonant frequency, f_{res}, will be less than the operating frequency of the induction machine. Therefore the slip of the resonant circuit (s') must be less than that of the natural circuit. When a voltage is applied to the induction motor, the speed of the rotor will increase until it is equal to the resonant speed, or frequency (speed is related to frequency). Beyond this speed, the resonant circuit will start to act as an induction generator, and the term $\frac{R_2'}{s'}$ will become negative. Therefore, there will be negative resistance in the resonant circuit, which, at a certain frequency (f_{res}) will cancel the effect of the resistance (R_1) in the circuit. At this frequency the resonant current of this circuit will not dissipate as previously suggested, because there will be no resistance to damp it. These conditions cause resonance.

Load Torque

It is important to mention load torque, as its characteristic will affect the way in which the motor behaves. The less torque imposed on the motor at start up, the faster it will reach synchronous speed, therefore reducing the possibility of SSR occurring.

The Petronet Induction Motor is used to drive a pump. Because the motor is being used to drive a pump, the load-torque varies with speed. In fact, the load torque is proportional to the square of the motor speed [24].

Determination of the resonant frequency [23]

Wagner used the fact that for oscillations to continue un-damped, the impedance of the resonant circuit needed to be zero. Therefore, the impedance of the circuit needs to be zero to guarantee oscillation.

The resonant circuit will now be looked at in isolation, and equations will be derived that relate to the frequency at which the resistance of the circuit is zero.

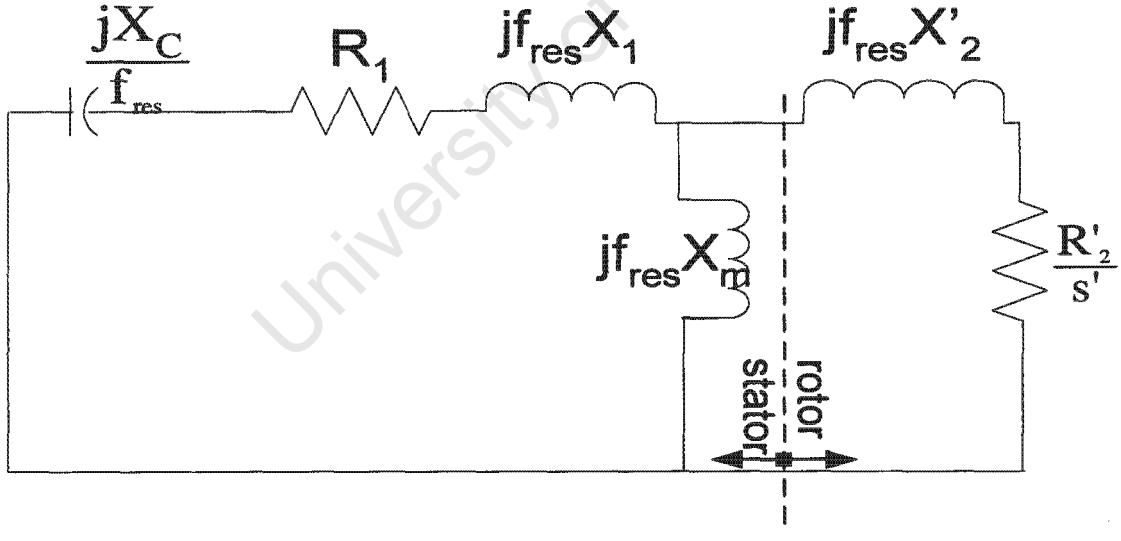

Figure 22: Resonant circuit [23]

University of Cape Town

For the resonant circuit to go into oscillation, it must have zero impedance as viewed from any point in the circuit. Viewing the resonant circuit from the point of view of the rotor, and making 'f_{res}' unity, Wagner derived the following equations:

$$\frac{jX_m(R_1 + j(X_1 - X_C))}{R_1 + j(X_m + X_1 - X_C)} + \frac{R'_2}{s'} + jX_2 = 0 \tag{3.3}$$

Which, once the imaginary part is removed from the denominator is the same as:

$$\frac{jX_m[R_1 + j(X_1 - X_C)][R_1 - j(X_m + X_1 - X_C)]}{R_1^2 + (X_m + X_1 - X_C)^2} + \frac{R'_2}{s'} + jX_2 = 0$$

The resonant circuit will self-excite when it has zero impedance.

Considering imaginary parts:

$$X_m R_1^2 + X_m(X_1 - X_C)(X_m + X_1 - X_C) + X_2 R_1^2 + X_2(X_m + X_1 - X_C)^2 = 0$$

which gives:

$$R_1^2 = -(X_m + X_1 - X_C)\left(X_1 + \frac{X_2 X_m}{X_m + X_2} - X_c\right) \tag{3.4}$$

Real parts:

$$-X_m R_1(X_1 - X_C) + X_m R_1(X_m + X_1 - X_C) + \frac{R_1^2 R'_2}{s'} + \frac{R'_2}{s'}(X_m + X_1 - X_C)^2 = 0$$

which gives:

$$\frac{s'}{R'_2} = -\frac{R_1^2 + (X_m + X_1 - X_C)^2}{X_m^2 R_1} \tag{3.5}$$

Squaring (3.5), and reinserting R_1 from equation (3.4):

$$\left(\frac{s'}{R'_2}\right)^2 = -\frac{X_m + X_1 - X_C}{(X_m + X_2)^2\left(X_1 + \frac{X_2 X_m}{X_m + X_2} - X_c\right)} \tag{3.6}$$

f_{res} can be reinserted into these equations by dividing it into all X_c terms, and multiplying it by all X_m terms.

Thus, equations (3.4) and (3.6) become:

University of Cape Town

$$R_1^2 = -\frac{1}{f_{res}^2}[f_{res}^2(X_m + X_1) - X_C] \times \left[f_{res}^2 \left(X_1 + \frac{X_2 X_m}{X_2 + X_m} \right) - X_C \right] \quad (3.7)$$

and

$$\left(\frac{s'}{R_2'}\right)^2 = -\frac{f_{res}^2(X_m + X_1) - X_C}{f_{res}^2(X_m + X_2)^2 \left[f_{res}^2 \left(X_1 + \frac{X_2 X_m}{X_2 + X_m} \right) - X_C \right]} \quad (3.8)$$

If

$$X_M = X_m + X_1 \quad (3.9)$$

and

$$X_B = X_1 + \frac{X_2 X_m}{X_2 + X_m} \quad (3.10)$$

then equations (3.7) and (3.8) can be simplified to:

$$R_1^2 = -\frac{1}{f_{res}^2}[f_{res}^2 X_M - X_C][f_{res}^2 X_B - X_C] \quad (3.11)$$

$$\left(\frac{s'}{R_2'}\right)^2 = -\frac{f_{res}^2 X_M - X_C}{f_{res}^2(X_m + X_2)^2(f_{res}^2 X_B - X_C)} \quad (3.12)$$

These "two equations represent the conditions which must be satisfied to produce self-excitation." Thus, for a given R_1, the value of f_{res} can be found from equation (3.7) Substituting this value into equation (3.8), the corresponding slip, and hence speed can be found.

From equation (3.7), the natural frequencies of the resonant circuit can be found. Using the same parameters that Wagner used (see appendix 'A'), the natural frequencies of the resonant circuit were plotted against R_1 in Figure 23. (Parameters used by Wagner, shown in appendix 'A'.)

University of Cape Town

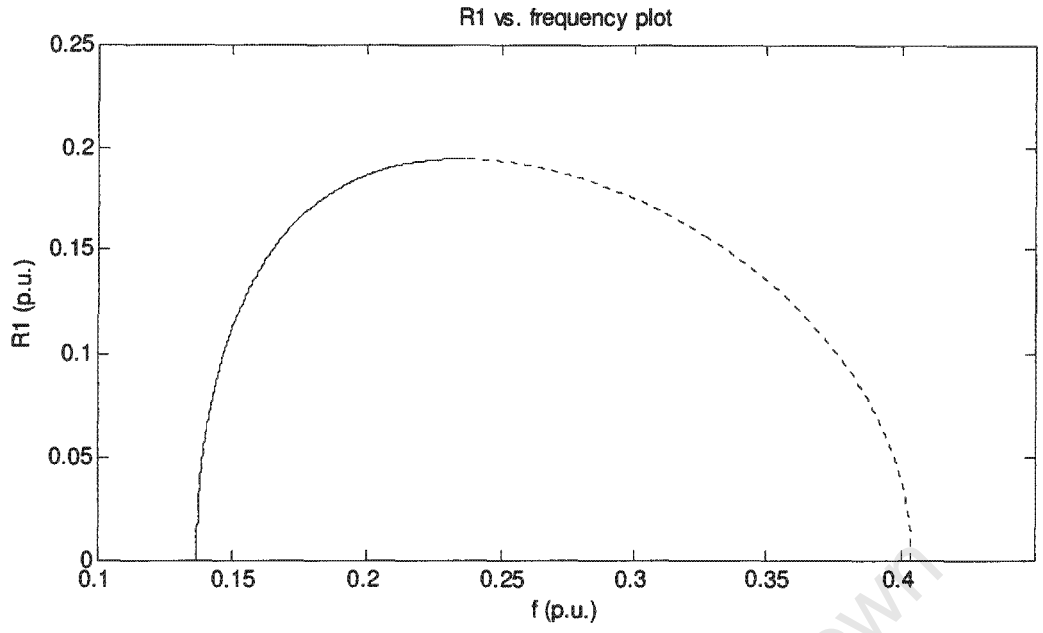

Figure 23: Natural frequency plotted against R_1 for the resonant circuit, using the same parameter values as Wagner [23]

It can be seen that for each value of R1, there are two values of f_{res}. The two values are differentiated in the graph as shown by the dotted and solid line.

The resonating region, as discussed by Wagner [23], is the region in-between the two resonant speeds of the CCS-IM circuit. The lower resonant frequency value can be inserted into equation (3.8) to find the corresponding slip, and therefore speed at which the motor will resonate. The speed that the motor reaches is directly related to the sub-synchronous-frequency of the system. If sub-synchronous oscillations are excessive, the speed the rotor reaches (in rpm) will be close to the speed as determined by $speed_{rotor} = \frac{120 f_{res}}{p}$, where f_{res} is in Hz. The less severe the oscillations, the closer the rotor's speed will be to synchronous speed.

The loss through the $\frac{1-s}{s} R_2^{'}$ resistor in the equivalent circuit of an induction machine (see eqn. (2.11)) represents the power transmitted to the shaft by the induction machine. The resonant circuit obtains its power from the natural circuit through the shaft, which is

University of Cape Town

the only connection between the two circuits. As the total resistance of the resonant circuit tends towards zero, the power it draws from the natural circuit will increase. This means there will be less power and therefore torque available for the appliance that is connected to the shaft. [eqn.(2.15)]

Once the resonant speed has been determined, it is then possible to work out whether the motor will resonate from a torque point of view. At that resonant speed, some torque is required by the load and the remainder is normally used to accelerate the rotor. However,

> "if the inertia of the rotor is quite high or the power available for acceleration is low, so that the current (in the resonant circuit) has sufficient time to build up"[23]

then the torque normally available for accelerating the rotor can be used to supply the resonant circuit. When all the power/torque available to accelerate the rotor is used by the resonant circuit, then the rotor will not reach its synchronous speed. This is illustrated graphically, in Figure 24:

University of Cape Town

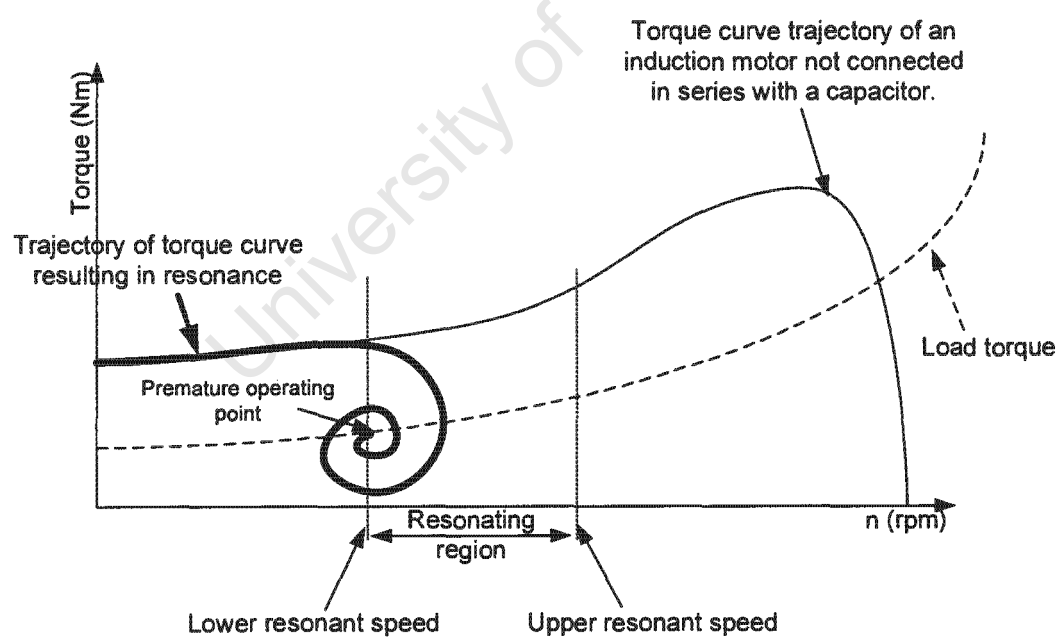

Figure 24: Graph used to explain how resonance occurs, from a torque point of view

In a scenario where SSR is just avoided, the region between the upper and lower resonant frequencies would resemble the machine torque curve of Figure 25.

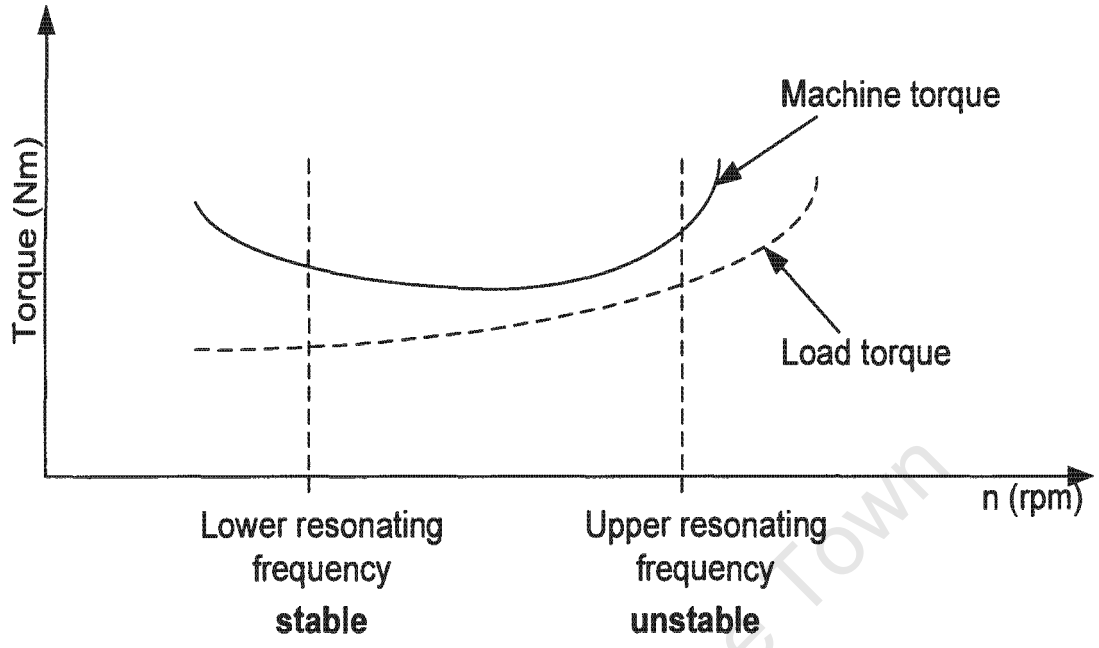

Figure 25: Zoomed-in region of the torque-speed plot of an IM

Wagner [23] showed that only the smaller resonant frequency results in sustained oscillations. This can be explained intuitively:

The equivalent positions of the resonant frequencies are shown on the speed axis of Figure 25. At a speed corresponding to the lower resonant frequency (n_{lower}), the IM torque curve has a negative slope. Therefore, if the rotor speed increases past n_{lower} there will be less torque to accelerate it, and hence the rotor will slow down. If the rotor speed drops below n_{lower}, then the opposite is true, and hence the rotor speeds up. It can be seen that the nature of the IM at this speed is the reason that the lower resonating frequency can lead to sustained oscillations.

The IM curve has a positive slope at a speed corresponding to the upper resonant frequency (n_{upper}), resulting in the opposite of what happens at n_{lower}. If the rotor speed were to increase past n_{upper} then there would be more torque available to accelerate the

University of Cape Town

rotor, and hence the rotor's speed would move further away from n_{upper}, which is the reason that the upper resonating frequency does not lead to sustained oscillation.

3.2.2 Prevention of self-excitation using a back-to-back converter

Here, the basic idea is to separate the CCS from the induction machine by means of a back-to-back converter [18].

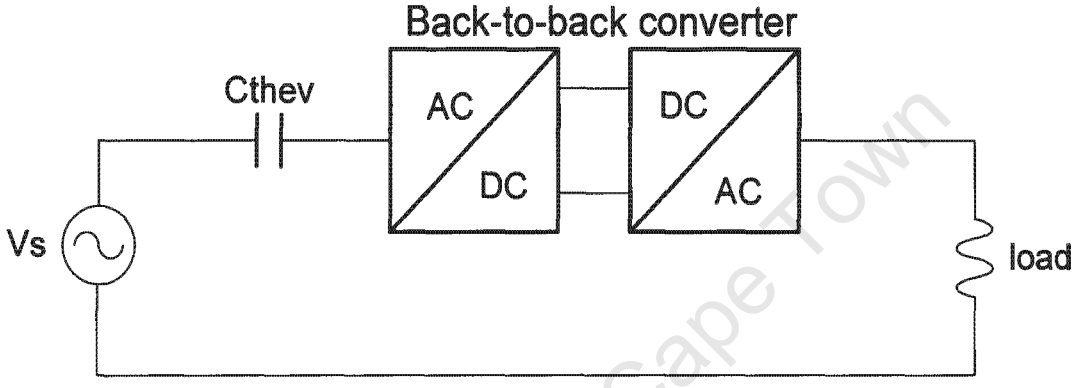

Figure 26: Back-to-back converter solution to CCS-IM SSR [18]

The first rectifier converts the AC to a DC-bus, where it is filtered by a smoothing capacitor. The second converter then recreates an undistorted ac waveform. "The rectifier is an active rectifier, which means that a sinusoidal current is always drawn from the supply establishing a linear current-voltage relationship. Any sub-cycle fluctuations in the current on the load will not influence the current waveform on the supply side." [18]

University of Cape Town

3.2.3 Prevention of self-excitation by changing CCS-IM parameters

A similar method was discussed by [18] and [21]. The basic concept is to change the lower resonant frequency as the speed of the motor increases. This is done by momentarily changing CCS-IM parameters.

If, for example, the motor was started with a lower resonant frequency of 35Hz, the motor will attain approximately 70% of its synchronous speed, without experiencing SSR. As the system begins to oscillate and parameters are modified to place the lower resonant frequency at 25Hz, for example, this would result in a corresponding resonant speed of 50% of synchronous speed (n_s). Because the motor is already at a speed faster that $0.5 \times n_s$ it is likely to continue to speed up to its synchronous speed.

Difficulties arise when changing the resonant frequency, as CCS-IM parameters cannot easily be changed without affecting other system characteristics. One such way to change the resonant frequency is to insert a resistor in series with the CCS capacitance, as described in section 3.2.4.

3.2.4 Prevention of self-excitation by introducing resistance

Passive compensation:

"Wagner [23] developed the theory of passive compensation for systems suffering from self-excitation of induction machines. [18]" He showed that, by modifying equation (3.11) slightly, it could be written as:

$$\frac{R_1}{X_c} = -\frac{1}{f}\sqrt{\left[f^2\frac{X_M}{X_C}-1\right]\left[f^2\frac{X_B}{X_C}-1\right]} \qquad (3.13)$$

Curves of r_s/X_B (see equations (3.9) and (3.10) for the definition of X_M and X_B) against Xc/X_B can be plotted for different values of X_M/X_B. The curves show the maximum series resistance (r_s - connected to the stator) above which the circuit will not resonate. The problem with this method is the steady state voltage drop caused by the series resistor [18].

Similar curves can be plotted for a resistance connected in parallel across the series capacitance, below which the circuit will not resonate. These curves show that for $Xc/X_B = 1$, a resistance equal to Xc is required to prevent resonance. In the case of a CCS, a series inductance (X_L) is added to compensate for the capacitance of the line. Therefore, X_B will be equal to $X_1+X_m+X_L$, and because the capacitance is 100%

University of Cape Town

compensated, the ratio Xc/X_B will be close to unity. If the shunt resistance is equal to Xc then half the power supplied by the CCS will be consumed by the shunt resistor.

If the CCS is not compensated by an inductor, then X_B will be much less. Typically X_L is 10 times as large as (X_l+X_m) so the ratio Xc/X_B will be less than 0.1. Therefore the shunt resistance needed will be ~5 times Xc. This means that at most, one sixth of the power supplied by the CCS will be used by the shunt resistor.

"These are the reasons why passive compensation is not an option for highly compensated lines," [18] as is the case with the Meru CCS.

Active compensation:
Switching the shunt resistor in and out of the circuit can solve the power loss problem. Thyristor-based systems are most appropriate for actively damping self-excitation at high power levels [18]. This system is similar to the ferroresonance damping method discussed by Sanaye-Pasand and Aghazadeh [21].

3.2.5 Prevention of self-excitation using current injection (FACTS)

Current injection is the compensation technique that was tested at Stellenbosch to prevent self-excitation of their CCS-IM model. The basic function of current injection is to supply the harmonic currents and reactive power demanded by the CCS-IM setup. Because the CCS will not be supplying harmonic currents, it will view whatever load is applied to it as purely resistive. The way in which a current injector works is explained using Figure 27.

University of Cape Town

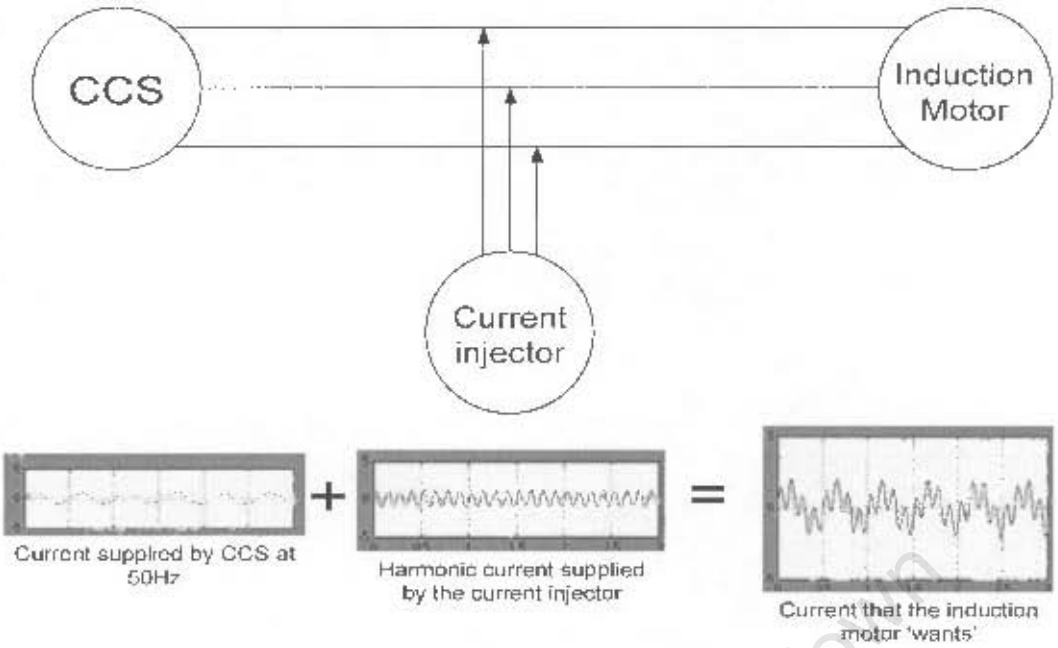

Figure 27: Diagram showing how the current injector works

University of Cape Town

Stellenbosch Current Injector (Active filter)

Current was injected between the CCS and the induction motor as shown in Figure 27. The current was injected using an active filter developed by Stellenbosch University in conjunction with Eskom Enterprises. The operation of this filter was based on the rotating reference plane.

The active filter uses the following z-plane, or digital filter:

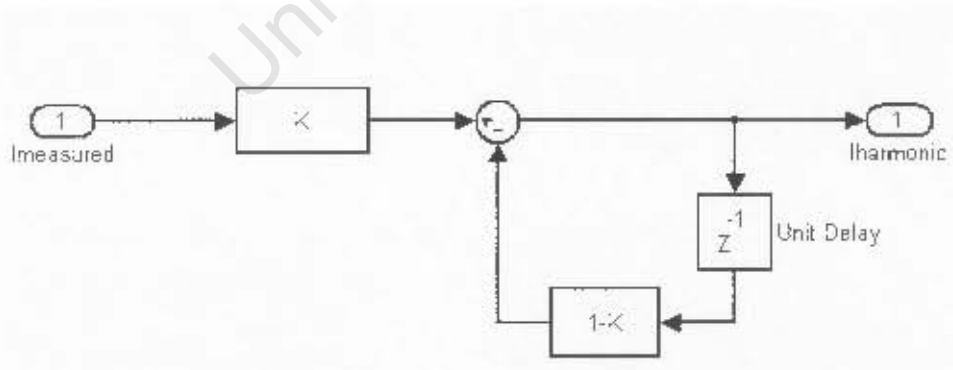

Figure 28: Discrete filter used to determine current to be injected

As the filter constant, K, is varied, the cut-off frequency of the filter changes. The filter used is a low pass filter, which may seem counter-intuitive as SSR occurs at sub-synchronous frequencies. However, the active filter is based on a rotating reference frame, and aligned so that 50Hz signals appear DC in this reference frame. Therefore, a band-pass filter will not attenuate the 50Hz signal, as it is 'seen' as DC. Frequencies other than 50Hz will be cut off by the filter, depending on the filter constant used.

The difference between the filtered current and the current demanded by the IM is then injected by the current injector.

Current source active filter:

A similar FACTS system is presented in [25]. A series active-power-filter works as a sinusoidal current source, in phase with the mains voltage. Because the current produced is in phase with the supply voltage, the supply will 'see' whatever load it provides as resistive. The control corrects power factor, harmonic distortion and allows for load voltage regulation.

There are many other FACTS solutions available but most operate according to the same principles that have been described in this sub-chapter.

Current injection from a torque point of view

From a torque point of view, a current injector would provide the necessary current, and therefore torque to the resonant circuit of the CCS-IM at its resonant speed. The injector supplies the torque necessary to prevent the induction machine from reaching a premature operating point.

University of Cape Town

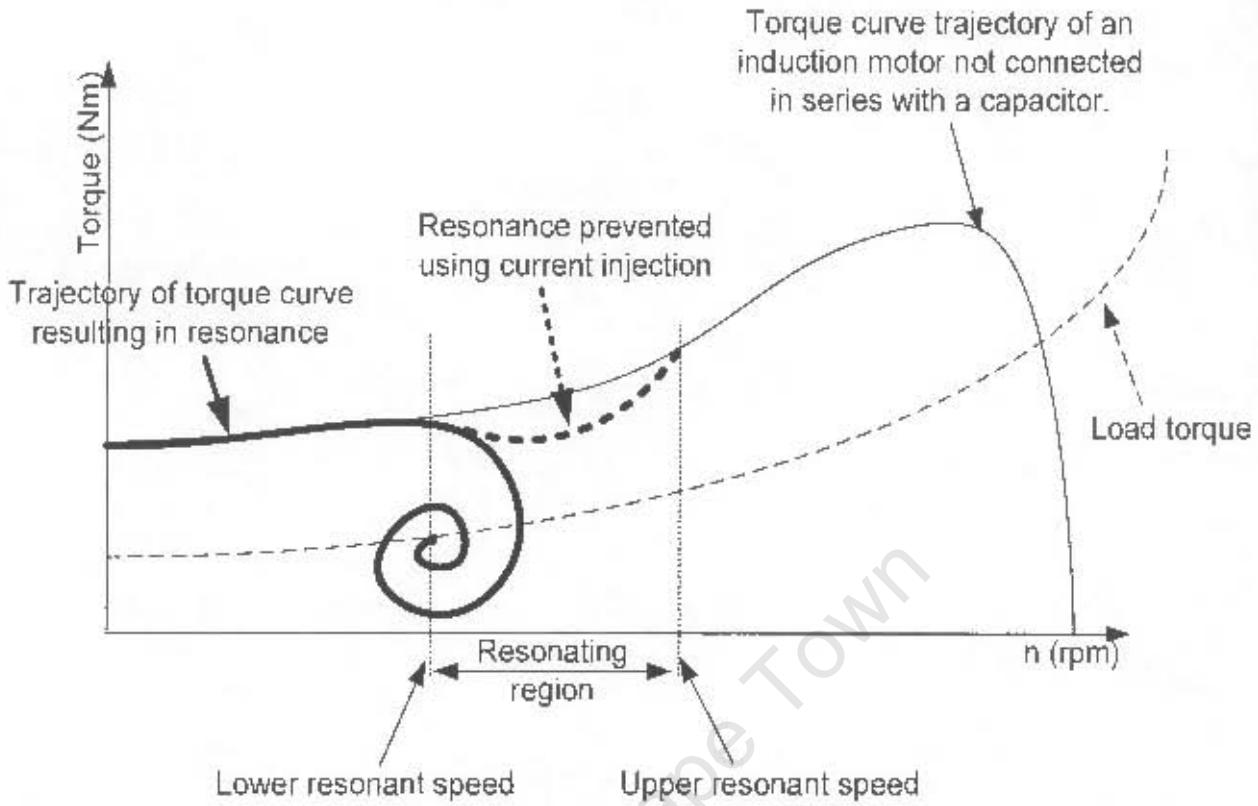

Figure 29: Graph used to explain how self-excitation can be prevented using current injection

If the resonating circuit absorbs power (and therefore) torque faster than the current injector can supply it, so that the induction motor torque curve intersects the load curve, then resonance will occur. The rate at which the resonant circuit absorbs energy is determined using the settling time of the torque transfer function (see sect. 2.2.3):

The settling time of the torque transfer function is $\frac{J}{B}\left(\frac{inertia}{friction\ and\ windage}\right)$. Thus, the larger the inertia, the longer the induction machine 'lingers' at a particular speed and the more energy the current injector will be required to provide.

In order to avoid resonance, enough energy must be added to the system so that the torque curve of the induction machine does not intersect the load curve at the upper

University of Cape Town

resonant speed (Figure 30).

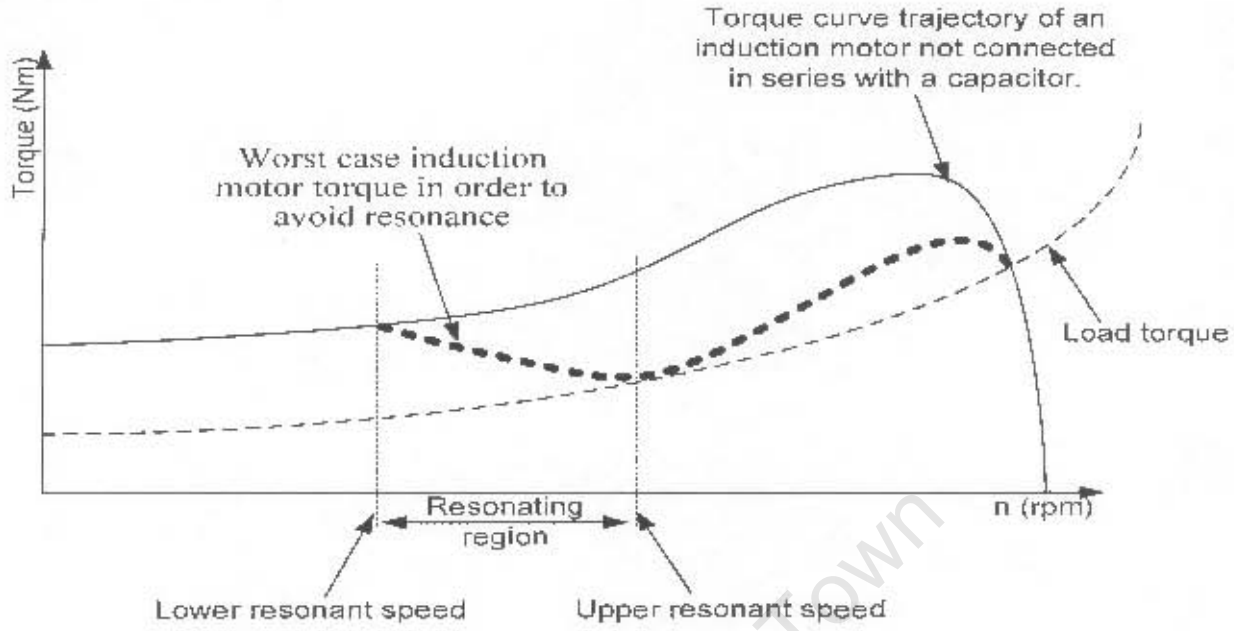

Figure 30: Worst-case induction motor torque in order to avoid resonance

Power required for the prevention of self-excitation:

If the equivalent positions of the resonant frequencies are plotted on the zoomed-in torque-speed plot of Figure 30, Figure 31 is obtained:

University of Cape Town

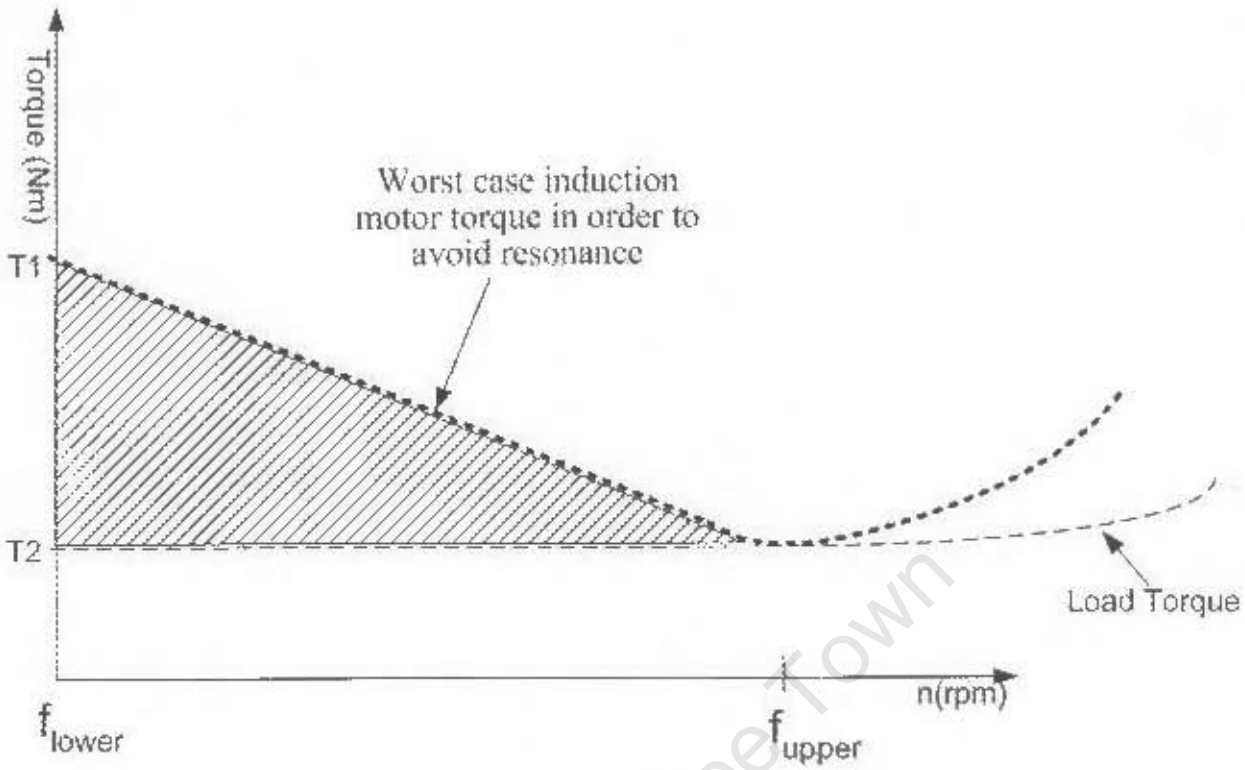

Figure 31: Torque-speed curve of the region between the two resonant frequencies

Then the power required to avoid resonance is the area under the curve between f_{lower} and f_{upper}. Assuming that the curve can be approximated by a parallelogram, as shown in Figure 31, then:

$$P_{compensator} = \frac{(T1-T2)}{2} \times 2\pi(f_{upper} - f_{lower}) \qquad (3.14)$$

T1 and T2 are the respective torques as shown in figure 5.

A rough calculation for a 3kW motor:

Assume T1-T2 = 10Nm and

$f_{upper} - f_{lower} = 20\text{Hz}$

Then the compensator should be about 600W in size.

University of Cape Town

3.3 Control-Systems Methods

In chapter 4, a model of the CCS-IM system is built using control engineering tools. It is therefore necessary to introduce those tools here.

3.3.1 Block Diagram Algebra

Block diagram algebra is a process of manipulating signals and variables algebraically. A system of inter-connected blocks is formed, each representing a relationship between important variables. The primary advantage of block diagrams is that larger systems can be re-arranged to a simpler block diagram [11], which can ultimately be represented as a transfer function, relating an input to its output. This is done by identifying potential feedback loops, and moving branches around to simplify those loops [27].

3.3.2 State-Space

State-space is advantageous because of its ability to handle non-linear time-varying systems, which the other model building techniques mentioned in this document do not deal with properly. State-space techniques are also able to analyse complex systems consisting of multiple inputs and outputs. The matrix format of state-space models makes it ideal for computerization [32]. State-space models are suitable for both discrete-time and continuous-time systems.

State variables are central to describing the dynamic evolution of a system. State variables collectively define the state of a system, by summarising those aspects of the past that are relevant to the future. Thus, they are typically associated with a system's memory mechanisms or energy storage devices. The laws that govern the evolution of state-space variables are embodied in the state-space model. [26]

3.3.3 Root-Locus

The root-locus method of analysing control-models and developing controllers for these models will now be discussed.

University of Cape Town

The following material is based on data collected from lecture notes of Braae, University of Cape Town (UCT) [11], lecture notes from the University of Calgary [27] and tutorials from the University of Michigan [28].

Consider the following system [27]:

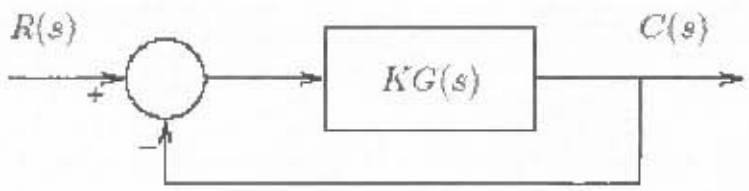

Figure 32: Root-Locus Example [27]

A Root-Locus Plot shows how the closed-loop pole positions change as the Root-Locus-gain, K, increases from zero to infinity.

The closed-loop transfer function is:

$$\frac{C(s)}{R(s)} = \frac{KG(s)}{1+KG(s)} = \frac{KN(s)}{KN(s)+D(s)} \tag{3.15}$$

The closed-loop pole positions are given by:

$$\begin{aligned} 1+KG(s) &= 0 \\ \text{Hence } KG(s) &= -1 \end{aligned} \tag{3.16}$$

Since K is a real positive number, and G is complex, the magnitude and angle of equation (3.16) can be determined:

$$\begin{aligned} |KG(s)| &= 1 \\ \arg(KG(s)) &= 180 + 360k \quad (k \in \mathbb{Z}) \end{aligned} \tag{3.17}$$

The magnitude condition implies that if s_0 is a closed-loop pole then:

$$K = \frac{1}{|G(s_0)|} \tag{3.18}$$

and the angle condition, since K is real and positive, arg(K) = 0, so

$$\arg(G(s_0)) = 180 + 360k \quad (k \in \mathbb{Z}) \tag{3.19}$$

Therefore, if s_0 is a closed-loop pole then the vector drawn from the open-loop pole to s_0 will satisfy equation (3.19) and have a gain by equation (3.18).

University of Cape Town

These two rules are the foundation of Root-Locus. From these rules, other rules are developed to assist in the drawing of Root-Locus Plots. Depending on where closed-loop poles lie on a Root-Locus indicates the stability of the system for that gain. Firstly, a Root-Locus will always be symmetrical about the real axis. This is because poles with imaginary components occur in complex conjugates. As shown in Figure 33, if the closed-loop poles are on the right half of the real axis then the system will be unstable. However if they fall on the left half, then the system is stable. The further the closed-loop poles are from the y-axis, the faster the dynamics of the system will be, in terms of settling time. Although a system may be stable, it could still be unsatisfactorily oscillatory. The imaginary axis is indicates the frequency of oscillation of a system. The greater the imaginary value of a closed-loop pole, the more oscillatory is will be. The shaded region labelled 'damped region' indicates a region where the damping factor of more that 0.707 i.e. $\cos(45^{\circ})$.

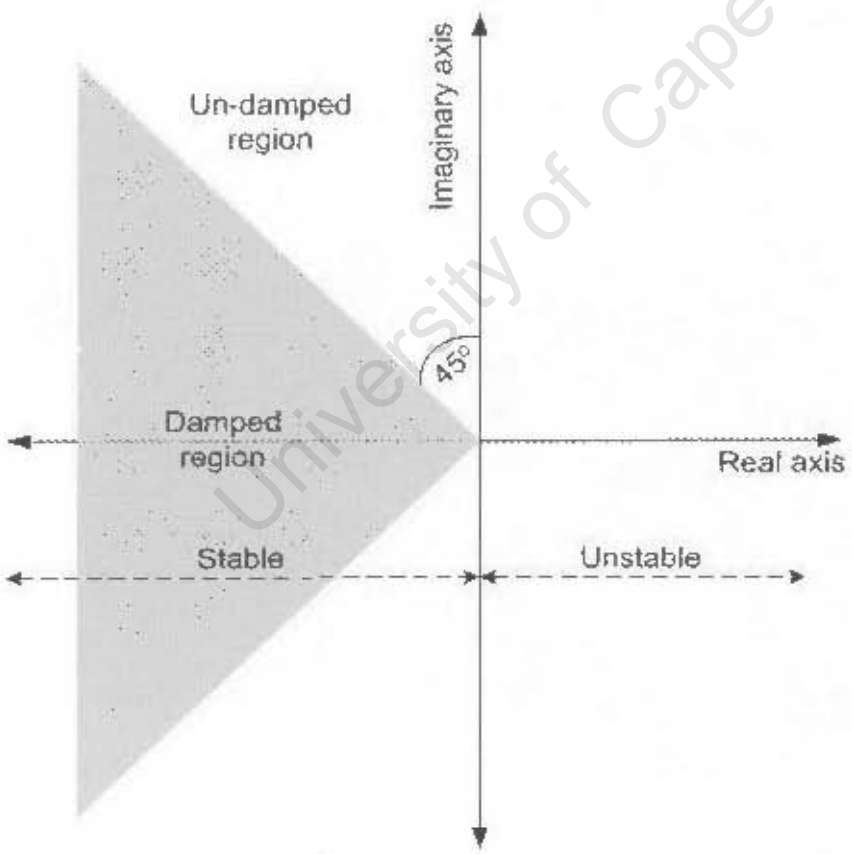

Figure 33: Stability regions of a Root-Locus plot

University of Cape Town

3.4 Summary

Ferroresonance arises as a result of inductor saturation. There are numerous ways of preventing ferroresonance. At the Meru CCS, series air-core compensating-inductors were used to eliminate the possibility of ferroresonance, following the approach of Bolduc et al. [14] . A filter-bank was also used to eliminate the possibility of ferroresonance from other inductors connected to the Meru bus. Ferroresonance causes dangerous over-voltages, and leads to SSR. SSR was experienced, but over-voltages were not characteristic with the problem. This makes it less likely that ferroresonance is the cause of the SSR experienced.

Beukes et al. [18] concur that ferroresonance is not the cause of SSR associated with the Meru-Petronet system. Furthermore, Bouldac et al. [14] showed that ferroresonance is successfully prevented using the filter-bank developed by Hydro-Quebéc.

Self-excitation results from the un-damped propagation of natural currents within a circuit. Wagner [23] showed that it is the result of a capacitor connected in series with an induction machine. Self-excitation results in SSR, at frequencies typical to those experienced in the Meru-Petronet system. The speed that a rotor reaches is directly related to the sub-synchronous-frequency of a system. Beukes et al. [18] attributed the cause of SSR experienced to self-excitation.

Based on data collected in this chapter, the hypothesis of chapter 2 is refined:

> *SSR associated with a CCS-IM setup arises because of an interaction between the CCS and IM. The most significant cause of such SSR is self-excitation.*

Some control-systems methods were discussed at the end of this chapter. These tools shall be used in the next chapter.

University of Cape Town

4 BUILDING OF A CCS-IM TRANSFER FUNCTION MODEL

Based on the hypothesis made at the end of the last chapter, self-excitation will now be studied in more detail.

In 1941, C. Wagner [23] showed that an induction motor, connected in series with a capacitor, would be unstable under certain conditions. However, he did not have the luxury of Root-Locus as it was yet to be invented. Authors such as Limebeer et al. [35] and Ojo [29] also attributed such SSR to self-excitation. Ojo essentially expanded on work done by Wagner, whereas Limebeer et al. touched briefly on the use of Root-Locus to analyse a series capacitor - IM system. A more thorough analysis shall be undertaken in this section.

Various dynamic models are constructed using the different control tools available. These will be used to predict the resonant frequencies of the CCS-IM system.

It will be important that

1. the control systems model be able to logically show how self-excitation leads to SSR,
2. the mathematical model behaves in a similar way to the model that was developed by Wagner,
3. that the results of the model concur with laboratory results and simulations,
4. that research, model results and physical results support the hypothesis that self-excitation is the cause of SSR,
5. that the model is capable of predicting instabilities in systems, such as the Meru-Petronet system,
6. possible solutions to the SSR problem be developed and analysed using the model.

University of Cape Town

Because of the valuable insight provided by the control-model, a possible solution to SSR is proposed at the end of this chapter.

The s-plane referred to here is the Laplace Domain, where 's' is shorthand for the derivative, $\frac{\partial}{\partial t}$. Note that when referring to the slip associated with an induction motor in this section, 'q' will be used, so as not to confuse this with the 's' of the s-plane.

Note that in each Root-Locus plot, the Root-Locus gain is the inverse of slip, 1/q. Thus, the Root-Locus gain increases with a decrease in slip, q. In other words, the Root-Locus gain increases with increasing speed.

4.1 Block Diagram Analysis of Wagner's resonant circuit

Wagner showed that the following circuit can lead to SSR [23]:

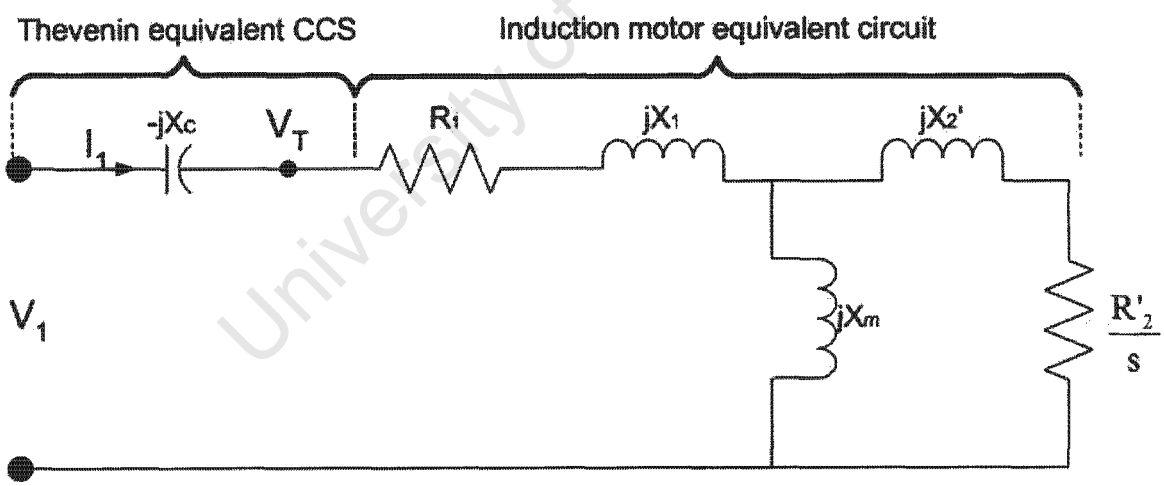

Figure 34: Circuit used by Wagner to show SSR [23]

Parameters that Wagner used are shown in appendix 'A'.

Using the method outlined by Braae et al. [30] to form a transfer function of the CCS-IM system and with the aid of Root-Locus, the stability of the circuit can be determined.

University of Cape Town

The transfer function relating the output, V_T, to the input, V_S, is as follows:

Figure 35: Block diagram showing how V_T relates to V_S

$G_1(s)$ can be calculated by simplifying the circuit shown in Figure 34.

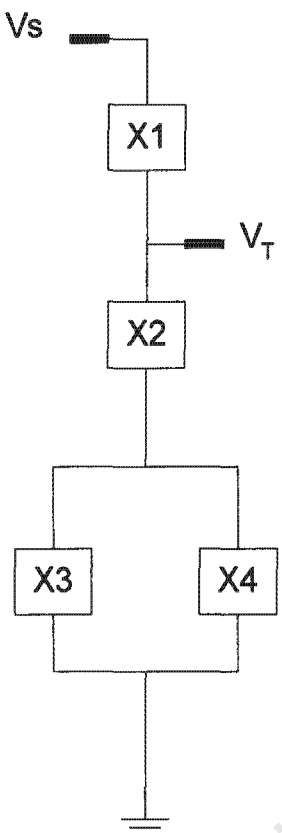

University of Cape Town

Figure 36: Simplified circuit diagram of Figure 34

Where:

$$X_1 = \frac{1}{sC}$$

$$X_2 = R_1 + sL_1$$

$$X_3 = sL_m$$

$$X_4 = sL_2 + \frac{R_2}{q}$$

Then: $V_T = V_S\left(\dfrac{X_2 + \dfrac{X_4X_3}{X_3+X_4}}{X_2 + X_1 + \dfrac{X_4X_3}{X_3+X_4}}\right)$

$= V_s\left(\dfrac{X_2X_3 + X_2X_4 + X_4X_3}{X_4X_3 + X_1X_4 + X_1X_3 + X_2X_4 + X_2X_3}\right)$

which becomes:

$$= V_s\left(\frac{[C(L_1L_m + L_1L_2 + L_mL_2)]s^3 + [C(R_1(L_m + L_2) + \frac{R_2}{q}(L_1 + L_m))]s^2 + [\frac{CR_1R_2}{q}]s}{[C(L_1L_m + L_1L_2 + L_mL_2)]s^3 + [\frac{CR_2}{q}(L_1 + L_m) + CR_1(L_m + L_2)]s^2 + [L_2 + L_m + \frac{CR_1R_2}{q}]s + \frac{R_2}{q}}\right) \tag{4.1}$$

We can now separate all terms containing 1/q from the characteristic equation, in order to plot an extended Root-Locus:

$$\frac{V_T(s)}{V_S(s)} = \frac{1}{q}\left[\frac{CR_2(L_m + L_1)s^2 + CR_1R_2s + R_2}{C(L_mL_2 + L_mL_1 + L_1L_2)s^3 + CR_1(L_m + L_2)s^2 + (L_m + L_2)s}\right] \tag{4.2}$$

Making equation 4.2 monic so that the Extended Root Locus gain is proportional to 1/q gives equation 4.3:

$$\frac{V_T(s)}{V_S(s)} = \frac{CR_2(L_m + L_1)}{C(L_mL_2 + L_mL_1 + L_1L_2)q}\left[\frac{s^2 + \frac{R_1}{(L_m + L_1)}s + \frac{1}{C(L_m + L_1)}}{s^3 + \frac{R_1(L_m + L_2)}{L_mL_2 + L_mL_1 + L_1L_2}s^2 + \frac{(L_m + L_2)}{C(L_mL_2 + L_mL_1 + L_1L_2)}s}\right] \tag{4.3}$$

The extended Root-Locus was plotted using the same values that Wagner [23] used (see appendix 'A'). From equation 4.3, the Root-Locus gain is 1/q. Note that the slip (q) here is the slip of the resonant circuit, which ranges from unity, when the rotor is stationary; to zero when the rotor speed corresponds to the resonant speed of the resonant circuit ($120f_{res}/p$); to about -1, when the rotor is running at the rated speed of the motor. If the resonant frequency corresponds to a rotor speed such that

$$\frac{120f_{res}}{p} = \frac{1}{2} \times \frac{120f}{p} \quad \text{where:} \quad \begin{matrix} f_{res} = \text{resonant frequency} \\ f = \text{supply frequency} \end{matrix}$$

then the Root-Locus gain will vary as shown in Table 1.

University of Cape Town

0^- is used to represent a negative number very close to 0, and 0^+ a positive number very close to 0.

Table 1: Variation of Root-Locus gain with the slip of the resonant circuit		
Typical slip of the resonant circuit	Corresponding rotor speed (rpm)	Root-Locus gain (1/q)
1	0% of $120 \times f_{res} / p$	1
0.5	25% of $120 \times f_{res} / p$	2
0	100% of $120 \times f_{res} / p$	+infinity when slip is positive -infinity when slip is negative
-0.5	125% of $120 \times f_{res} / p$	-2
-1	200% of $120 \times f_{res} / p$	-1

Figure 37 shows part of a Root-Locus plot for which the slip is negative. When the slip is 0^-, the Root-Locus gain is negative infinity and the corresponding position on the Root-Locus plot is close to the system-zeros (indicated by small circles). If the rotor speed were to increase past $120f_{res}/p$ the corresponding resonant slip would become more negative, as illustrated in Table 1 and the Root-Locus plot would follow the trajectory of Figure 37 in a direction indicated by the arrows; tending towards the system-poles, which are indicated by a small crosses.

The real-axis trajectory of the Root-Locus plot of Figure 37 is assumed stable for all values of Root-Locus gain. It starts at the origin, and moves to negative infinity (stable) as the resonant slip changes from 1 to 0^+. When the resonant slip becomes 0^-, the position of the real-axis closed-loop pole moves to positive infinity (unstable). It is not mathematically plausible that a system be infinitely stable in one instant, and infinitely unstable at the next. This peculiarity can be attributed to a set of mathematical circumstances for which the Root-Locus rules do not hold. It is for this reason that the

University of Cape Town

real-axis trajectory of the Root-Locus is assumed stable for all Root-Locus gains, and therefore ignored in Figure 37, and in all similar Root-Locus plots.

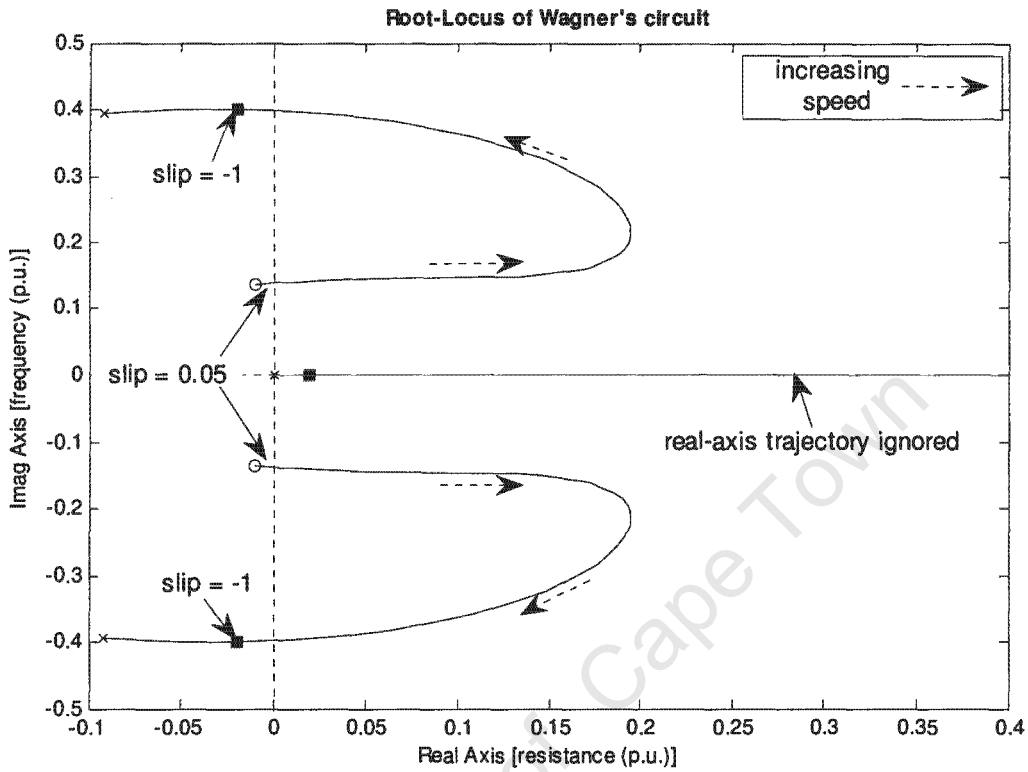

Figure 37: Extended Root-Locus for $V_T(s)$, where root-locus gain = 1/q

Inclusion of Torque in the Block Diagram Analysis:

The CCS can also be analysed with respect to its torque, and therefore rotational speed. This analysis is more complete, because it includes the inertia of the machine. The transfer function with respect to the rotational speed of the machine can be obtained as follows in Figure 38.

From Figure 38, it can be seen that the mechanical power delivered by the induction machine is:

University of Cape Town

$$P_m = R_2\left(\frac{1-q}{q}\right)I_2^2 \tag{4.4}$$

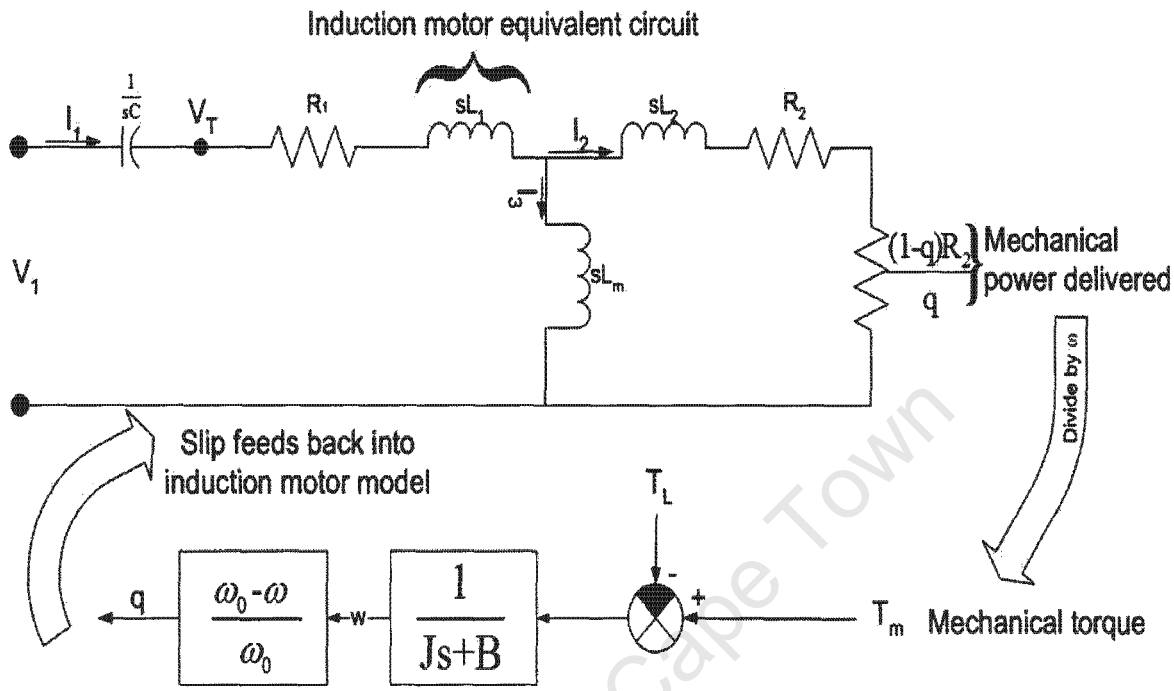

Figure 38: CCS model that includes mechanical torque, and rotor speed

Since P = Tω, the mechanical torque can be found. This is fed into the torque transfer function and the resulting speed and therefore slip is obtained. The slip determines the amount of mechanical power available, and is therefore fed back into the induction motor model.

The transfer function that relates the input voltage to I_2, the rotor current, can be found, beginning with Figure 39:

University of Cape Town

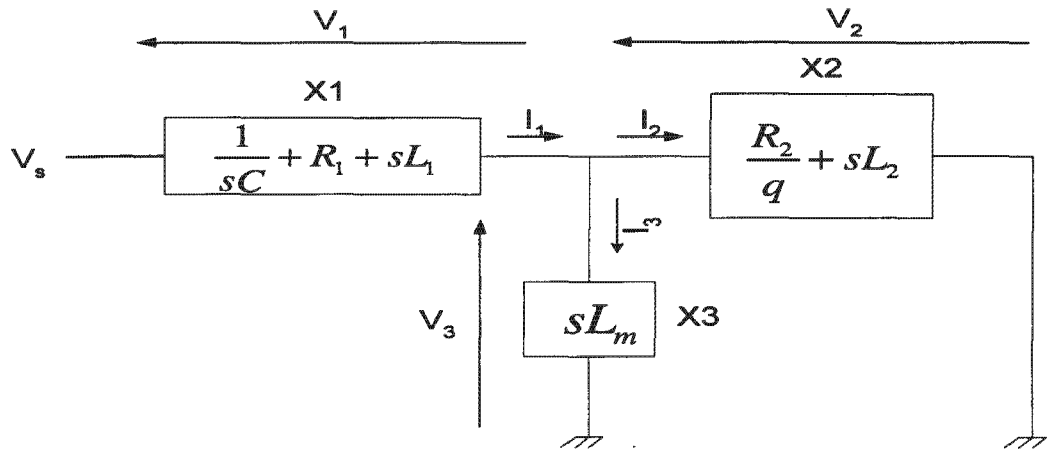

Figure 39: Foundation for the block diagram that relates Vs to I_2

The electrical circuit can then be converted into block diagrams as follows:

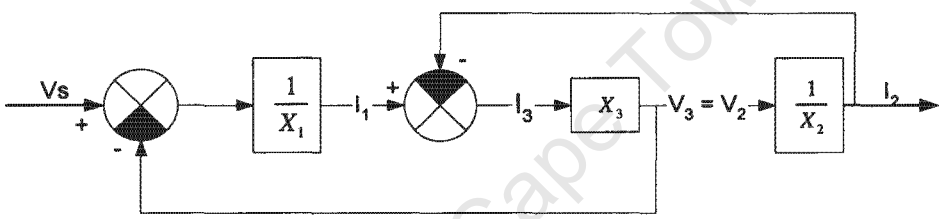

This can be simplified:

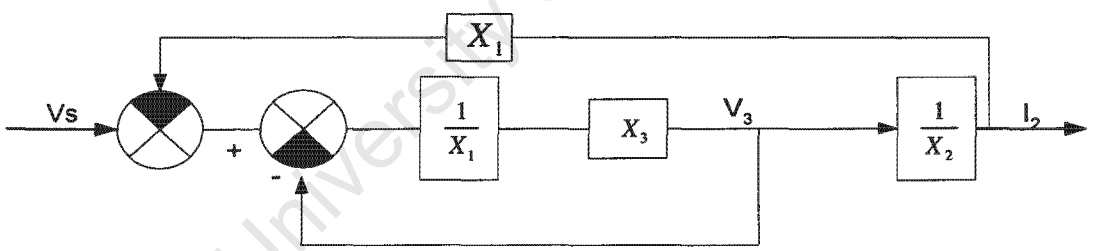

Further simplified:

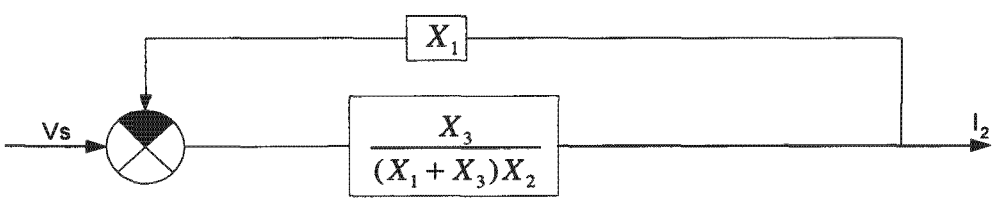

The final transfer function is:

University of Cape Town

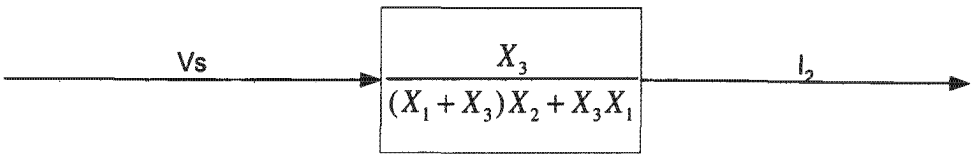

Figure 40: Block diagram reduction to find the transfer function relating Vs to I_2

The transfer function of $\frac{V_S}{I_2}$ can be expanded to give:

$$\frac{V_S}{I_2} = \frac{L_m s^2}{[L_2(L_m+L_1)+L_mL_1]s^3+[\frac{R_2}{q}(L_1+L_m)+L_2R_1+L_mR_1]s^2+[\frac{R_2R_1}{q}+\frac{1}{C}(L_2+L_m)]s+\frac{R_2}{qC}} \quad (4.5)$$

We must now extend this transfer function to include torque. Since the mechanical power delivered by the shaft is equal to:

$$P_m = R_2\left(\frac{1-q}{q}\right)I_2^2,$$

and because $P_m = T_m\omega_m$ and $q = \frac{\omega_s - \omega_m}{\omega_s}$

where ω_m is the mechanical speed of the rotating shaft, in rad/s,

and ω_s is the synchronous speed of the rotating shaft, in rad/s.

Then the mechanical power available from the shaft is:

$$T_m = \frac{R_2\left(\frac{1-q}{q}\right)I_2^2}{\omega_m}, \text{ since } \omega_m = \omega_s - q\omega_s$$

$$\text{thus } T_m = \frac{R_2\left(\frac{1-q}{q}\right)I_2^2}{\omega_s(1-q)} = R_2\left(\frac{1}{q\omega_s}\right)I_2^2$$

University of Cape Town

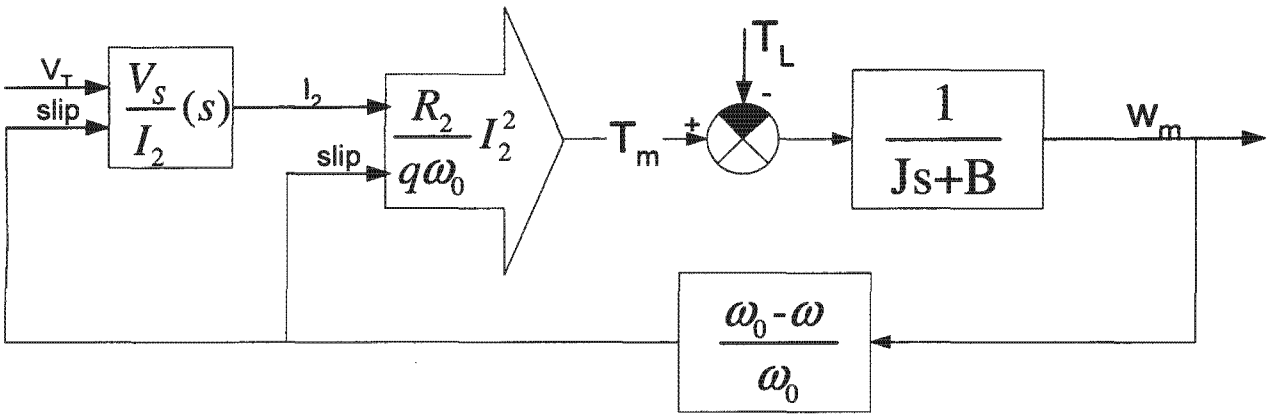

Figure 41: Torque block diagram

From this diagram, it can be seen that the slip is an input to both the $\frac{V_S}{I_2}(s)$ and the torque transfer function. Slip affects the current, which in turn affects the mechanical torque (T_m). If the inertia of a machine is small, then the $\frac{V_S}{I_2}(s)$ transfer function will dominate the dynamics of the system. However, if the inertia of the machine is large then the torque-transfer function will govern the dynamics of the system. A larger inertia will have an amplification effect on resonations, allowing more time for current build up in the $\frac{V_S}{I_2}(s)$ part of the circuit.

This transfer function of equation (4.5) has exactly the same pole positions as the V_T transfer function of equation (4.1). This is to be expected, as each system is identical, except one is a current analysis and the other, a voltage analysis. Therefore, the only real value that the inclusion of torque in the block diagram model has been to confirm what Wagner [23] stated: that a CCS-IM system that has a large inertia is more susceptible to SSR.

University of Cape Town

4.2 Prevention of self-excitation by introducing resistance

In chapter 3.2.4, Wagner's [23] method of the use of either a series resistance, or a shunt resistance across the series capacitors in order to damp self-excitation was described. It shall be shown how easily control-systems methods demonstrate the effect such resistance has on the closed-loop system-poles.

Effect of series resistance:

The effect of increasing series resistance (on the stator side) can be shown by increasing the value of R_1 in Figure 34.

As shown by Wagner [23], and confirmed using with a Root-Locus plot of the system transfer function in Figure 42, an increase in series resistance moves the system towards the stable half of the Root-Locus plot. However, this is at the cost of an increasing voltage drop across the series resistor, and hence a decrease in efficiency.

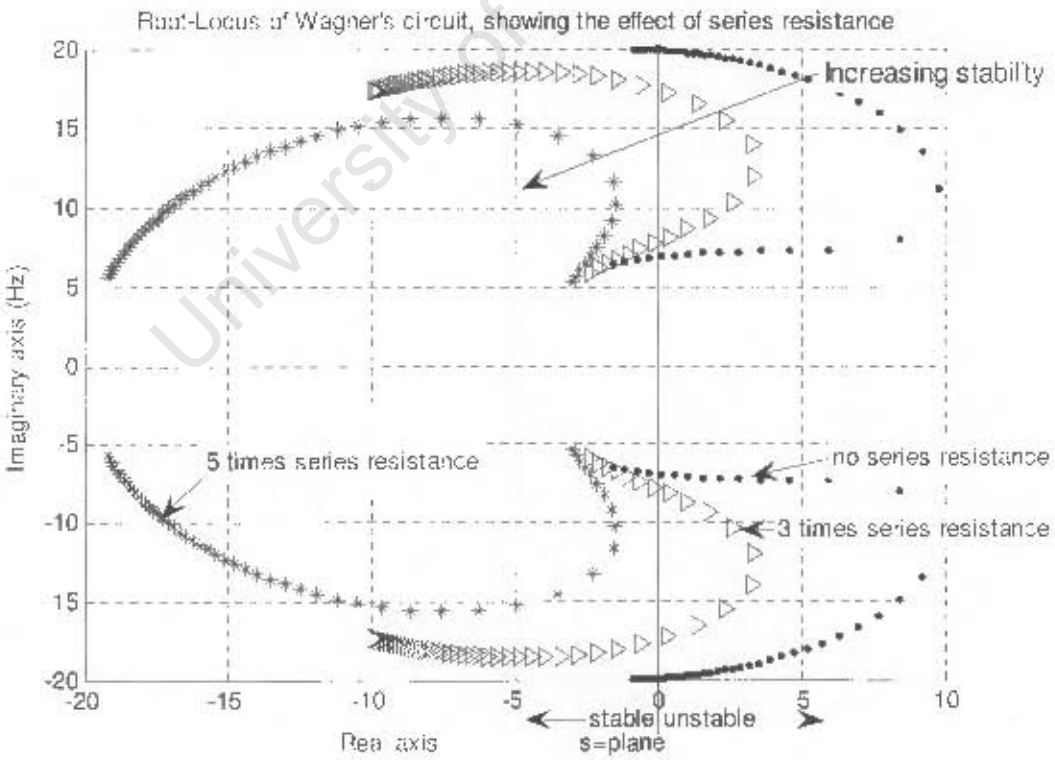

University of Cape Town

Figure 42: Effect of series resistance

It must noted that the vertical line drawn through the origin was inserted to differentiate between the stable and unstable regions of the Root-Locus plot. Here-forth, this line will be inserted however it will not be labelled.

Shunt resistance:

The effect of a shunt resistance across the Thevenin equivalent capacitor of Figure 34 is shown in Figure 43. This confirms what was stated by Wagner: [23] that a decrease in shunt resistance reduces the likeliness of self-excitation.

In order to observe the effect of the shunt resistor, the dynamic model represented by equation (4.3) was modified slightly. This was done with the help of a Matlab® program called SCAM that was developed by Cheever [31]. (See sect. 4.5 for more information.)

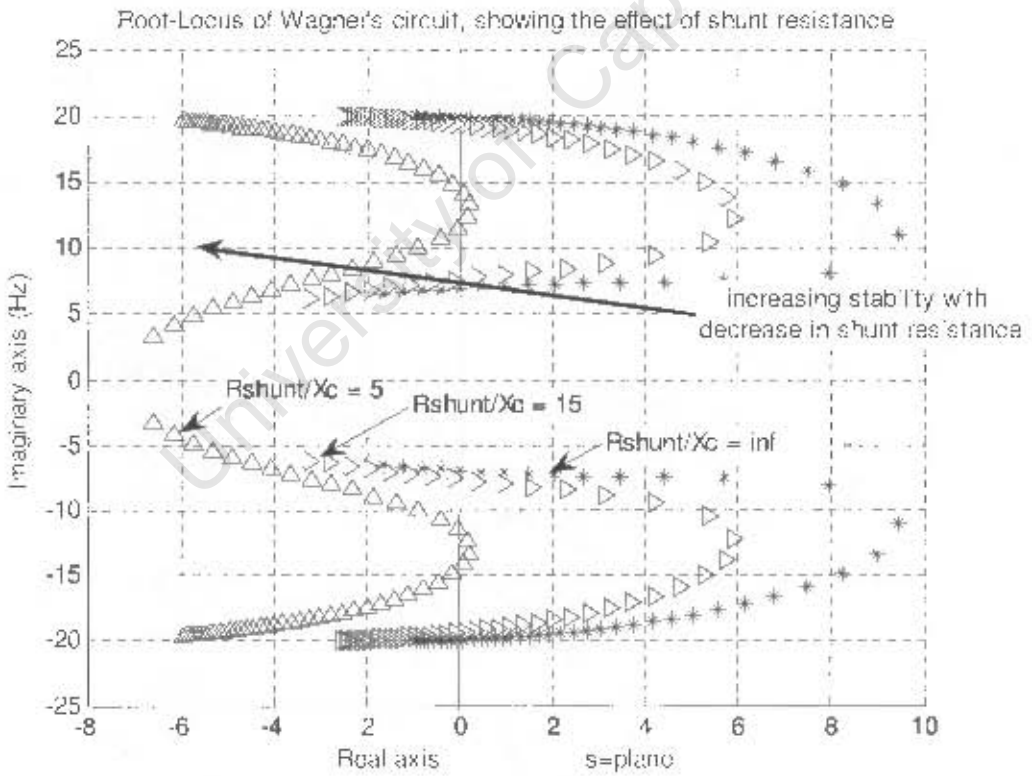

Figure 43: Effect of shunt resistance

University of Cape Town

4.3 CCS with compensating reactance

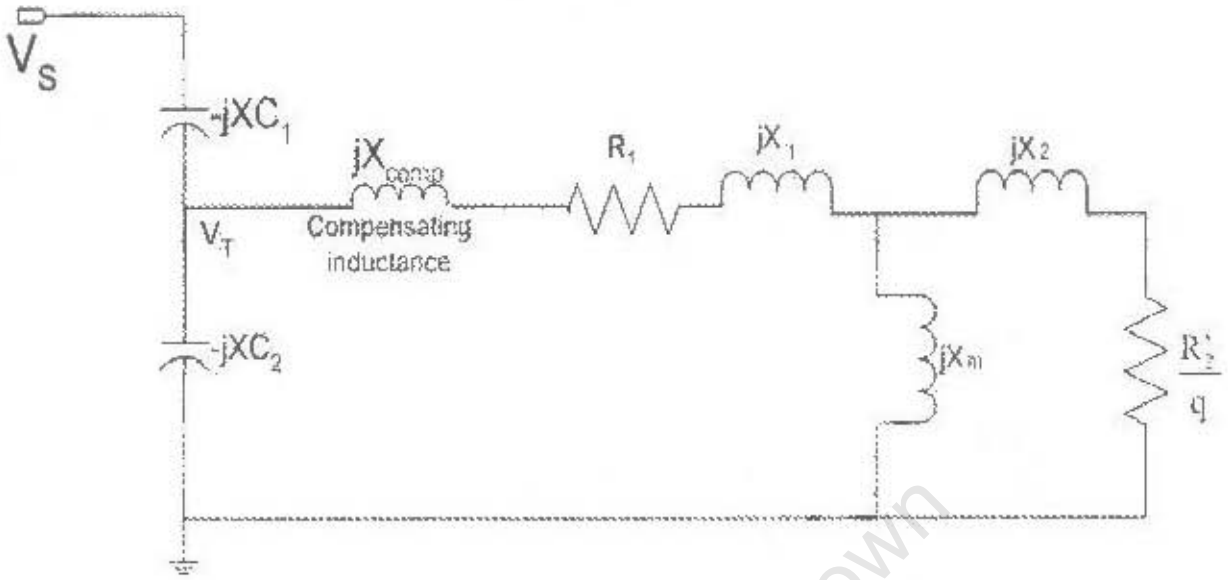

Figure 44: CCS-IM set-up, with compensating inductance

The Meru-Petronet setup includes an inductance inserted to cancel the effect of the Thevenin Equivalent capacitance of the CCS, as shown in Figure 44.

Various values of series inductance are inserted into Wagner's circuit, the Root-Locus plot of Figure 45 was obtained. Note that only the top half of the Root-Locus plot is shown.

University of Cape Town

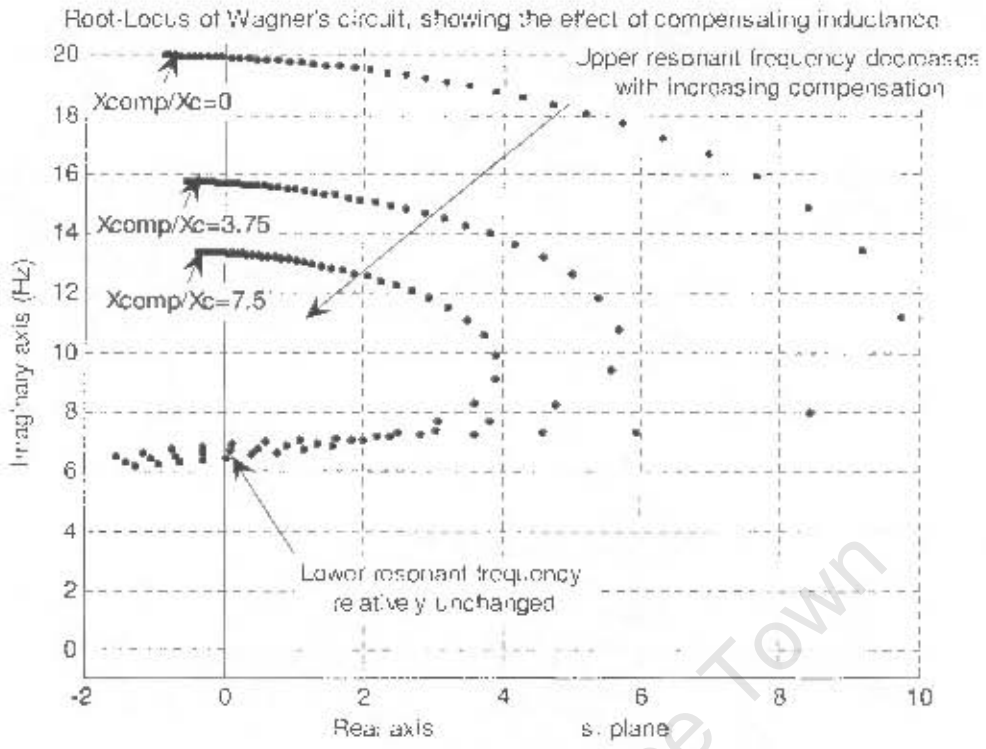

Figure 45: Root-Locus of Wagner's circuit, showing the effect of compensation

The addition of series compensation leaves the lower resonant frequency (f_{lower}) relatively unchanged. However, the upper resonant frequency (f_{upper}) is seen to decrease with an increase in compensation. As explained in section 3.2.1, only (f_{lower}) is stable. f_{upper} has effect on the stability of the system, in that the closer it is to f_{lower}, the less energy is required to avoid resonance (see sect. 3.2.1). The frequency at which a system will resonate is determined by f_{lower}.

Therefore, the addition of a compensating inductance does not have a significant effect on the sub-synchronous-frequency of a system, although it does reduce the amount of power a current injector needs to supply, but only when the amount of compensating inductance is of the order four times the capacitance of the CCS, which is not practical (see Figure 45).

The compensating inductance cancels reactive effects of the CCS, making the CCS an ideal source at supply frequency. However, a compensated CCS will not improve the

University of Cape Town

power factor of the overall power supply - grid network that a CCS may be part of. If shunt resistors are used to prevent self-excitation, more power is wasted through them if the CCS is inductively compensated than if it is not, as shown using Meru parameters:

	CCS inductively compensated [18,23]	CCS not inductively compensated [23]
Power used by shunt resistors, as a percentage of total power supplied to CCS [23].	~50%	<16%

Therefore, although a CCS will not be an ideal source at supply frequency, it may be more economical not to compensate a CCS. In this way, less energy will be used by shunt resistors. A CCS that is not inductively compensated will also improve the power factor, and therefore the transmitting ability of the overall grid. Thus, some of the energy that is lost because the CCS is not perfectly compensated for will be recovered by improving the power factor of the overall grid [4].

4.4 State-Space analysis of an induction-motor in series with a capacitor

Based on the complexity of the block diagram model of the system, a state-space model was constructed in an attempt to simplify the model.

The following state-space equations were developed using notes from [32], [28], and with the help from the 2005 EEE369W Control Class, at the University of Cape Town.

University of Cape Town

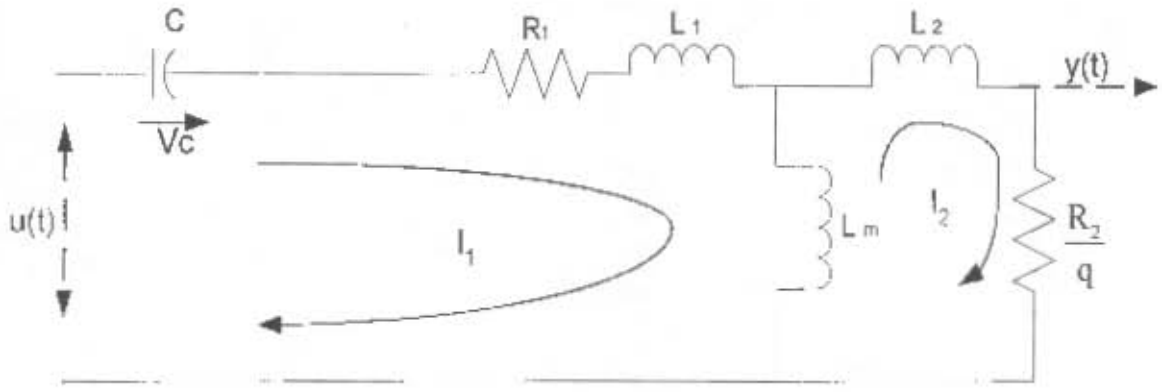

Figure 46: State-space equivalent circuit

Firstly, the states of the system need to be chosen. Generally, there are as many states as there are energy storage elements. Here, three states are chosen: V_c, I_1 and I_2. The reason that the current through L_m is not selected as a 4th state is because it is a linear combination of I_1 and I_2.

Important relations needed are:

Capacitor

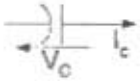

$$I_C = C\frac{\partial V_c}{\partial t}$$

Inductor

$$V_L = L\frac{\partial I_L}{\partial t}$$

Therefore, the states are:

$$\underline{x} = \begin{bmatrix} Vc(t) \\ I_1(t) \\ I_2(t) \end{bmatrix} \tag{4.6}$$

The current flowing through C is I_1, therefore:

$$\frac{\partial V_c(t)}{\partial t} = \frac{I_1(t)}{C} \tag{4.7}$$

Now,

$$y(t) = \frac{R_2}{q} I_2(t) = L_m \frac{\partial I_1(t)}{\partial t} - (L_2 + L_m)\frac{\partial I_2(t)}{\partial t} \tag{4.8}$$

and

$$u(t) = R_1 I_1(t) + (L_1 + L_m)\frac{\partial I_1(t)}{\partial t} - L_m \frac{\partial I_2(t)}{\partial t} + Vc(t) \tag{4.9}$$

University of Cape Town

From equation (4.8)

$$\frac{\partial I_1(t)}{\partial t} = \frac{R_2}{qL_m} I_2(t) + \frac{(L_2 + L_m)}{L_m} \frac{\partial I_2(t)}{\partial t}$$

(4.10)

Substituting this into equation (4.9)

$$u(t) = R_1 I_1(t) + (L_1 + L_m)\left\{\frac{R_2}{qL_m} I_2(t) + \frac{(L_2 + L_m)}{L_m} \frac{\partial I_2(t)}{\partial t}\right\} - L_m \frac{\partial I_2(t)}{\partial t} + Vc(t) \qquad (4.11)$$

Therefore

$$\frac{\partial I_2(t)}{\partial t}\left[\frac{L_m^{\,2} - (L_1 + L_m)(L_2 + L_m)}{L_m}\right] = -u(t) + R_1 I_1(t) + Vc(t) + \frac{(L_1 + L_m)R_2}{qL_m} I_2(t)$$

(4.12)

Substituting equation (4.11) into (4.10)

$$\frac{\partial I_1(t)}{\partial t} = \frac{R_2}{qL_m} I_2(t) + \frac{(L_2 + L_m)}{L_m^{\,2} - (L_1 + L_m)(L_2 + L_m)}\left[-u(t) + R_1 I_1(t) + Vc(t) + \frac{(L_1 + L_m)R_2}{qL_m} I_2(t)\right]$$

(4.13)

This can be simplified to:

$$\frac{\partial I_1(t)}{\partial t} = \frac{(L_2 + L_m)}{L_m^{\,2} - (L_1 + L_m)(L_2 + L_m)}\left[-u(t) + R_1 I_1(t) + Vc(t) + \frac{L_m R_2}{q(L_2 + L_m)} I_2(t)\right] \qquad (4.14)$$

$$Let\ \mathrm{A} = \frac{(L_2 + L_m)}{L_m^{\,2} - (L_1 + L_m)(L_2 + L_m)}$$

and

$$\mathrm{B} = \frac{L_m^{\,2} - (L_1 + L_m)(L_2 + L_m)}{L_m}$$

Then a state-space equation of the system can be formed:

$$\dot{\underline{x}} = \begin{bmatrix} \frac{\partial}{\partial(t)} Vc(t) \\ \frac{\partial}{\partial(t)} I_1(t) \\ \frac{\partial}{\partial(t)} I_2(t) \end{bmatrix} = \begin{bmatrix} 0 & \frac{1}{C} & 0 \\ \frac{1}{A} & \frac{R_1}{A} & \frac{L_m R_2}{Aq(L_2 + L_m)} \\ \frac{1}{B} & \frac{R_1}{B} & \frac{(L_1 + L_m)R_2}{BqL_m} \end{bmatrix} \begin{bmatrix} Vc(t) \\ I_1(t) \\ I_2(t) \end{bmatrix} + \begin{bmatrix} 0 \\ \frac{-1}{A} \\ \frac{-1}{B} \end{bmatrix} u(t)$$

University of Cape Town

$$y(t)=[0 \quad 0 \quad \frac{R_2}{q}]\begin{bmatrix} Vc(t) \\ I_1(t) \\ I_2(t) \end{bmatrix} \tag{4.15}$$

This model proved to be as complicated to solve as the block-diagram model presented in section 4.1, and was not used for analysis. Instead, a similar analysis conducted by Limebeer et al. [35] will be examined:

SSR examination by Limebeer et al. [35]

Limebeer et al. used machine equations of an induction machine, connected in series with a capacitor (see the natural circuit of Figure 21), to form loop equations. The determinant of these loop equations determines the pole positions of the induction machine, capacitor system, which can be plotted on a Root-Locus diagram.

The loop equations were of the form:

$$|V|=|Z(s)||I| \tag{4.16}$$

or

$$\begin{bmatrix} 0 \\ 0 \end{bmatrix}=\begin{bmatrix} R_1+s(L_1+L_m) & -sL_m \\ -s(L_m) & s(L_s+L_m)+R_2/s_{slip} \end{bmatrix}\begin{bmatrix} I_1 \\ I_2 \end{bmatrix} \tag{4.17}$$

now,

$$\det[Z]=C(L_1L_2+L_1L_m+L_2L_m)s^3+C\left(R_1[L_m+L_2]+\frac{R_2}{s_{slip}}(L_1+L_m)\right)s^2+\left(L_2+L_m+\frac{CR_1R_2}{s_{slip}}\right)s+\frac{R_2}{s_{slip}} \tag{4.18}$$

The position of the poles of this equation are identical to those of equation (4.1), validating the correctness of the block-diagram model developed.

4.5 CCS-IM with filter-bank

A useful tool was uncovered when dealing with state-space equations. A Matlab® tool was developed by Erik Cheever [31] called SCAM (Symbolic Circuit Analysis in Matlab). It is a tool for deriving and solving equations symbolically. The program

University of Cape Town

requires a netlist to do this. A netlist defines the interconnection between circuit elements. This tool can be used to find the transfer function of systems. SCAM was tested with Figure 34, and the same pole positions as those of equation (4.18) were found (see appendix 'G' for the comparison).

This tool shall now be used to produce equations for a Root-Locus plot of the Wagner's circuit with the filter-bank included.

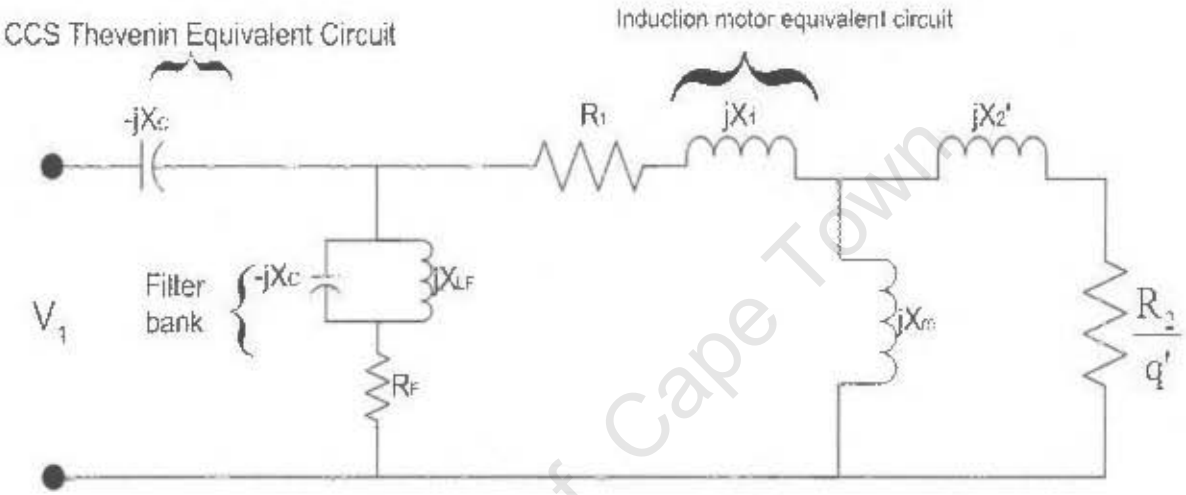

Figure 47: CCS-IM circuit with filter-bank

The Root-Locus plot of Figure 48 is shown with and without the filter-bank, and is plotted for resonant slip values starting at 0.05 and decreasing to -1, as the speed of the rotor increases. The filter-bank reduces the upper and lower resonant frequencies of the circuit, resulting in less energy being required to prevent SSR as determined by equation (3.14). However, the circuit is still unstable, and therefore this is not an adequate solution.

University of Cape Town

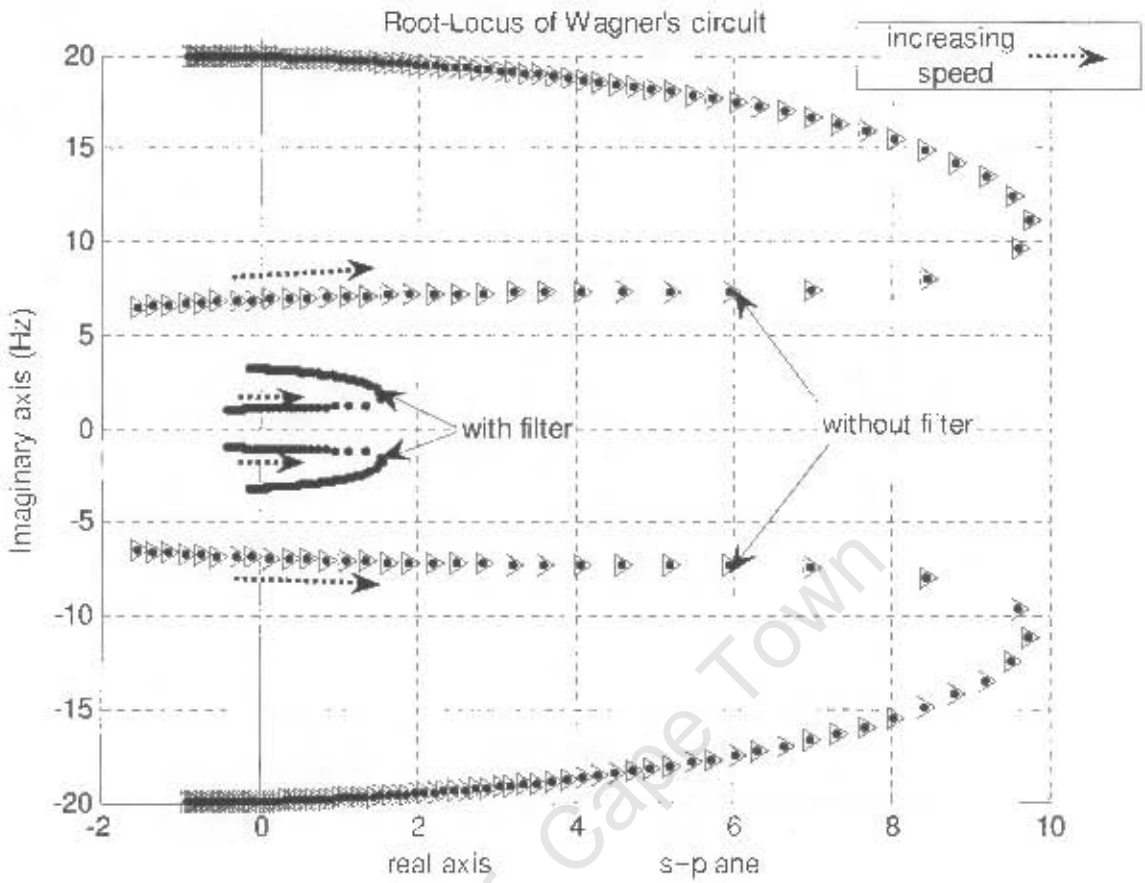

Figure 48: Root-Locus of Wagner's circuit with, showing the effect of the filter-bank

University of Cape Town

4.6 Proposed solution

An example of the ease with which a solution can be developed is now illustrated. Using the transfer function model developed for the CCS-IM system (see equation (4.3)), a controller of $k(s) = \frac{1}{1+28s}$ is proposed. Before moving on, it must be pointed out that although the CCS-IM system is being treated as a control system, it does not imply that the author intends to control the output to a set-point dictated by the input. The sole intention of this control analysis is to evaluate whether it is theoretically possible to stabilise the system. Therefore, discussion of open-loop and closed-loop poles does not imply that the physical CCS-IM system is/ will become a feedback loop if a theoretical controller is found.

If it is found that the system can be theoretically stabilised, converting the theoretical controller to a practical solution may prove difficult, as adding circuit elements to the CCS would have repercussions; such as on the tap voltage or system efficiency. In practice, such a controller may take the form of a lag circuit [32], which would be inserted after the CCS, in the same position as the filter-bank of Figure 4.

The position of the controller pole is shown before it is implemented, in the left-hand Root-Locus diagram of Figure 49. The effect of the controller can be observed in the right-hand Root-Locus plot. It can be seen that the controller moves the closed-loop-poles (solid black line) into the left-hand-side (stable region) of the Root-Locus plot.

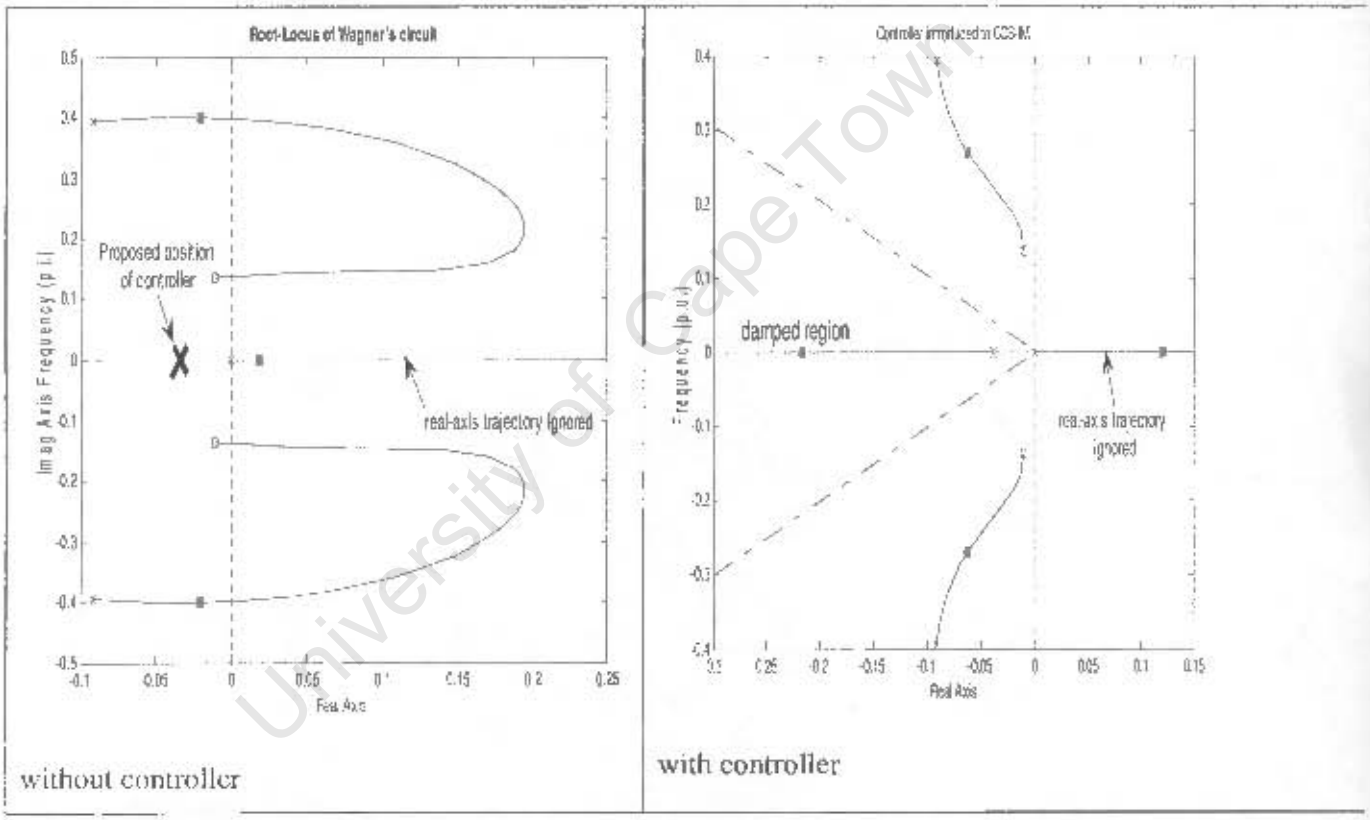

Figure 49: CCS-IM circuit with and without controller

Although the system is now stable, oscillations are not damped enough. When q is close to -1, the closed-loop poles will be close to the open-loop poles, of the transfer function that represents the system. Thus, when the IM is running close to synchronous speed, there will be strong harmonics of about 40% of the supply frequency. For oscillations to

University of Cape Town

be suitably damped, the closed-loop poles should be within the demarcated triangle, which represents a damping factor of 0.707.

As already mentioned, the Root-Locus gain is equal to $\frac{1}{slip_{resonant}}$. Therefore, the resonant slip is close to zero at the lower resonant frequency, and so the Root-Locus gain is large. However, at synchronous speed, the resonant slip will be close to -1, so the Root-Locus gain will be small. Therefore, the positions of the system-poles at synchronous speed will be close to those of the open-loop system. This means that the system is uncontrollable by means of a hypothetical feedback control loop. Therefore, there is no need to try control the system with other controllers, such as a second order controller.

In conclusion, because the dynamics of the transfer function that represents the CCS-IM system are ultimately controlled by open-loop pole positions, the system is practically uncontrollable, by means of a passive controller, such as a passive filter.
Therefore, either the system configuration must be changed, for example, using a shunt resistor (see sect. 3.2.4); or the system must be controlled actively using FACTS devices, as discussed in section 3.2.5.

4.7 Summary

A block-diagram-model was constructed in this section to replicate the mathematical model of self-excitation developed by Wagner [23], these results are shown chapters 7 and 8.

It was shown that the model could be adapted, using a Matlab® application called SCAM [23] to include components such as compensating inductance, or a filter-bank. These methods are compared and discussed in chapters 7 and 8 respectively.

It was also shown that a passive controller is not suitable for a CCS-IM system, and other means of control (such as the use of a shunt resistor or FACTS devices) should be used.

University of Cape Town

5 COMPUTER SIMULATION OF RESONANCE

Matlab's® Simulink® and Power Systems® Toolbox was used to simulate various aspects of the CCS-induction motor system. The simulation was used to assist in the design of the lab-model. The model was not a dynamic model, so it could not be used in the validation process. However, it was useful in predicting steady-state torque and speed values.

5.1 Simulink Model

A simulation of self-excitation was constructed. Other aspects of the CCS system such as ferroresonance and inductor saturation were omitted. These characteristics were omitted so that self-excitation could be studied in isolation. Therefore, instead of building a simulation involving a capacitor in series with an induction motor, a simulation was conducted that focused specifically on self-excitation.

Self-excitation is essentially the undamped oscillation of energy between two reactive devices in a system. When oscillating continuously, self-excitation can be represented by two alternating power supplies: a fundamental, and a sub-harmonic supply.

The simulation model of Figure 51 was used. The parameters of the induction machine were the same as those that of the 3kW induction motor that was used in the UCT laboratory. (See section 6.1.2) The parameters of the three-phase programmable voltage source were determined using dynamic model predictions of the lower resonant frequency (see section 4). With this model, graphs of the voltage, current, power and torque of the system could be plotted. These graphs are shown in chapter 7, and discussed in chapter 8 of this thesis.

In summary, a 'steady-state' self-excitation simulation was developed that did not predict transients well. However, it could predict values such as the final speed and torque that an induction-motor experiencing self-excitation would be likely to reach. It was used as a stepping-stone to implement a laboratory CCS-IM setup.

University of Cape Town

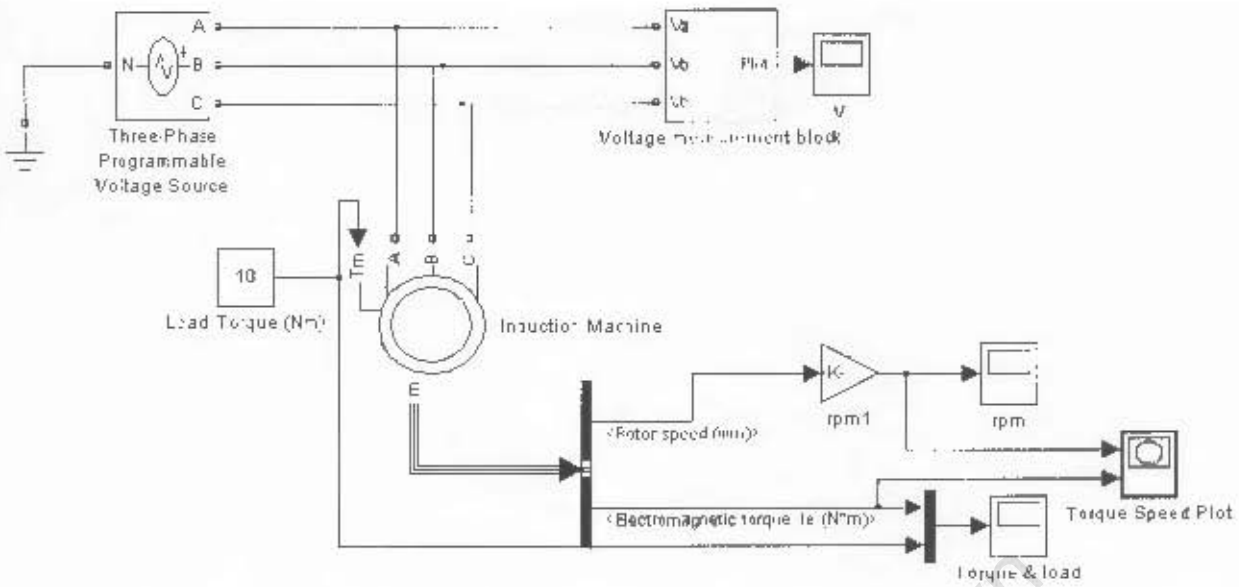

Figure 50: Matlab®, Simulink® simulation model

The characteristics of the induction motor and three-phase programmable voltage source were:

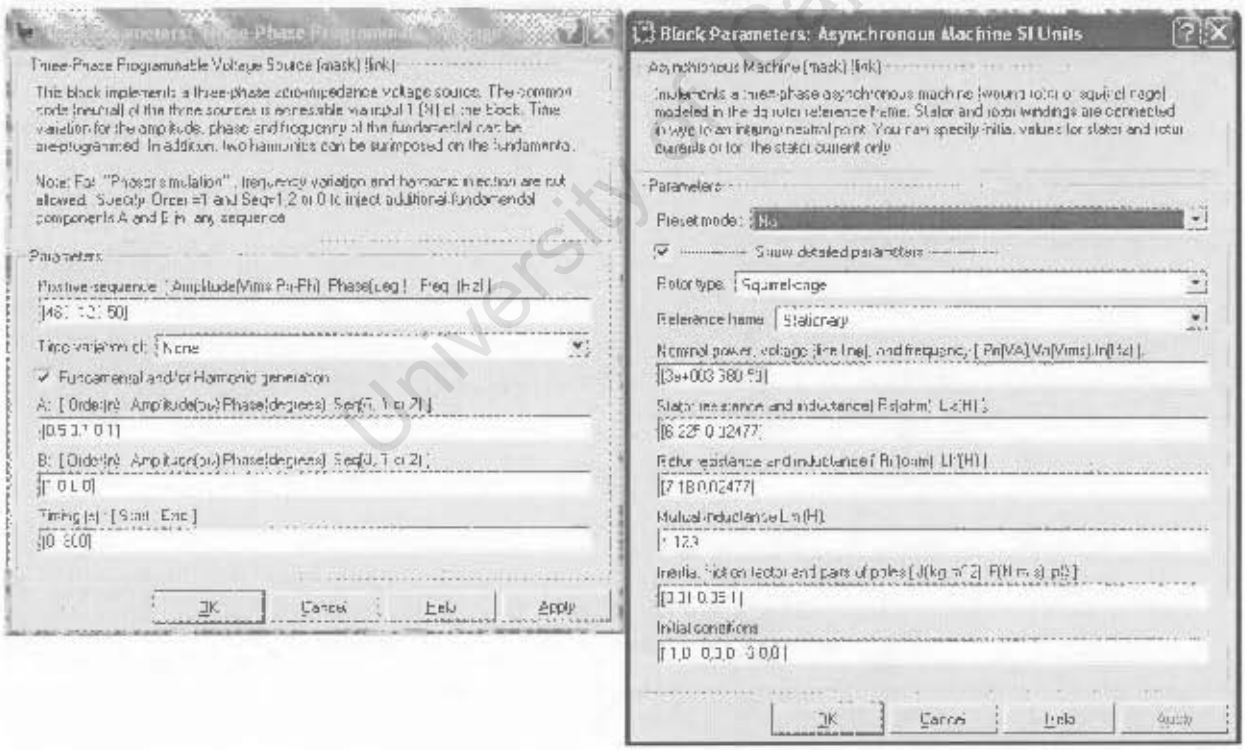

Figure 51: Characteristics of the induction motor and three-phase programmable voltage source

University of Cape Town

6 PHYSICAL MODEL

In this chapter, the process used to construct a physical model at UCT is presented. The intention of this model was to recreate instabilities that are found in the field [16], and validate the dynamic model of chapter 4. This model was built in the UCT Machines Laboratory.

6.1 Laboratory model

A 3kW Thevenin Equivalent physical model was built by the author in order to validate theoretical predictions. A 3kW motor was used based on the availability of a 3kW motor test-rig in the UCT Machines Laboratory. The induction motor was coupled to a dc motor, sufficiently increasing the inertia of the IM-system to make self-excitation more likely (see section 3.2.1). Other advantages of using a relatively small motor were ease of circuit manipulation (cable sizes, component availability), and the safety compared to constraints and safety hazards associated with high power levels.

To record parameters of interest, such as torque, speed, current and voltage a DSP (Digital Signal Processor)-based motor logger was designed and built. The conceptual intention of the data logger is shown pictorially in Figure 52.

University of Cape Town

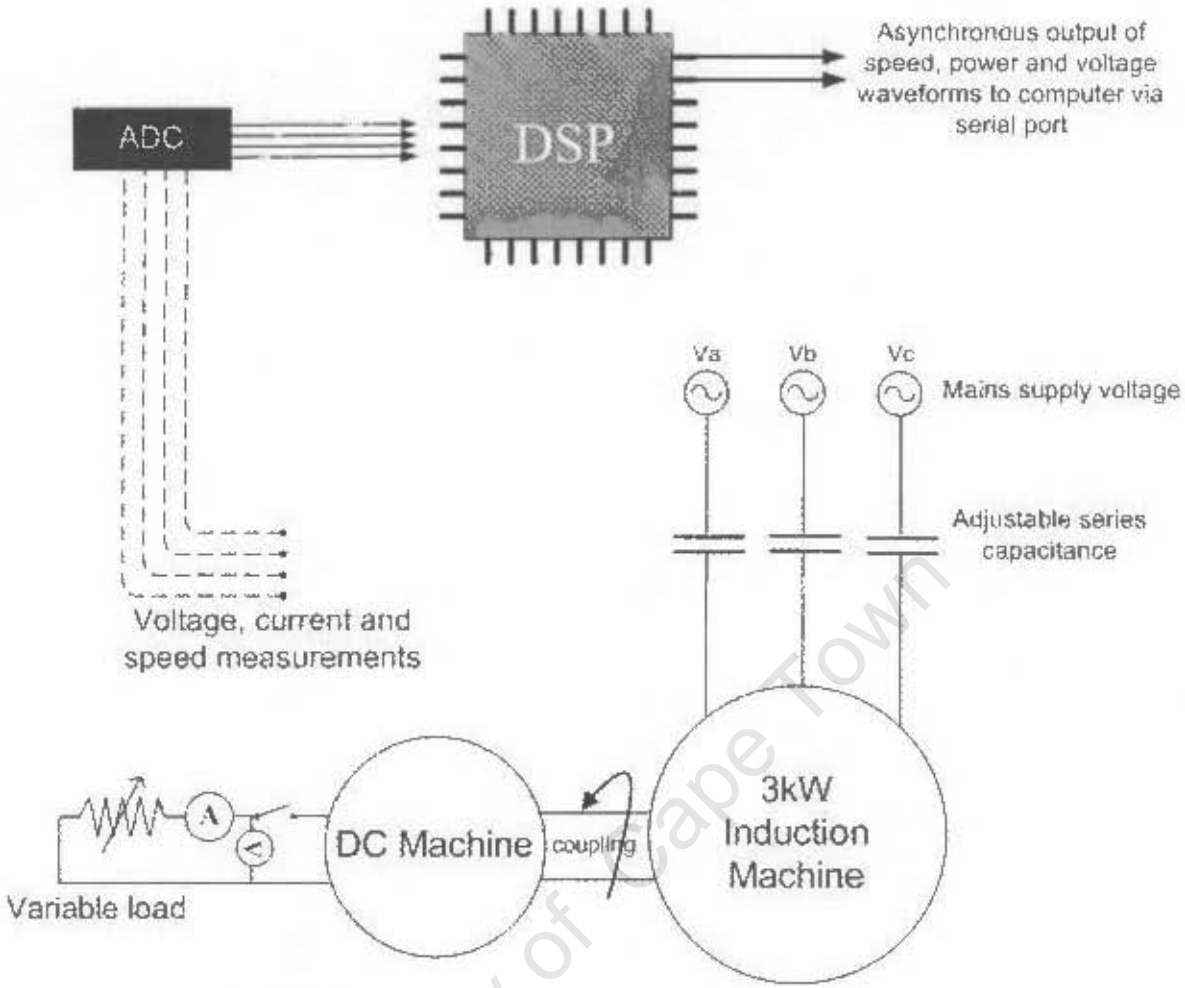

Figure 52: Laboratory model flow chart

The various elements of the laboratory model shall now be discussed.

University of Cape Town

6.1.1 Capacitor bank

A three-phase bank of capacitors was set-up. The capacitance of this bank could be varied from 50μF to 200 μF.

6.1.2 Induction machine parameters

Parameters of the laboratory induction machine were determined using the blocked rotor and no-load test described by P.C. Sen [8].

The parameters of the induction machine were found using the equivalent circuit of Figure 7. Firstly, R_c was excluded from the equivalent circuit as the core losses associated with it were lumped together with friction and windage losses [8].

Under no-load, during the no-load test, the only power consumed by the motor is that due to the core, friction and windage loss. Thus, a negligible amount of current will flow through R'_2 and X'_2. In addition, the machine is operating at a slip close to zero. Therefore, the resistance $\frac{R_2'}{s} + X_2$ is much larger than that of X_m. So, the equivalent circuit is simplified to that shown in Figure 53(A).

When the rotor is prevented from rotating, the slip is one. Thus $\frac{R_2'}{s} + X_2'$ will be much larger than X_m, so that the equivalent circuit will resemble that of Figure 53.B. To obtain the characteristics of the machine under normal operating conditions, the supply voltage to the machine should be increased until rated current flows in the stator windings.

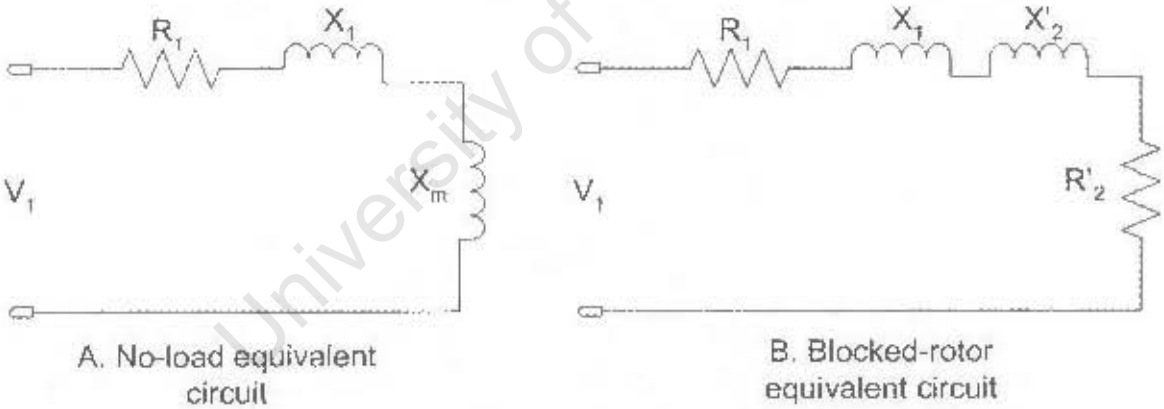

Figure 53: No-load and blocked rotor tests on an induction machine

The no-load and blocked-rotor tests were carried out, and the results were evaluated as shown in appendix 'A'. The results are summarised here:

University of Cape Town

Table 2: Laboratory 3kW induction motor parameters	
Parameter	**Value**
Number of poles	**2**
Rated frequency	**50Hz**
Rated voltage (L.L)	**380V**
Rated speed	**2800rpm**
Values below are per-phase	
R_1	6.6Ω
$X_1=X'_2$	7.7Ω
$L_1=L'_2$	24.8mH
R'_2	7.2Ω
X_m	353Ω
L_m	1.12 H

Friction and windage, and torque were estimated using the method described in sections 2.2.4 and 2.2.5. These estimations were validated using the Matlab Simulation. Estimated values were:

Inertia: 0.01 kgm^2

Friction and windage: 0.01 Nms/rad

6.1.3 Motor logger

A motor logger was built to collect data from the Lab model, and send this data via serial port using RS232, to a computer. At the computer, the data was manipulated, using Matlab®, to make it useful for analysis. A custom-made data-logger was used as opposed to a commercial one because of the freedom that it allowed: to record different parameters at different sampling rates and resolutions, and manipulate those variables as required, at a low cost. A flow chart of the workings of the data-logger is shown in Figure 54.

University of Cape Town

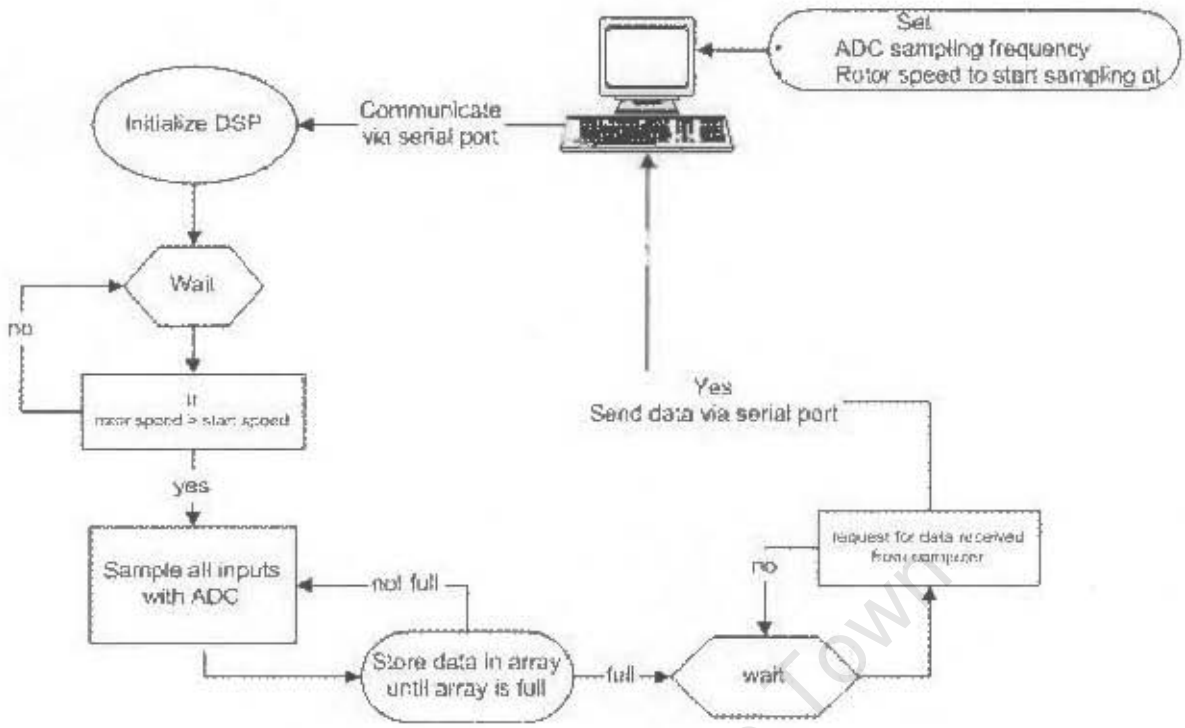

Figure 54: Code structure of data-logger

Before the data logger can be used, it must first be set up. The sampling rate and rotor speed at which to start sampling are inputted to the instrument via the serial cable. The motor logger works by waiting for the rotor speed to reach a certain value. It then starts logging. In this way, the dynamic start-up of the machine can be observed. Once memory of the DSP is full, the logger stops. It then waits for a request from a computer before sending whichever set of data was requested to the computer via the serial port. The C++ code for the data logger can be found in appendix 'D'.

6.2 Summary

In this chapter, the workings of the 3kW Thevenin Equivalent CCS-IM system were shown. A useful instrument was constructed (using a DSP) that was capable of recording and logging various parameters of interest. This device was capable of communicating with a computer, so that the data could be further analysed using Matlab©.

These results obtained from this model shall be used in chapters 7 and 8 to test the hypothesis presented at the end of chapter 3.

University of Cape Town

7 RESULTS AND MODEL VALIDATION

Collection of results forms the first part of the validation process of the hypothesis presented in section 3.4. The second, and last, part of this process is the discussion of results, in chapter 7.

The following systems are analysed:

1. The circuit used by Wagner,
2. The Laboratory model that was built at UCT,
3. The Laboratory model that was built at Stellenbosch,
4. The commercial Meru-Petronet system.

A brief summary of these systems shall now be presented:

7.1 Description of the models to be analysed

7.1.1 The circuit used by Wagner

The circuit and parameters used by Wagner in [23] have already been presented in chapter 3.2.1. He represented self-excitation as two equivalent circuits of an IM, a resonant and a natural circuit. The resonant circuit is shown here:

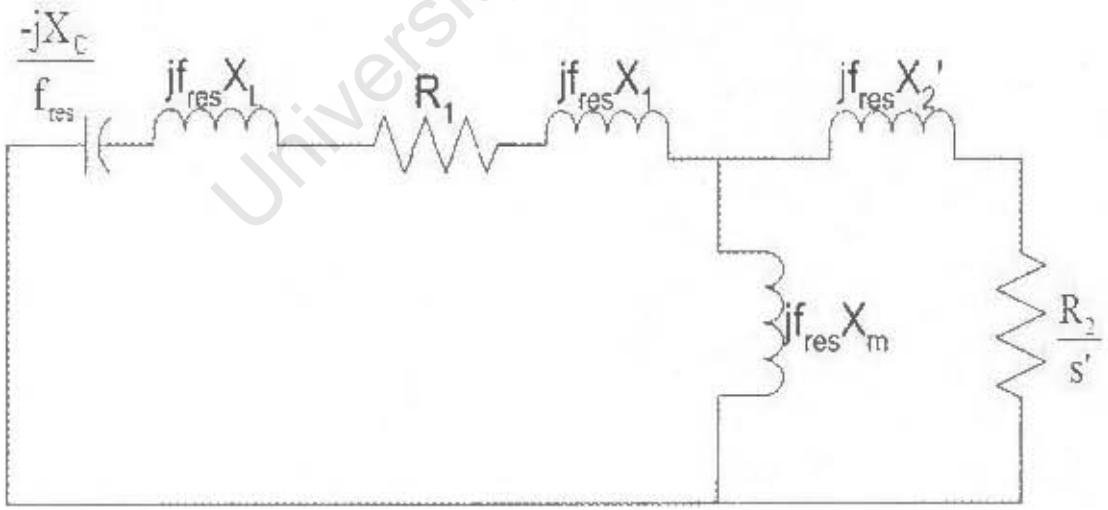

Figure 55: Resonant circuit used by Wagner [23]

University of Cape Town

As a reminder, the resonant circuit operates at its resonant frequency, f_{res}. Therefore the slip of the resonant circuit is not the same slip that is associated with the natural circuit, and is denoted by s'.

7.1.2 The Laboratory model that was built at UCT

A Thevenin Equivalent CCS-IM laboratory model was built at UCT to replicate the phenomenon of self-excitation. The model was constructed using the same circuit diagram tested by Wagner (Figure 34). However, the values of the parameters used were different.

The series capacitance consisted of a capacitor bank that could be adjusted from 25μF to 200μF, in 25μF steps. A 3kW squirrel-cage motor was used based on its availability and ease of use, due to its relatively small power rating. It was also coupled to a dc motor, allowing load tests to be conducted, and resulting in higher system inertia. Equivalent circuit values were determined in section 6.1.2, and are shown in Table 2.

University of Cape Town

7.1.3 The Laboratory model that was built at Stellenbosch

The Stellenbosch lab-setup was as follows:

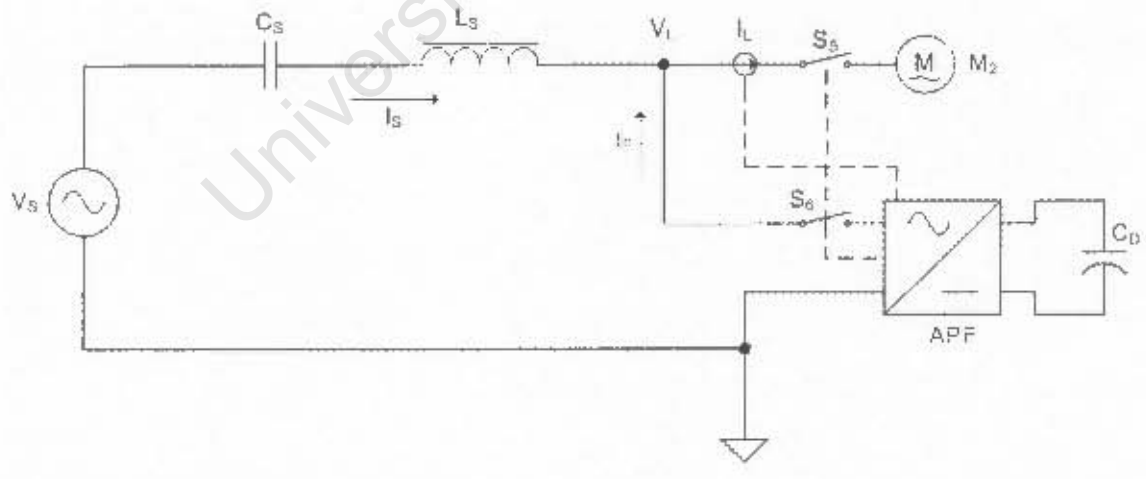

Figure 56: Stellenbosch laboratory setup [33]

The block labelled APF is the Active Power Filter, or current injector that was used to damp sub-synchronous oscillations. The C_S and L_S values were 3mF and 2.8mH respectively [33].

The motor that was used to test the APF was a 65kW squirrel-cage induction machine. However, tests were not done to determine the equivalent circuit parameters of this motor. So the parameters have been estimated by the author, and are based on those parameters given by the Matlab Power Systems Toolbox® for a 100HP (horsepower) induction machine. Component values are shown in appendix 'A'.

7.1.4 The commercial Meru-Petronet system

The Meru-Petronet system is shown in Figure 4, where the Petronet IM was connected to V_{out}, which is V_T in Figure 57 as $V_{out} = V_T$. Schilder et al. [16, page 4] and Braae et al. [30] showed that the shunt-filter was not the cause of SSR. For this reason, the shunt filter was not included in the analysis of the Meru-Petronet system. In addition, the Thevenin Equivalent CCS of Figure 3 was used. Therefore, the Meru-Petronet equivalent circuit analysis was much like the circuit used by Wagner (Figure 34) with an additional compensating inductance, as shown in Figure 57. Component values are shown in appendix 'A'.

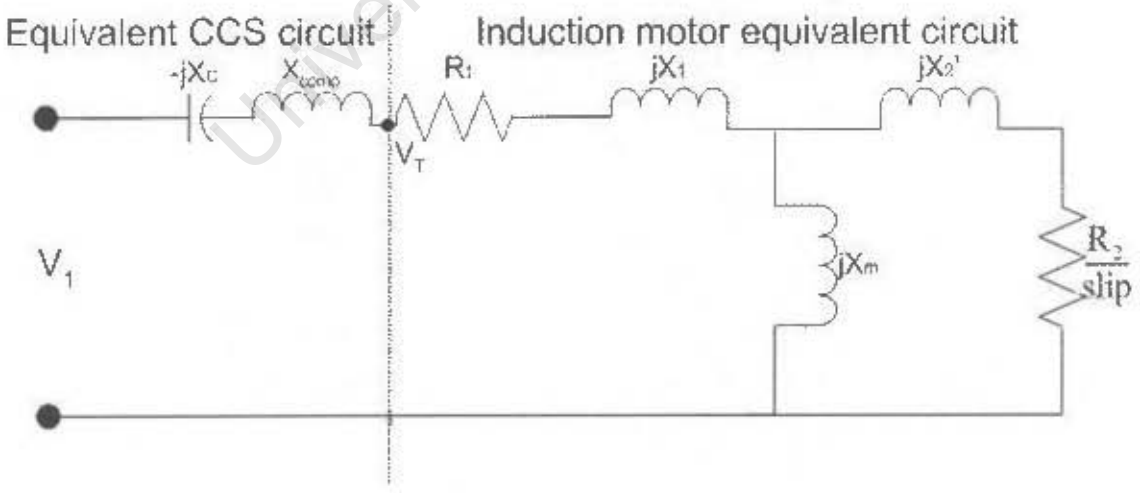

Figure 57: Meru-Petronet Equivalent System

University of Cape Town

For the purpose of completion, the circuit of the Petronet-Meru system was analysed as it was built, with the filter-bank included; i.e. with the output of Figure 2 connected to the input of Figure 8 (R_c ignored). Results of this analysis were very similar to those conducted using the circuit of Figure 57, except for the presence of new stable system-poles as a result of the filter-bank and are therefore shown in appendix 'E-1.3'.

7.2 Comparison of the different methods of determining the resonant frequency

Here, the various methods of predicting the resonant frequency of a CCS-IM system are compared. At the end of this chapter, these predictions are tested against physical results.

Two methods of finding the resonant frequency of a CCS-IM have been discussed in this document namely:

- The Root-Locus method and
- Wagner's method (discussed in section 3.2.1)

To plot the Root-Locus of the CCS-IM system, its transfer function must first be determined, using slip as the Root-Locus gain. In other words, slip would be an internal model parameter. A transfer function can be obtained in many ways, such as using block-diagram algebra, or by forming state-space equations for the system. The transfer function formed is a theoretical construct representing the system. Useful insight into the dynamic behaviour of the real-life system can be gained by analysing Root-Locus plots of the transfer function. A Root-Locus of the transfer function in open-loop is plotted rather than that of the system in closed-loop, which would falsely represent the system, as it contains no such feedback loop.

University of Cape Town

7.2.1 The circuit used by Wagner

Wagner's resonant frequency prediction method:

Using the method developed by Wagner for finding the resonant frequency, the following graph was obtained:

Figure 58 shows how the resonant frequency changes with the stator resistance (R_s) of the induction motor. The slip (of the resonant circuit) that corresponds to a particular R_s value and the frequency at which that slip occurs is also shown. Wagner showed that there are two resonant frequencies for each R_s value (see sect. 3.2.1).

Figure 58: Frequency vs. Rs, and corresponding slip for Wagner's circuit

Root-locus method:

When a transfer function was constructed for the circuit of Figure 55, and the same parameters used, the Root-Locus of Figure 59 was plotted.

University of Cape Town

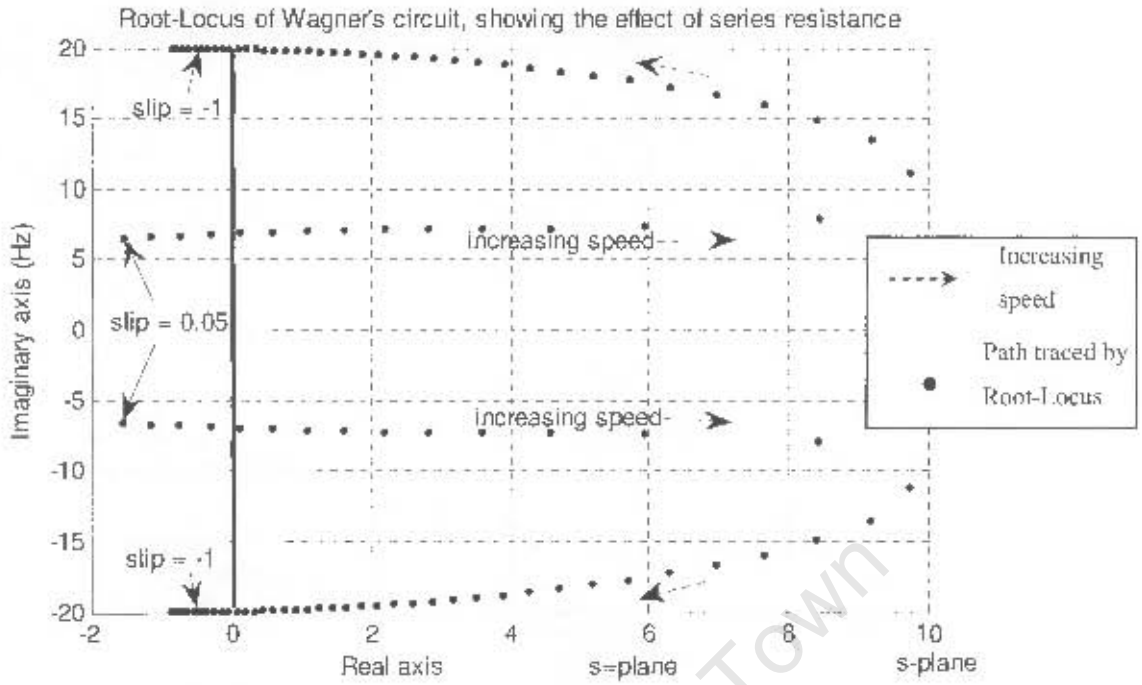

Figure 59: Root-Locus response of Wagner's Circuit

Each dot in Figure 59 shows the system-pole positions for a particular slip. Starting at 0.05, the slip is repeatedly decreased by 0.01 until it is equal to -1.

Comparison of the Wagner and the Root-Locus Methods:

Table 3: Table of resonant frequency and corresponding slip for Rs = 0.1 (p.u.)				
	Determined using Wagner's method		Determined using Root-Locus	
	Freq. (p.u.)	**Slip**	**Freq. (p.u.)**	**Slip**
Lower freq.	0.15	-0.1	0.15	-0.12
Upper freq.	0.37	-0.37	0.36	-0.3

It can be seen that the two methods of finding the resonant frequency correlate closely. Note, the resonant frequency, which leads to sustained SSR, is the smaller of the two frequencies for a particular Rs.

7.2.2 The Laboratory model built at UCT

Wagner's resonant frequency prediction method:

Using the method developed by Wagner, the following frequency vs. stator resistance graph of Figure 60 is formed:

University of Cape Town

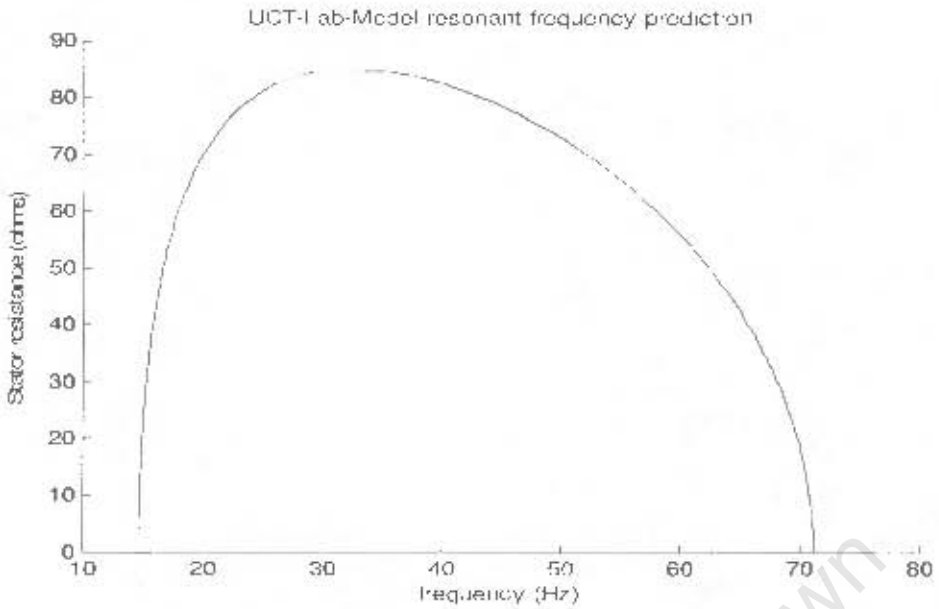

Figure 60: UCT-Lab-Model resonant frequency prediction

In Figure 60, the slip plot was not shown as it resembles that of Figure 58. It can be calculated for any frequency by substituting that frequency value, and the relevant circuit parameters into equation (3.12).

When the stator resistance is 6.2 ohms, the lower and upper resonant frequencies are 15Hz and 71Hz; which correspond to resonant circuit slips [using equation (3.8)] of -0.01 and -1 respectively.

Root-locus method:

By constructing a transfer function of the UCT-Lab-Model, the Root-Locus of Figure 61 was plotted:

University of Cape Town

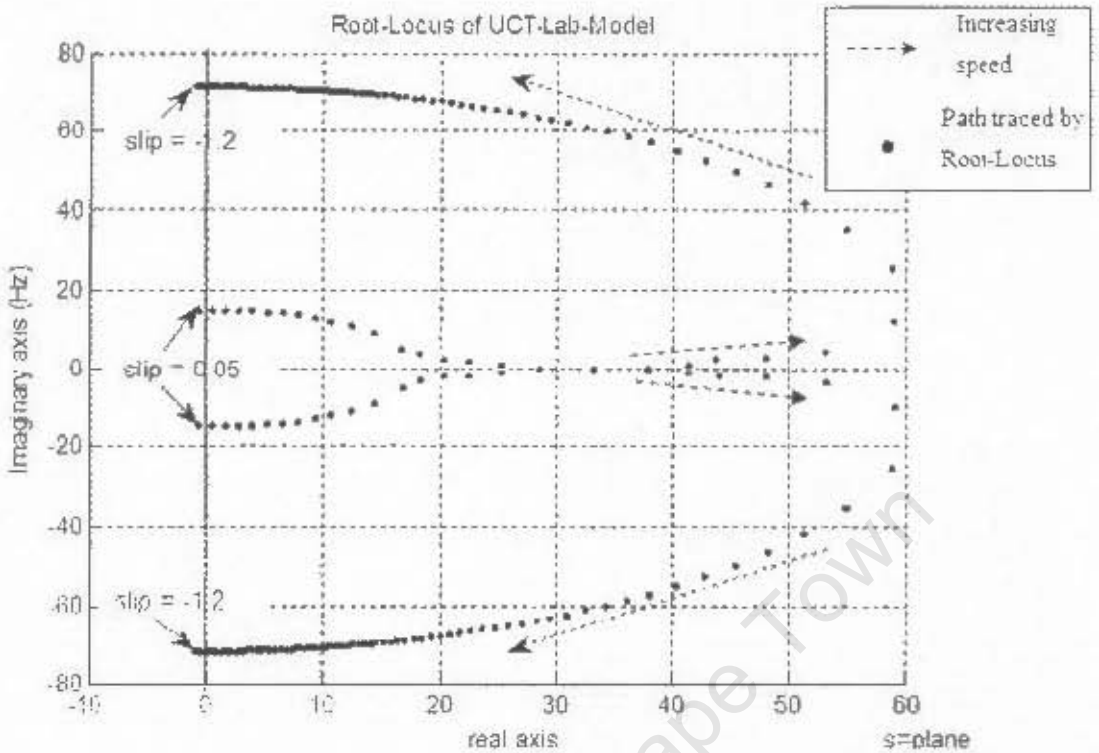

Figure 61: Root-Locus plot of UCT-Lab-Model

Each dot in Figure 61 shows the system-loop pole positions for a particular slip. Starting at 0.05, the slip is decreased in steps of 0.01 until it is equal to -1.2. Root-Locus predicts lower and upper resonant frequencies of approximately 15Hz and 72Hz respectively, the corresponding lower and upper slip (for the resonant circuit) values are approx. -0.01 and -1.2.

Comparison of the Wagner and the Root-Locus Methods

Table 4: Table of resonant frequency and corresponding slip for Rs = 6.2 Ω

	Determined using Wagner's method		Determined using Root-Locus	
	Freq. (Hz)	**Slip**	**Freq. (p.u.)**	**Slip**
Lower freq.	15	0.01	15	-0.01
Upper freq.	71	-1	72	-1.2

It must be noted that the two methods predict very similar resonant frequency values.

University of Cape Town

Capacitance variation:

The UCT-Lab-Model has an adjustable capacitor bank. The effects of capacitor variation shall be discussed in chapter 8. Results obtained using different capacitor values are shown in appendix 'B'.

7.2.3 The Stellenbosch Laboratory model

The same procedure that was conducted in sections 7.2.1 and 7.2.2 is also conducted here. Plots are shown in appendix 'E-1.1', and a summary of the findings shown:

Table 5: Table of resonant frequency and corresponding slip for Rs = 0.04 Ω				
	Determined using Wagner's method		Determined using Root-Locus	
	Freq. (Hz)	**Slip**	**Freq. (p.u.)**	**Slip**
Lower freq.	21	-0.001	21	-0.01
Upper freq.	48	-0.5	48	-0.5

7.2.4 The commercial Meru-Petronet system

The same procedure that was conducted in sections 7.2.1 and 7.2.2 is also conducted here. Plots are shown in appendix 'E-1.2', and a summary of the findings in Table 6:

Table 6: Table of resonant frequency and corresponding slip for Rs = 0.012 Ω				
	Determined using Wagner's method		Determined using Root-Locus	
	Freq. (Hz)	**Slip**	**Freq. (p.u.)**	**Slip**
Lower freq.	48.8	-0.001	49	-0.01
Upper freq.	50.5	-1.3	51	-1.3

7.3 Simulink® Simulation Results

Simulations of the UCT laboratory model were conducted using Matlab's Power Systems® Toolbox. Results obtained were compared to the physical results of the UCT-Lab Model.

University of Cape Town

7.3.1 Simulation of system with no self-excitation

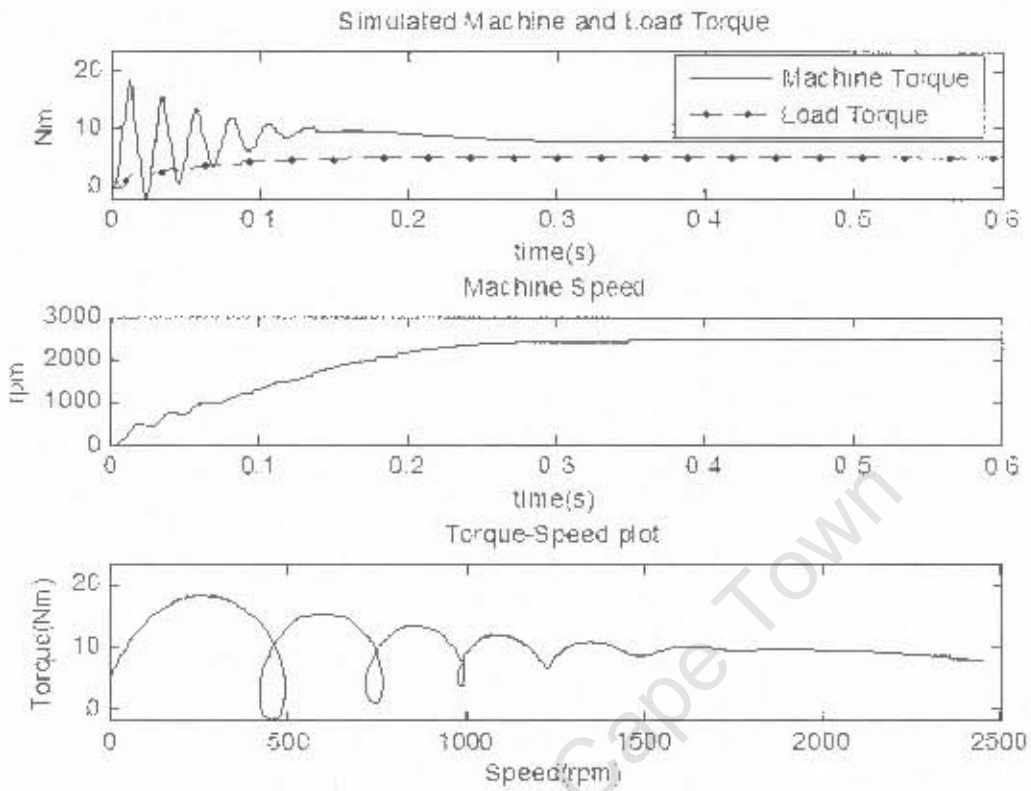

Figure 62: Simulation of 3kW UCT system with no self-excitation

In Figure 62, it can be seen that:

- The induction motor runs close to its synchronous speed (2800rpm) in approximately 0.4 seconds.
- The induction motor torque reaches a final value as determined by the sum of the load torque and the torque due to friction and windage.

7.3.2 Simulation of system with 25 Hz self-excitation

25Hz was chosen as the SSR frequency in this instance because of its similarity to the SSR frequency of the physical UCT model.

University of Cape Town

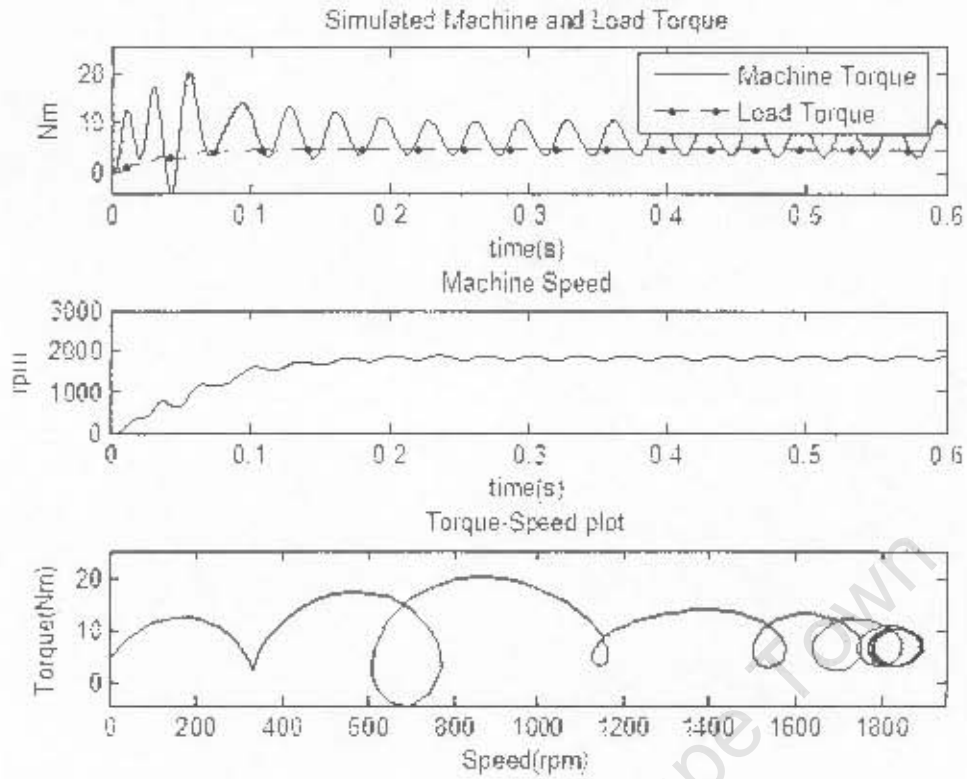

Figure 63: Simulation of 3kW UCT system with 25Hz self-excitation

Here, it can be seen that:

- The induction motor does not reach its synchronous speed.
- The induction motor torque reaches a final value as determined by the sum of the load torque and the torque due to friction and windage, but it is more oscillatory than it was with no self-excitation in Figure 62.

A discussion of the similarities and differences between the simulated and laboratory results is conducted in chapter 8.

7.4 Laboratory Model Results

Using the motor logger, the following results were obtained for the 3kW UCT laboratory model connected to a load of ~1kW.

University of Cape Town

7.4.1 Induction motor with no series capacitor

First, the system was tested with no series capacitor, so that normal operating conditions could be observed.

Torque speed plots:

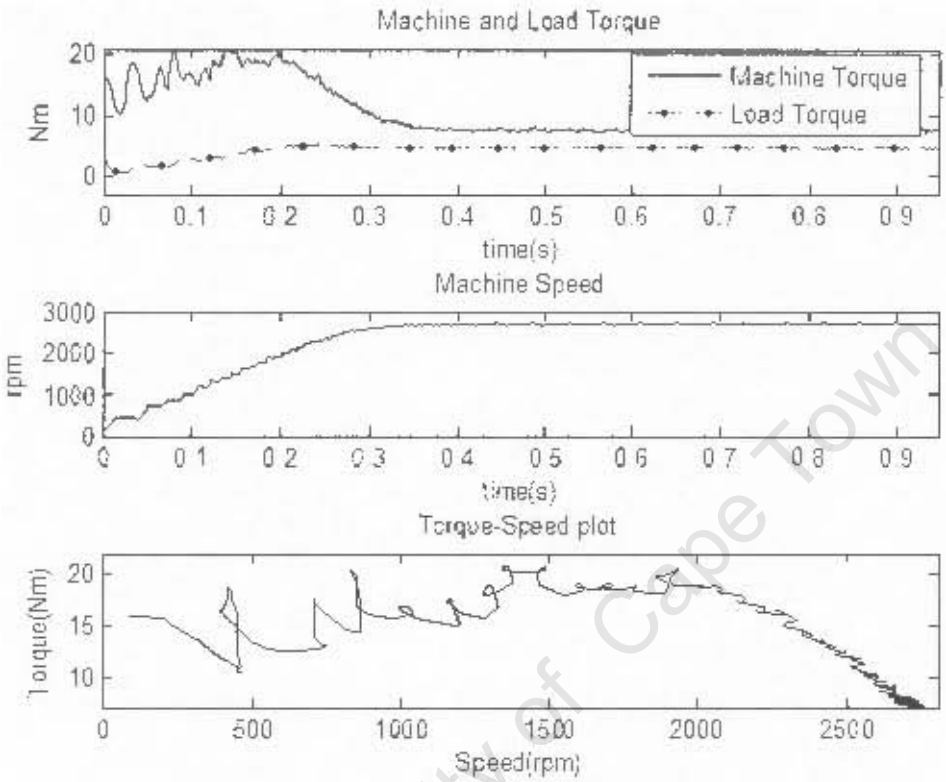

Figure 64: Torque-speed plot of 3kW UCT system with no series capacitor

Here, it can be seen that:

- The induction motor reaches its synchronous speed in approximately 0.4 seconds.
- The induction motor torque reaches a final value as determined by the sum of the load torque and the torque due to friction and windage.
- Although the torque-speed curve has some significant torque-dips in it, these are similar to those of the simulation, but slightly distorted because of too coarse a sampling rate, which was used to collect data over a longer time period.

Voltage and Current plots:

The voltage and current waveforms were captured. The DFFT (Discrete Fast Fourier Transform) was taken (see Figure 65 and Figure 66) to show the contribution of various frequencies to the system.

University of Cape Town

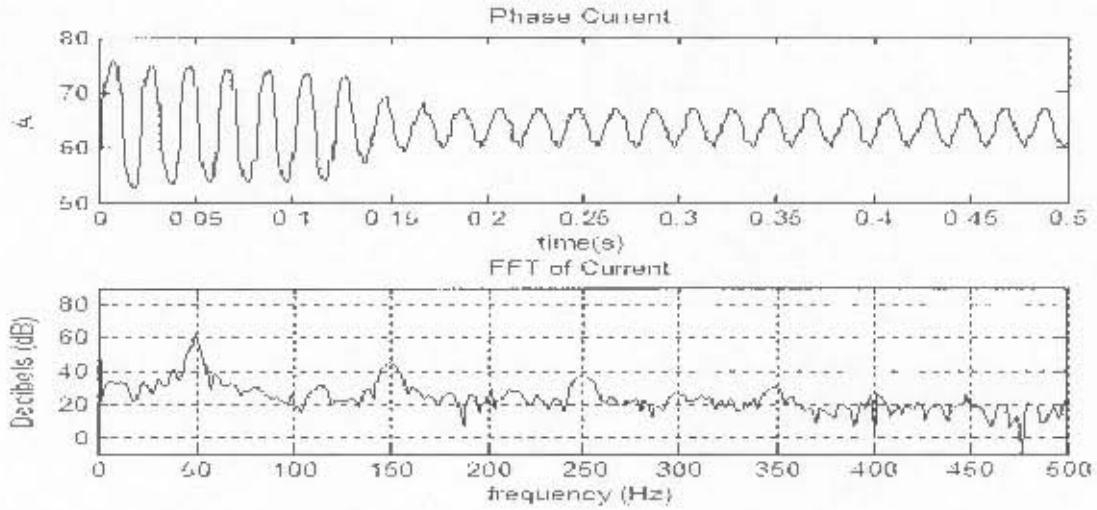

Figure 65: Current and DFFT waveform of 3kW UCT system with no self-excitation

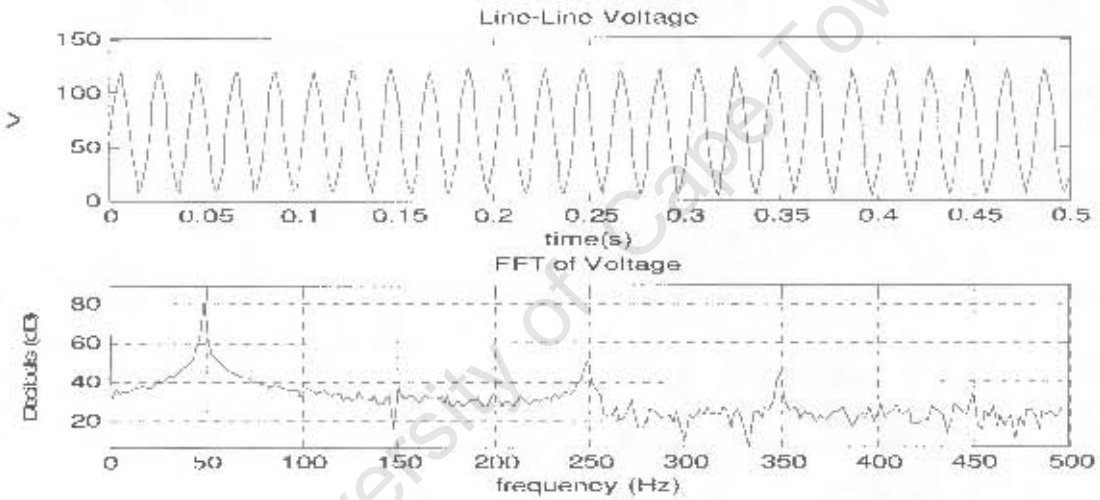

Figure 66: Voltage and DFFT waveform of 3kW UCT system with no self-excitation

University of Cape Town

7.4.2 Induction motor with 100µF series capacitor

Figure 67 shows the torque speed plot obtained when the 3kW UCT system was tested with a 100µF series capacitor, coupled to a ~1kW load.

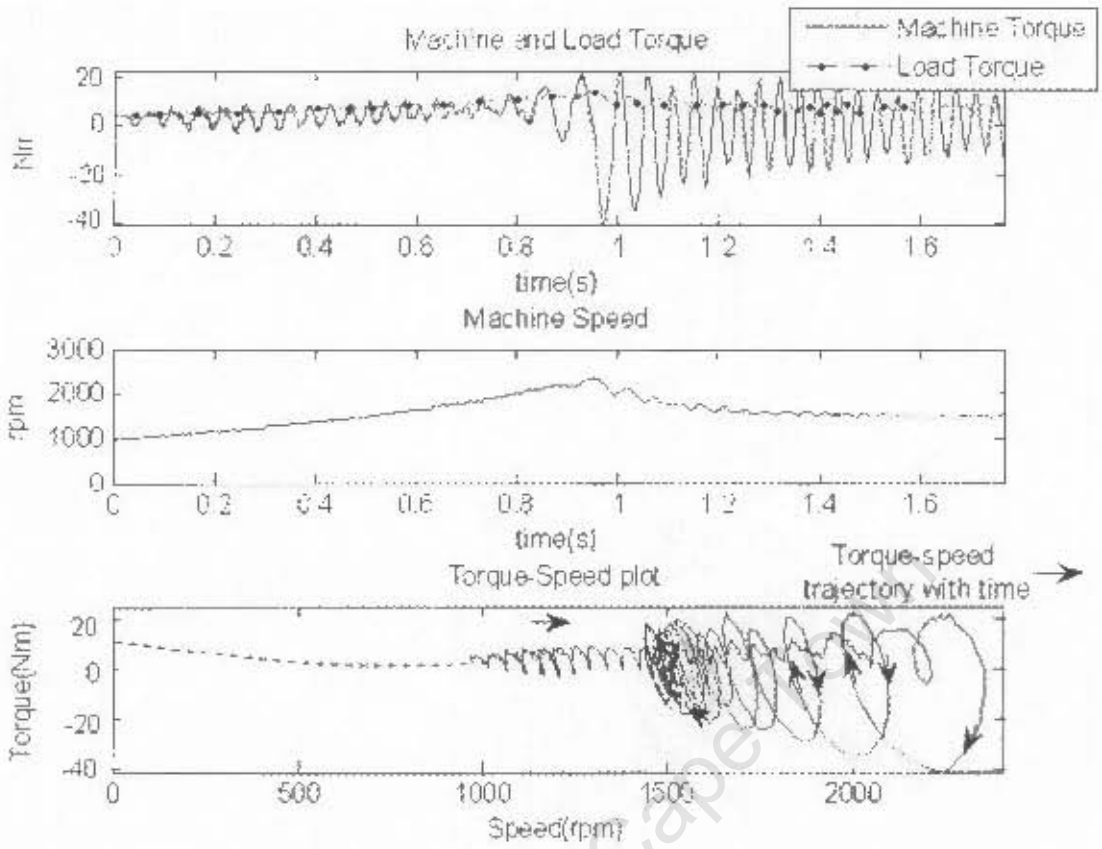

Figure 67: Torque-speed plot of 3kW UCT system with no 100μF series capacitor

It can be seen:

- Firstly, that the induction machine does not reach its synchronous speed,
- secondly, that the torque is more oscillatory here than it was when the IM was run without a series capacitor, in Figure 64.
- More such plots are collected in appendix 'C', showing the repeatability of this experiment, and the way in which the system behaves under different loading conditions, using different capacitor values.

University of Cape Town

Voltage and Current plots:

The voltage and current waveforms were captured while the system was oscillating. The DFFT (Discrete Fast Fourier Transform) was taken to show the contribution of various frequencies to the system.

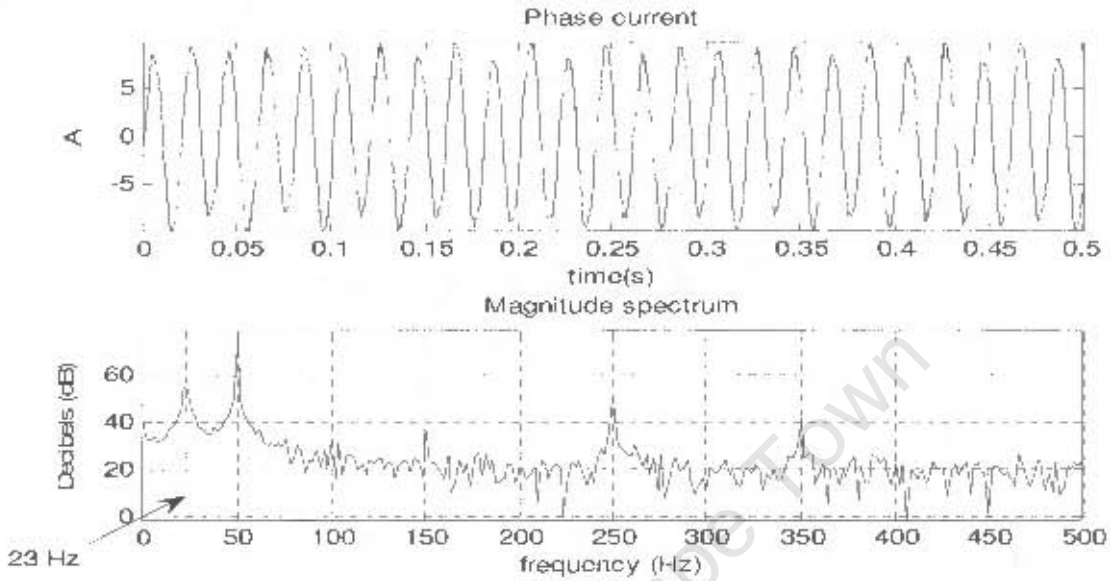

Figure 68: Current and DFFT waveform of 3kW UCT system with 100µF series capacitor

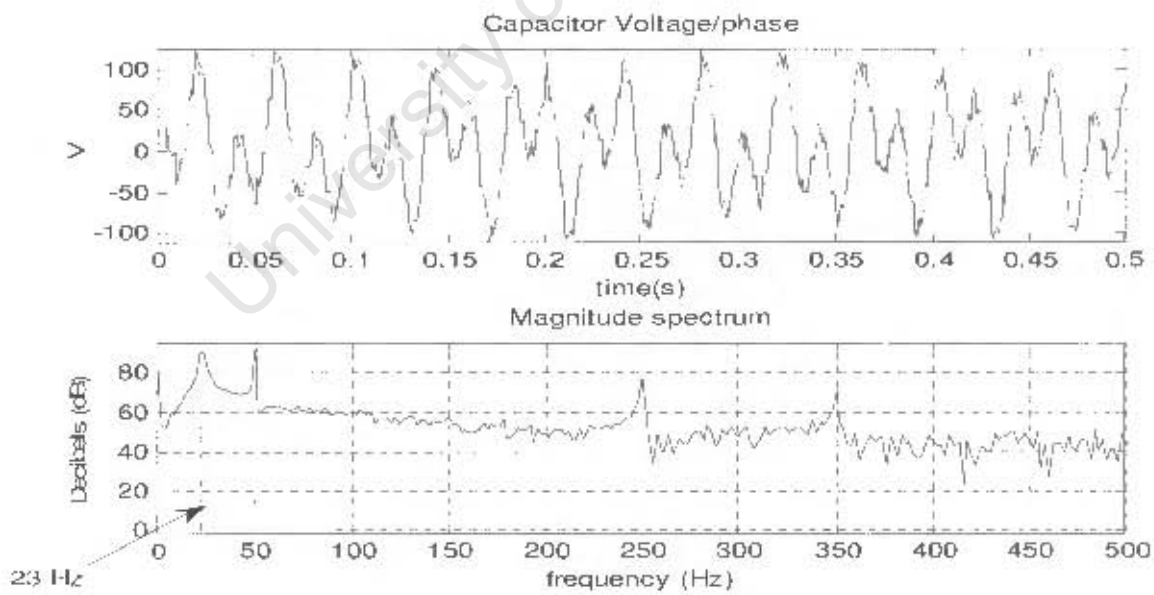

Figure 69: Voltage and DFFT waveform of 3kW UCT system with 100µF series capacitor

University of Cape Town

7.4.3 IM in series with other capacitors

Tests were carried out with the UCT-Lab model to investigate the variation in SSR frequency with capacitance. Results are summarised here and raw data shown in appendix 'B'.

Table 7: Summary of DFFT results collected from the UCT-Lab model

Capacitance (μF)	Average resonant frequency (Hz)	Speed reached by rotor
62	30.5	1810
75	27.5	1700
100	23.5	1400
112	22.8	1360
125	22.0	1350
150	21.0	1240
162	20.0	1230
200	19.3	1220

In chapter 8, these results are plotted on a graph, and the equation of the best-fit line calculated. A best-fit line was plotted in an attempt to establish an empirical relationship between capacitance and the lower resonant frequency. The resulting equation was then examined theoretically, in chapter 8, in order to determine its validity.

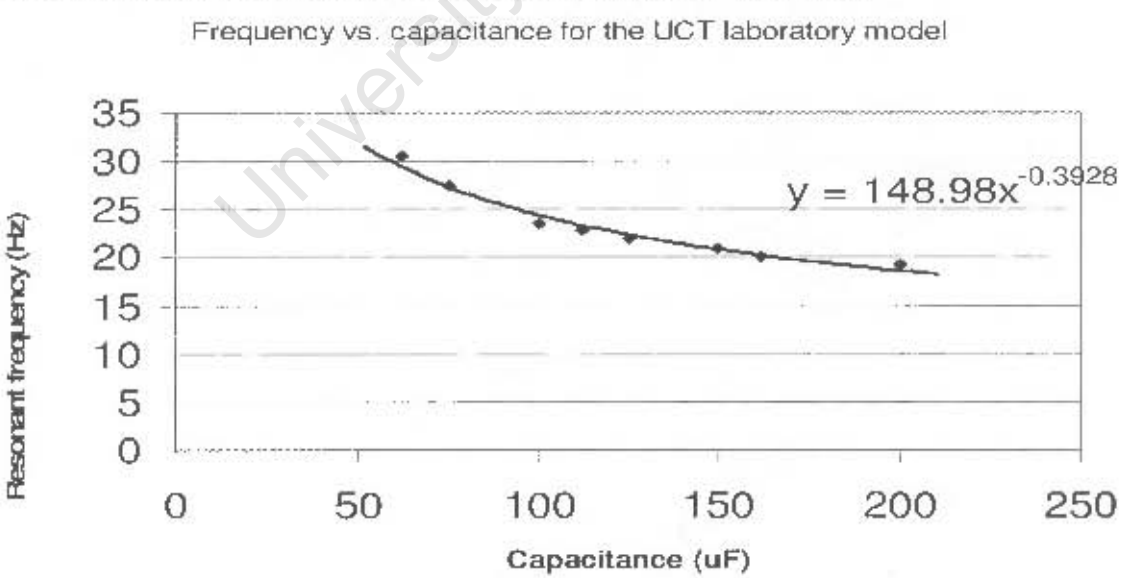

Figure 70: Resonant frequency of UCT-Lab model with different capacitances

University of Cape Town

Figure 70 shows that increasing the series capacitance decreases the resonant frequency. The speed that the rotor reaches is approximately

$$\frac{f_{res}}{50} n_s \tag{7.1}$$

where n_s is the synchronous speed, which is 2800 rpm in this case.

7.4.4 Effect of changing load

Tests were conducted to observe the effect of a changing load on the speed of an induction motor connected in series with a 50μF capacitor:

Two separate tests were conducted:

1. Start-up with load, and then remove it.
2. Start-up with no-load, and then introduce one.

The results are as follows:

1. The induction motor did not run up to speed (27% of synchronous speed), but once the load was released, the induction motor sped up to within 10rpm of the synchronous speed, as shown during the first seven seconds of Figure 71.
2. With no load, the induction motor sped up to within 10rpm of the synchronous speed. However, when the load was applied, the speed did not dip, and remained within 20rpm of the synchronous speed, as shown during the last two seconds of Figure 71.

These results are expected from a self-excitation point of view. If the induction machine settles pre-maturely at a sub-synchronous speed, or the lower resonant frequency, it is expected to reach full speed when loading is removed.

However, a capacitor-IM operating at synchronous speed is not expected to move to a speed corresponding to the lower resonant frequency when loaded, as it has already passed the region that could lead to sustained SSR. Unless the disturbance is very large, and the speed of the rotor drops to within the region where self-excitation will be experienced.

University of Cape Town

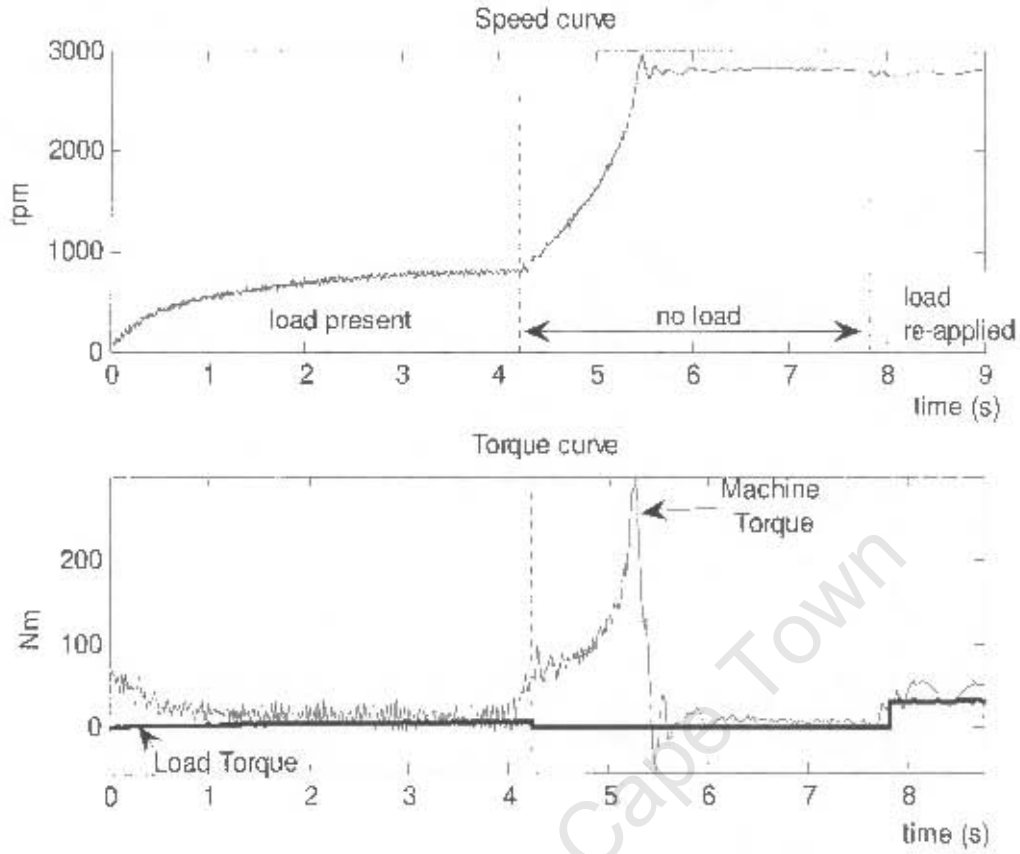

Figure 71: Effect of load change on the UCT 3kW system with a 50μF series capacitor

These tests show how self-excitation influences the speed of an induction machine. At low speeds and high loading, an induction machine connected to some form of series capacitance is likely to settle at a speed corresponding to its lower resonant frequency.

University of Cape Town

7.4.5 Stellenbosch Model Results

Laboratory results for the Stellenbosch Thevenin Equivalent of the CCS (The 'Stellenbosch mini-CCS') are show in Figure 72 and Figure 73. Components were arranged in the lab-setup as shown in Figure 56.

Voltage and current plots and DFFTs:

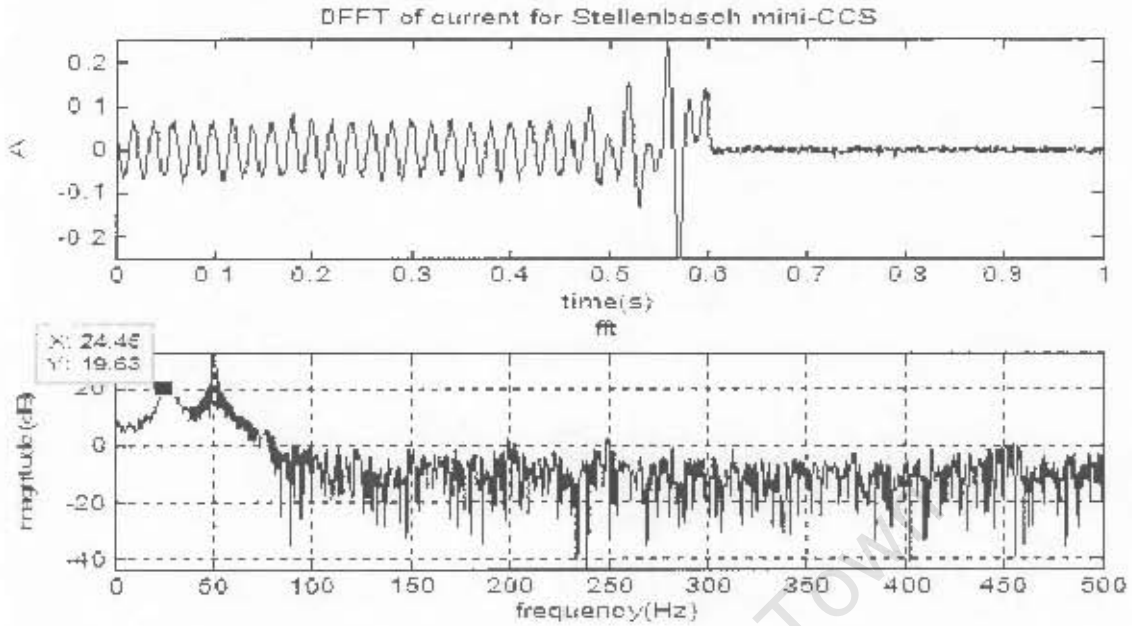

Figure 72: Current DFFT of the Stellenbosch mini-CCS

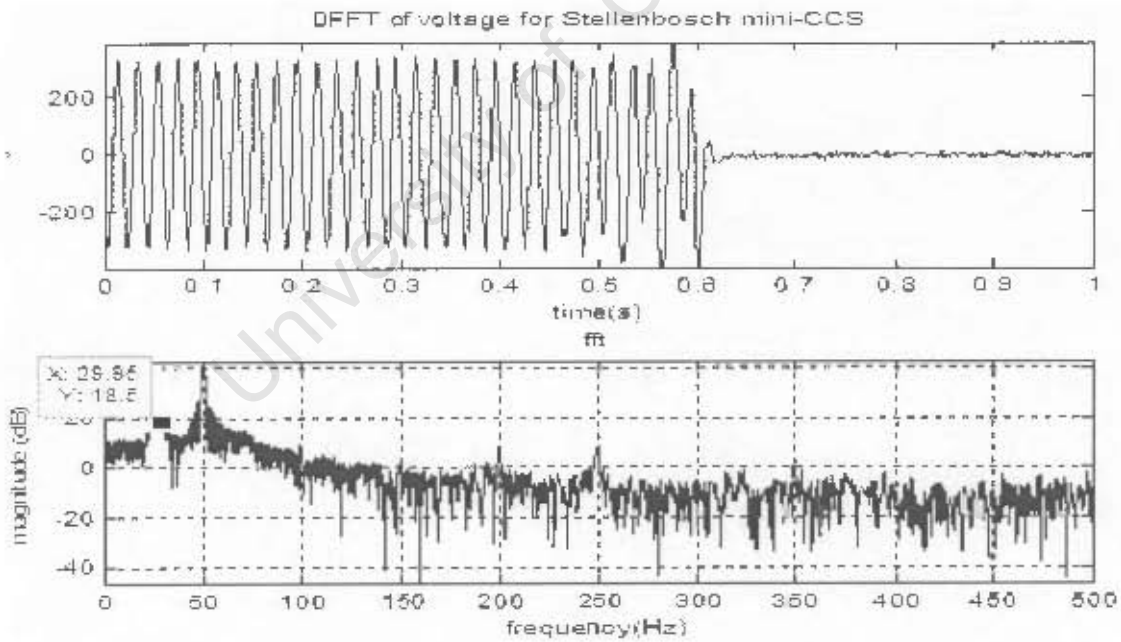

Figure 73: Voltage DFFT of the Stellenbosch mini-CCS

University of Cape Town

From the DFFT plots, it can clearly be seen that there is a dominant sub-harmonic at about 28Hz. This agrees with Wagner's theory of self-excitation; that a sub-harmonic frequency exists, and is the cause of SSR.

7.5 Meru results

Literature of section 2.3 showed that:

- "Severe flicker was experienced when running the (Petronet) motor at 60% of full speed (from the Meru-CCS)" with a strong 40Hz and 60Hz components observed in the voltage DFFT. [16]
- Significantly less flicker was observed at speeds greater than 89% of full speed, with weak 48Hz and 52Hz components observed in the voltage DFFT. [16]
- "The shunt filter at Meru is not the cause of the CCS/Petronet instability." [16]
- "It was shown that the captap system suffers from induction machine self-excitation problems and not from ferroresonance as initially suspected." [18]
- Results showed that "Sub-synchronous modes were found at about 30Hz in the Matlab dynamic analysis and laboratory model, which corresponds with the reported field measurements." [30]
- Two oscillatory modes exist, the lower being at ~30Hz. [30]
- SSR was only observed when the Meru CCS was used. "Normal operating conditions exist when the Petronet load is powered from the Ruston rural 22kV supply." [16]
- "It seems that a resistive load may be run successfully off Meru, provided that no or only very small motors are run from the CCS." However, SSR was also experienced when smaller motors were run from the Meru substation. [16]
- "Two resonant points (31.7Hz and 77.9Hz) occur when Petronet is supplied from the CCS. These increase during high loading conditions to about 33Hz and 86Hz respectively." [15]

In summary, oscillatory modes from Meru-Petronet tests and model results were found to lie within the 30Hz to 40Hz range. Severe speed fluctuations were observed

University of Cape Town

when the Petronet motor was supplied form the Meru-CCS, however such oscillations were not observed when the motor was run from a conventional substation [16], or when the CCS was used to supply power to a resistive load. This behaviour indicates that of the Meru-Petronet system is suffering from self-excitation.

The lower resonant frequency of the system was calculated to be approximately 30Hz by Braae et al [30], corresponding to the oscillations observed at 60% of synchronous speed by Scholder et al. [16] (60% of 50Hz is 30Hz). Nene and Naido [15] calculated such oscillations to lie within a range of 32Hz to 33Hz.

7.6 Solutions to self-excitation that have been proposed

Four methods have been discussed, and are summarised here.

1. **Introduction of series or shunt resistance [23]**

   The use of a series resistor to prevent self-excitation results in a steady-state voltage drop, which is unwanted [18].

   A CCS requires a large compensating inductor to cancel the capacitive effect of the sub-station. This condition leads to the need for a shunt resistance that is equal to the impedance of the capacitor that it is connected in parallel with [23]. Thus, half the power that was to be transferred by the CCS will be consumed by the shunt resistors that are used to prevent self-excitation. This is uneconomical.

   Switching the shunt resistor on and off can solve the power loss problem. Thyristor-based systems are most appropriate for actively damping self-excitation at high power levels [18].

University of Cape Town

2. Current injection using FACTS

The basic function of current injection is to supply the harmonic currents and reactive power demanded by the IM–CCS setup. Because the CCS will not be supplying harmonic currents, it will 'see' whatever load is connected to it as purely resistive. The injector also separates the IM and the CCS preventing a path through which oscillations can build-up.

Although this is a good method of solving the self-excitation problem, it is also costly. In terms of the goal of a CCS as a low-cost means of distributing electricity [1], the cost factor may prove to prohibit this goal.

Based on equation (3.14), and the assumption that $f_{upper} - f_{lower}$ is 30Hz, T1-T2 is half the rated machine torque and the rated IM speed is 2800rpm, then some examples of the approximate current injector sizes required to prevent resonance are shown in Table 8.

Table 8: Typical current injector sizes required to prevent self-excitation

Induction motor size (kW)	ΔT (Nm)	Δf (Hz)	Current injection size required (kW)
0.01	0.015	30	0.0015
0.1	0.16	30	0.015
1	1.6	30	0.15
10	16	30	1.5
100	160	30	15
1000	1600	30	150

From Table 8, it can be seen that 15% of the rated power of the induction motor is typically required to prevent self-excitation. However, these figures are estimates of the actual power that will be required. For results that are more accurate such calculations should be conducted with the aid of the dynamic model developed in chapter 4, and with accurate system parameters.

University of Cape Town

3. Passive filter (Tank circuit)

The filter-bank reduces the upper and lower resonant frequencies of a Wagner's capacitor-IM system. However, the circuit is still unstable, and therefore the passive filter (developed by Hydro-Quebec) is not the solution to self-excitation, as illustrated by Figure 48. It is, however useful in damping ferroresonance [14].

The effects of the passive filter on the UCT and Meru-Petronet systems are similar to those of Figure 48, and hence are shown in appendix 'G'.

4. Control-systems proposal

Because the dynamics of the transfer function representing the CCS-IM system are ultimately controlled by its open-loop pole positions, the system if practically uncontrollable by means of a passive controller, such as a passive filter. Therefore, to prevent self-excitation, either the system configuration must be changed, for example, using a shunt resistor to damp oscillations (see sect. 3.2.4); or the system must be controlled actively using FACTS devices, as discussed in section 3.2.5.

7.7 Summary

The aim of this chapter was to present the various results in a way in which they could be properly analysed and used to validate the hypothesis of sect. 3.4. In the next chapter, the results shall be discussed, as the final stage of the hypothesis validation process.

University of Cape Town

8 DISCUSSION OF RESULTS

Here, results are discussed, and the hypothesis presented in section 3.4 validated/disproved as the results indicate.

At the beginning of chapter 4, certain expectations were proposed regarding the mathematical model to be used in the analysis of self-excitation. The aim of this chapter is to discuss whether the model met those expectations, in order to validate both the model, developed in chapter 4; and the hypothesis of section 3.4, that self-excitation is the cause of SSR. The following questions shall be answered in this chapter as part of this process:

- Can the dynamic model be used to explain how self-excitation leads to SSR?
- Does the dynamic model of Wagner's circuit behave as predicted by Wagner?
- Do the CCS-IM models behave as computer simulations predict?
- Do the results from the various laboratory models concur with predictions of the dynamic model?
- Can the CCS-IM model be used to predict the SSR experienced at the Meru-Petronet System?
- Do research, model results and physical results support the hypothesis that self-excitation is the cause of CCS-IM SSR?
- What are possible solutions to self-excitation?

University of Cape Town

8.1 Can the dynamic model be used to explain how self-excitation leads to SSR?

The way in which SSR occurs can be explained using Figure 74, which shows a zoomed-in region of the Root-Locus diagram of Figure 37, which is typical for a capacitor-IM system. Note; only the upper half of the Root-Locus is shown, as the lower half is symmetrical to it, being its conjugate pair (see section 3.3.3).

Lower resonant frequency:

1. At point (a), the system stable, and therefore the rotor speeds up, moving the system-pole to point (b) on the Root-Locus diagram.
2. At point (b), the system is unstable, resulting in an increase in power used by the resonant circuit (of Figure 21). This means that there is less energy available to accelerate the rotor, and may result in a decrease in rotor speed. This will result in the system-pole moving back to point (a), and so steps 1 and 2 will be repeated, resulting in oscillation. This type of oscillation is referred to as Van der Pol oscillation [34].

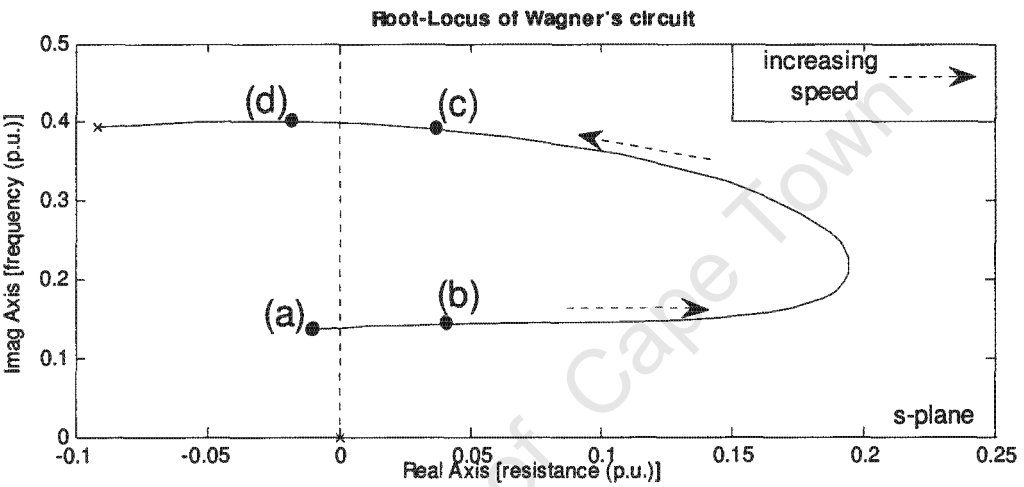

Figure 74: Explanation of how self-excitation leads to SSR using the dynamic model developed

Upper resonant frequency:

3. As the motor speeds up, and the system-pole moves towards point (c), it is becoming less unstable. Hence, the resonant circuit will require less energy, and so there will be more available to accelerate the rotor. Therefore, the rotor speeds up until the system-pole reaches point (d).
4. At point (d), the system is stable, and so will not slow down unless there is a disturbance resulting in:
    i. A decrease in speed that moves the system-pole to any point, on the upper Root-Locus diagram, that has a positive slope. This will result in a repetition of step 2, and therefore cause SSR.

University of Cape Town

ii. A decrease in speed that moves the system-pole to any point, on the upper Root-Locus diagram, that has a negative slope. This will result in a repetition of step 3, and therefore not cause SSR.

8.2 Dynamic model vs. Wagner's predictions

This section answers the question:

"Does the dynamic model of Wagner's circuit behave as predicted by Wagner?"

From the Root-Locus plot, data about the resonant frequency of Wagner's circuit can be deduced. If the top half of the Root-Locus response is super imposed on Figure 58, Figure 75 is obtained:

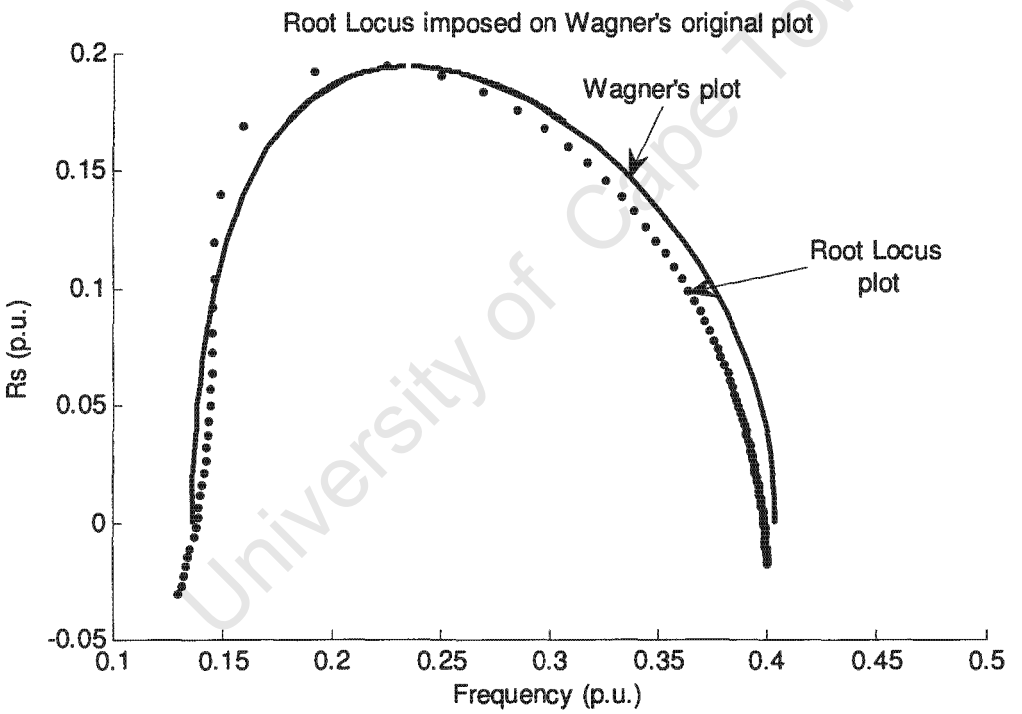

University of Cape Town

Figure 75: Root-Locus imposed on Wagner's plot

It can be seen that the Root-Locus plot closely resembles what was predicted by Wagner. This is to be expected, as each model is valid from a mathematical point of view. The slight discrepancies between the two results can be attributed to subtle model inaccuracies, implying that neither model is complete, but that each is useful.

Because Root-Locus was not an available tool at the time of his research, Wagner did not using it in his examination. Now that it is available, and it has been shown that the two methods predict similar resonant frequencies, Root-Locus can be used instead of Wagner's method, making analysis quicker and easier. Limebeer et al. [35] used a similar approach to the dynamic-systems analysis method used in this study, further validating the use of Root-Locus with respect to SSR of a CCS-IM system.

8.3 Do the CCS-IM models behave as computer simulations predict?

Here, simulations are compared to UCT-laboratory results. It was not possible to use this simulation to compare results of the Stellenbosch or Meru-Petronet systems as data required to do this was not available, such as induction machine equivalent circuit parameters.

8.3.1 System with no self-excitation:

Compared in Figure 76, are the simulated and the physical laboratory results. The induction motor was connected without a series capacitor, and coupled to an approximately 1kW load. This means that the induction motor would be expected to run up to its synchronous speed, and settle there.

University of Cape Town

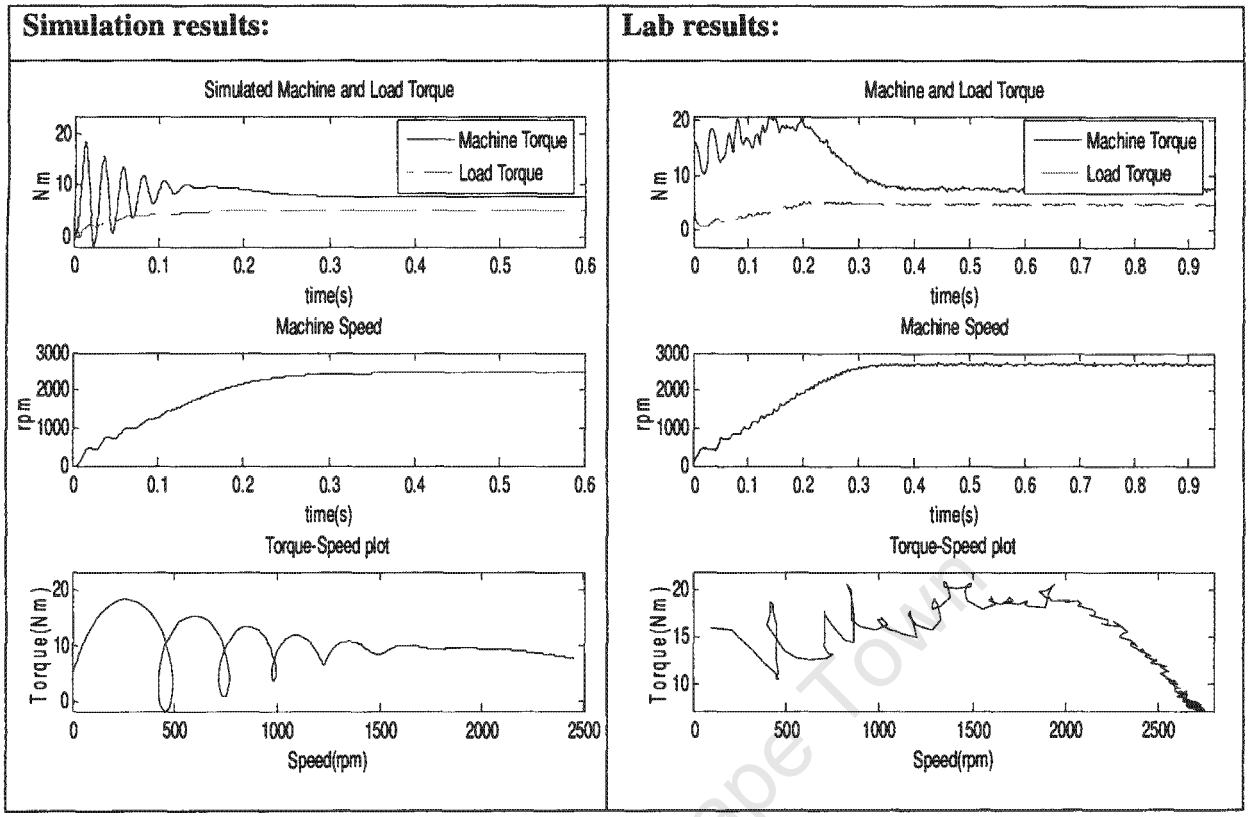

Figure 76: Comparison of laboratory and simulated results for the UCT system with no series capacitor

It can be seen that the simulation and the physical system behave similarly, especially with respect the speed-time plots. The simulated torque is smaller but more oscillatory than the measured torque. These differences shall now be explained:

- The lack of oscillations measured in the laboratory can be attributed to averaging of results in order to reduce the effect of noise. Each data point was obtained by taking the average of it and that of the two samples nearest to it, leading to results being slightly less oscillatory.
- The lower initial torque value of the simulated results can be attributed to torque losses experienced in the physical system. The laboratory IM was coupled to a dc motor, so it has more friction and windage losses, as well as more static friction. These additional losses and the non-linear behaviour of static friction were not modelled by the simulation system.

University of Cape Town

8.3.2 System with self-excitation

In Figure 77, simulation results are compared to those of a physical IM that is connected in series with a 100μF capacitor in, and coupled to an approximately 1kW load.

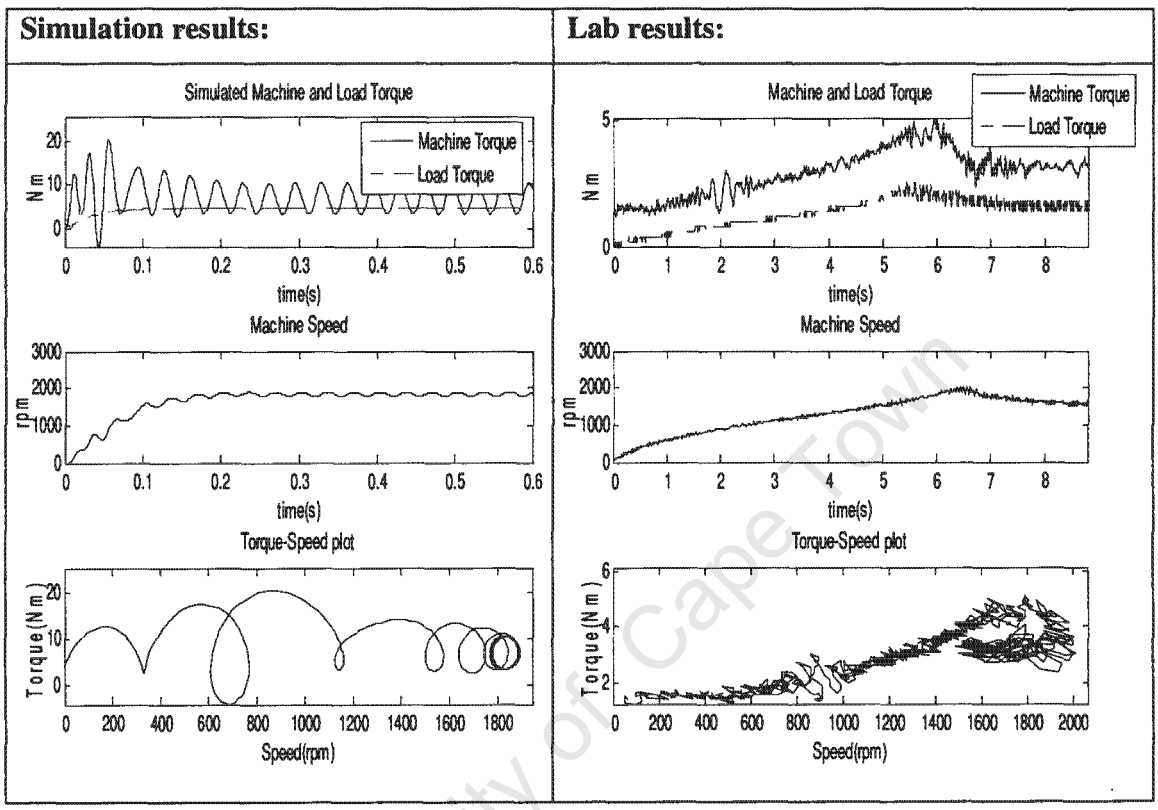

Figure 77: Comparison of laboratory and simulated results for the UCT system with a 100μF series capacitor

We can conclude that the simulation is inaccurate with respect to the time that it takes the IM to speed up. However, it provides useful information about the final speed that will be reached, and the steady-state torque that will be experienced. Such data was useful when building and testing the UCT laboratory model.

It is to be expected that the simulated results do not exactly concur with physical results. The simulator is very specific, and only simulates 'steady-state' self-excitation. The model does not take into account dynamic factors, such as voltage dips, which would slow the IM down. Therefore, the simulator can predict both the speed and torque that an induction motor experiencing self-excitation will reach, but not the time that it would

University of Cape Town

take to reach those values. Simulation data was useful in the design and testing of the UCT physical model.

8.4 Do the results from the various laboratory models concur with the dynamic model predictions?

Central to the hypothesis that self-excitation is the cause of SSR is the mathematical model of the capacitor-IM system. This model was first proposed by Wagner [23], and adapted later by Limebeer [35] so that it could be analysed using Root-Locus.

Figure 75 showed that Wagner's model and the dynamic model of the CCS-IM system were adequately similar, meaning that the latter could be used in lieu of Wagner's model; therefore, simplifying and speeding up associated analysis. It must be reiterated that there are two resonant frequencies for each CCS-IM system. The lower of these frequencies can lead to SSR, whilst the upper frequency will not lead to any lasting form of oscillations. The resonant frequency predictions shall now be compared with laboratory results.

8.4.1 UCT Laboratory system

Laboratory results:

These are shown in section 7.4.

Model predictions:

Examining the lower resonant frequencies, and plotting a graph of frequency vs. capacitance, Figure 78 is obtained:

University of Cape Town

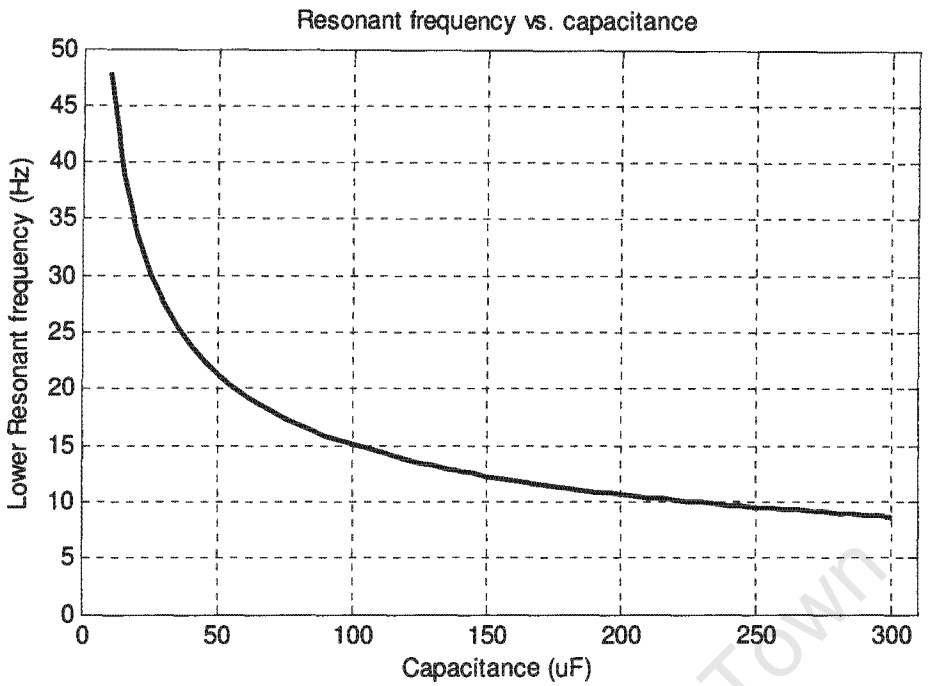

Figure 78: Lower resonant frequency vs. capacitance for the UCT-Lab model

It can be seen that there is a relationship between the resonant frequency and the capacitance of the IM set-up. This relationship is:

$$f_{res} \propto \frac{50\pi}{\sqrt{C_{\mu F}}} \tag{8.1}$$

so,

$$f_{res} \propto \frac{1}{\sqrt{C_{\mu F}}} \tag{8.2}$$

Where $C_{\mu F}$ is the series capacitance, in micro-Farads.

Thus, the resonant frequency is inversely proportional to the square root of the series capacitance. Wagner showed that resonant frequency can be determined using the following equation (see sect. 3.2.1):

$$R_1^2 = -\frac{1}{f_{res}^2}[f_{res}^2(X_m + X_1) - X_C] \times \left[f_{res}^2 \left(X_1 + \frac{X_2 X_m}{X_2 + X_m} \right) - X_C \right] \tag{8.3}$$

Where f_{res} is the resonant frequency.

University of Cape Town

From this equation, the relationship between the resonant frequency and capacitance is not immediately obvious. To test the validity of relation (8.2), some simplification was performed.

Using the Matlab Symbolic Toolbox®,

$$\frac{X_C}{f_{res}} = \frac{Gf_{res}}{2} + \frac{1}{2}\left[(G^2 - 4D)f_{res}^2 + 4R_1^2\right]^{1/2} \tag{8.4}$$

Where:

$$A = X_m + X_1$$
$$B = X_1 + \frac{X_2 X_m}{X_2 + X_m}$$
$$G = A + B \text{ and } D = AB$$

Typically, $(G^2 - 4D)$ is much larger than $4R_1^2$ therefore we can say that

$$\frac{X_C}{f_{res}} \approx \frac{Gf_{res}}{2} + \frac{1}{2}\left[(G^2 - 4D)f_{res}^2\right]^{1/2} \tag{8.5}$$

Because G and D are constant,

$$X_C \propto f_{res}^2 \text{ and so, } \frac{1}{C} \propto f_{res}^2$$
$$\text{or } f_{res} \propto \frac{1}{\sqrt{C}} \tag{8.6}$$

This means that equation (8.2), relating resonant frequency to capacitance is valid.

It must be noted that the predicted frequency is lower than the actual resonant frequency experienced in the laboratory. To investigate the reason that the difference exists, some sensitivity analysis of the mathematical model is required. This means that predictions need accommodate the possibility of incorrect parameter values.

To perform the sensitivity analysis, each parameter is varied by ±20% of its calculated value.

University of Cape Town

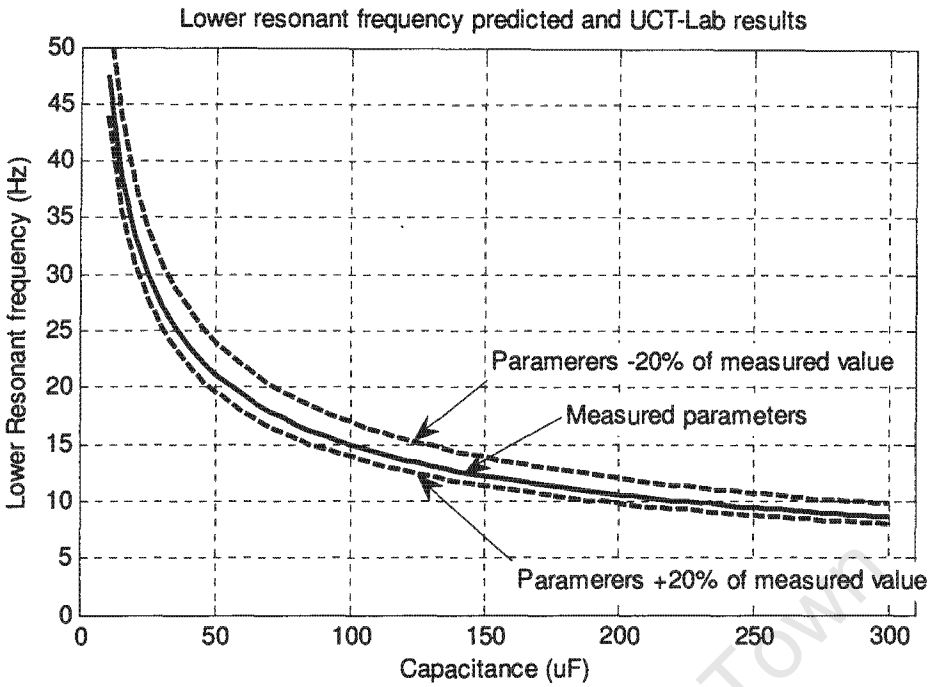

Figure 79: Sensitivity plot of lower resonant frequency vs. capacitance for UCT-Lab model

It can be seen that for each capacitance value there is a range of possible f_{res} values. A better sensitivity analysis would be one in which all the possible combinations of incorrect parameters were tested. Such a sensitivity analysis was conducted and results are shown in appendix 'H'. They are not included in the body of the thesis because the range of results fell within the same region as those of Figure 79, unless parameters were varied by ±50% of their measured value.

Laboratory results compared to theoretical predictions

As a way of concluding, the predicted results are plotted on the same graph as the actual UCT laboratory results, from Table 7, in Figure 80.

University of Cape Town

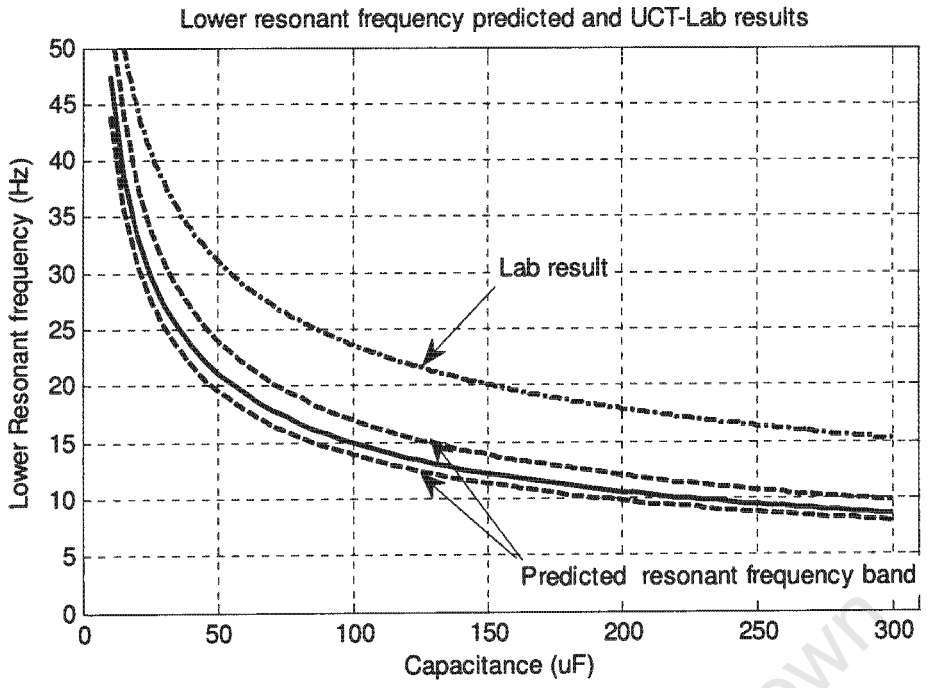

Figure 80: Comparison of UCT-Lab and predicted results

The equation of the predicted results is:

$$f_{res} = \frac{157}{(Cap\ in\ \mu F)^{0.5}}$$

Whilst that of the laboratory results was:

$$f_{res} = \frac{149}{(Cap\ in\ \mu F)^{0.4}}.$$

In both cases, f_{res} is approximately proportional to $\sqrt{Cap\ in\ \mu F}$. The agreement of the theoretical calculations [see equations (8.3) to(8.6)] with empirical results indicates the presence of self-excitation in the physical system.

Model predictions do not exactly match lab results, but the general trends are the same. This implies that the model is correct, but not complete. Influences such as, the effect of the type of rotor (deep-bar/ squirrel-cage) have not been included in the model.

Note that the speed that the rotor reaches is predominantly determined by $\frac{f_{res}}{50} n_s$. This is to be expected because when the system is oscillating, the sub-synchronous component is

University of Cape Town

more dominant than the supply (50Hz in this case), and so has the biggest influence on the rotor speed.

The effect of load change on an induction motor connected to a 50μF series capacitor:

The results of Figure 71 are expected from a self-excitation point of view. If the induction machine settles prematurely at a sub-synchronous speed, or the lower resonant frequency, it is expected to reach full speed when loading is removed.

However, a capacitor-IM system operating at synchronous speed is not expected to move to a speed corresponding to the lower resonant frequency, as it has already passed the region where it could possibly become unstable. Except in the case where the disturbance is very large or the IM is re-started, so that the speed of the rotor drops to within the region where self-excitation could result. This implies that a current injector, or damping device, is only required to 'pull' a CCS-IM system past the region in which SSR is likely to occur. Once the induction motor is running at or close to its synchronous speed, the device will no longer be required, unless there is a large speed disturbance, or the motor is required to run at a speed with in the SSR region, using a speed control device, such as a VSD.

University of Cape Town

8.4.2 The Stellenbosch Mini-CCS

Model predictions shall be compared to the results obtained from the Mini-CCS at Stellenbosch.

Test results:

Firstly, the 65kW induction motor under test at Stellenbosch was found to run up to within 2% of its synchronous speed (n_s). The fact that the IM motor was unloaded would explain why the motor did not get 'stuck' at a lower speed.

Data was collected from Stellenbosch during a number of visits. Johan Beukes, who was involved in the project, compiled a report of data that he collected.

Table 9: Results collected from the Stellenbosch Mini-CCS		
	Resonant frequency	Speed reached by rotor
Results 1	24 Hz	98% n_s
Results 2	30 Hz	98% n_s
Results 3	26 Hz	98% n_s
Results 4	28 Hz	98% n_s
Average	**27 Hz**	**98% n_s**

Predicted results and sensitivity check:

In chapter 7 predictions were made for the Stellenbosch Mini-CCS, predicting a lower resonant frequency of 21Hz. This is smaller than the physical 27Hz test result.

Because of the unavailability of induction machine parameters for the IM that was used at Stellenbosch, the parameters were estimated. The estimation was based on parameters of a 100HP (74kW) IM as given in the Matlab Power Systems Toolbox®. There is therefore an immediate possibility of error, which is the reason that a sensitivity plot is once again used to predict the lower resonant frequency.

There is less uncertainty about the capacitance and inductance of the CCS; therefore, those parameters are only varied by ±5%. The IM parameters are varied by ±20%.

University of Cape Town

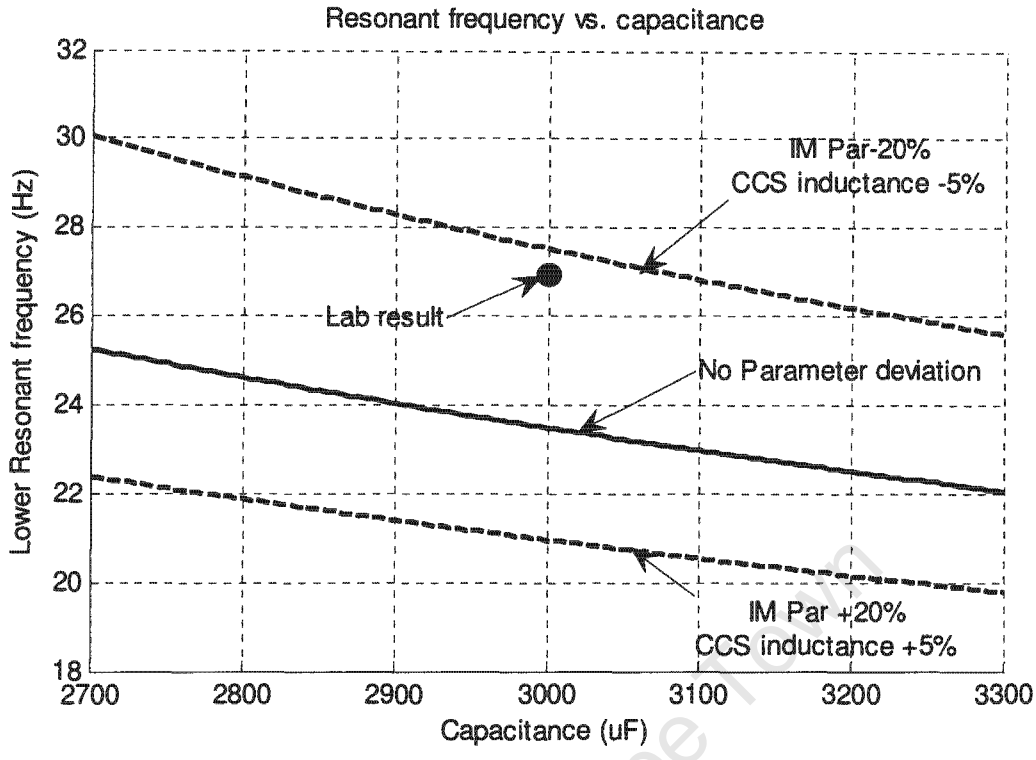

Figure 81: Sensitivity plot of f_{res} vs. capacitance for Stellenbosch Mini-CCS

The laboratory-measured resonant-frequency falls inside the sensitivity band of the previous figure. This means that IM parameters used are slightly incorrect but that the dynamic model is useful in approximating resonant frequencies.

8.4.3 The Meru-Petronet system

Based on both the scale and remoteness of the Meru-Petronet system, the author was unable to do any testing in person. Therefore, all results that are presented here have been collected from technical and research reports conducted on the system. On average, voltage and current oscillations were reported to consist of a strong 30Hz to 33Hz component.

Once again, the actual parameters of the Petronet IM were unavailable, and needed to be estimated. This estimation was done based on IM parameters used by Schilder in her Digsilent simulation (see appendix 'F') of the Petronet-Meru system. However, accurate

University of Cape Town

data with respect to the capacitance and inductance of the Meru-CCS was available, as verified by Scholder et al. [16].

A sensitivity plot of the possible resonant frequencies is plotted:

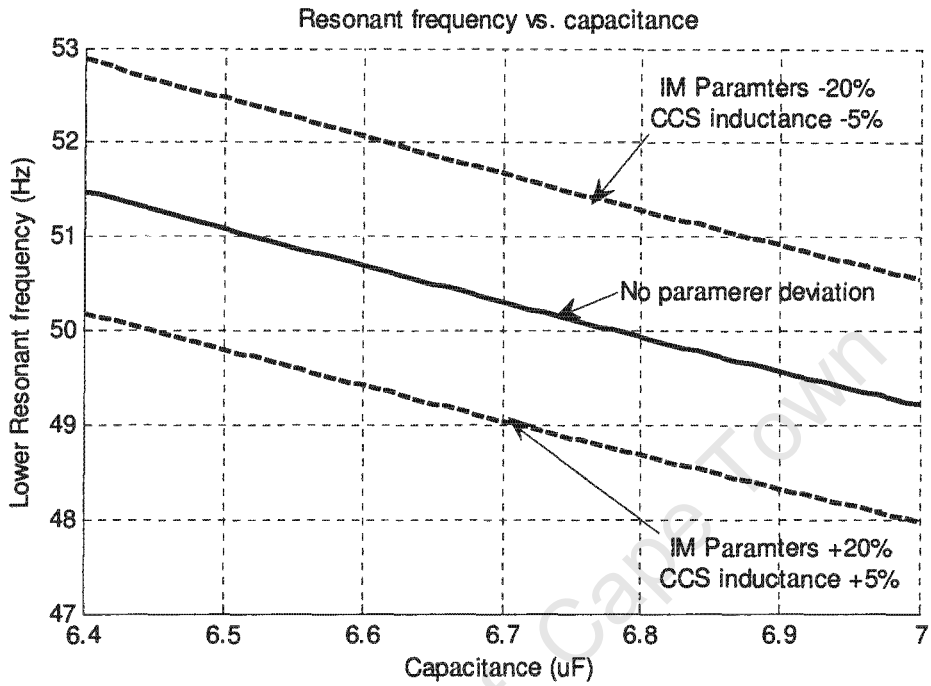

Figure 82: Sensitivity plot of f_{res} vs. capacitance for Meru-Petronet system

The resonant frequency was predicted to be about 50Hz using the dynamic model. However, it was reported to lie between 30Hz and 33Hz. Thus, the predicted resonant frequency is 17Hz and 20Hz higher than that of the actual system. For the Meru system, IM parameters were not measured, and were based on predictions made by Schilder (see appendix 'F'). This is a source of error, and with accurate parameters, the predicted results could resemble actual results more closely.

Another reason that the predicted and actual results did not correlate could be due to model inaccuracies. It was not known what type of induction machine was used by Petronet. Subtle changes to its makeup such as a deep-bar squirrel cage would result in a different equivalent circuit, and therefore cause model inaccuracies. The assumption that the source was ideal, and that the transmission network did not influence results, also makes results less accurate. This leads to the question:

University of Cape Town

8.4.4 Can the CCS-IM model be used to predict the SSR experienced at the Meru-Petronet System?

The dynamic model has been shown to predict and explain SSR well. However, the weakness of the model is its sensitivity. Before accurate Meru-Petronet predictions can be made, the parameters and characteristics of the Petronet IM must be known. Slight model adjustments as well as the inclusion of the transmission network in the model would also need to be made before it would be useful in designing systems such as the Meru CCS.

8.5 Do research, model results and physical results support the hypothesis that self-excitation is the cause of CCS-IM SSR?

In chapter 2, research of similar SSR studies that have been conducted showed signs of self-excitation to be present [see section 2.3]. Literature studied in chapter 3 revealed that the current and voltage oscillations associated with a CCS-IM system were caused by self-excitation, and not ferroresonance. In chapter 4, a mathematical, dynamic-systems model was developed to represent a CCS-IM system. It was shown (Figure 75) that the model developed behaved in a very similar to an existing model developed by Wagner [23].

Although theoretical predictions did not exactly match the physical results obtained from the UCT, Stellenbosch or Meru systems, such differences were attributed to parameter and model inaccuracies. Theoretical and predicted capacitance vs. frequency results of the UCT laboratory model were found to follow similar mathematical trends, strengthening the validity of the model. The way in which the UCT laboratory model reacted to changes in loading (see Figure 71) showed it to behave in a way that was expected of a system experiencing self-excitation.

This information leads to the conclusion that self-excitation is the cause of SSR associated with a capacitor-IM system.

University of Cape Town

8.6 Various solutions to self-excitation

Using resistance to prevent self-excitation is possible, as shown by results of authors such as Wagner [23] and Limebeer et al. [35], and concurs with theoretical predictions. In the case of a CCS, this is not a viable solution because of the high power loss incurred through such resistors.

The filter-bank (developed by Hydro-Quebec to damp ferroresonance) brings the upper and lower resonant frequencies of a CCS-IM system closer together, resulting in less energy being required to prevent SSR. However, the circuit is still susceptible to SSR, and is not useful in preventing self-excitation. This is to be expected, because the dynamics of the transfer function that represents the CCS-IM are ultimately controlled by open-loop pole positions, which means that the system is practically uncontrollable, by means of a passive controller, such as a passive filter. (See section 4.6.)

The use of FACTS systems to prevent self-excitation was shown by J. Beukes [33] to be a viable solution to self-excitation. Aghazadeh et al. [21] also showed that the power-loss through damping resistors could be reduced by actively switching damping resistors in and out of the circuit.

To prevent self-excitation, either the system configuration must be adjusted, for example, by inserting series resistance into the CCS circuit; or the system must be controlled actively with FACTS devices, such as a current injector. It must also be noted that damping or current injection is only required to 'pull' a CCS-IM system past the region in which SSR is likely to occur. Once the induction motor is running at or close to its synchronous speed, such devices will no longer be required; unless there is a large speed disturbance, or the motor is required to run at a speed within the SSR region using a speed control device, such as a VSD.

University of Cape Town

8.7 Summary

Based on the analysis of the results presented in this chapter, it was seen that:

- The way in which self-excitation can cause SSR was logically explained using the model developed in chapter 4.
- The dynamic model of Wagner's circuit did behave as predicted by Wagner.
- Simulations were valuable in predicting steady-state speed and torque values that at CCS-IM system is likely to reach.
- Research, model results and physical results support the hypothesis that self-excitation is the cause of CCS-IM SSR.
- The capacitor vs. resonant frequency trends for the UCT laboratory model concurs with those obtained from the dynamic model developed.
- With accurate equivalent circuit parameters, some small model adjustments and the inclusion of the transmission system, the CCS-IM model could be used to predict the SSR experienced by the Meru-Petronet System.

Based on theory studied, and results obtained, there is strong evidence supporting the hypothesis (presented at the end of chapter 3) that the cause of CCS-IM SSR is self-excitation.

University of Cape Town

9 CONCLUSIONS

From the findings of this dissertation, conclusions are made.

9.1 Overview

At the beginning of this thesis, it was stated that the overall aim was to determine the cause of SSR experienced at the Meru-Petronet system, and other similar systems, and investigate various compensation techniques. After the cause had been established, it was required that various compensation techniques be investigated.

All aspects of the CCS and induction motor were studied in the search for the cause of SSR. After becoming familiar with the components and concepts involved, documents referring to similar resonance problems were studied. Reports associated with the Meru-Petronet system indicated that either self-excitation or ferroresonance was the cause of SSR. Beukes et al. [18], Limebeer et al. [35] and Ojo [29] and attributed the cause of SSR to self-excitation. Other authors such as Schilder et al. [16], Braae et al. [30] and Nene et al. [15] also studied SSR associated with the Meru-Petronet system, documenting oscillatory modes at about 30Hz and 70Hz. It was also found that the ferroresonance filter worked properly, and was not the cause of oscillation [30, 16].
These reports revealed that SSR was most likely caused by self-excitation. For the purpose of completion, the possibility of ferroresonance being the cause of SSR was also investigated, as it was initially suspected to be the problem [18]. For these reasons, a hypothesis was made stating that ferroresonance or self-excitation were the most likely causes of SSR, and therefore, literature specific to ferroresonance and self-excitation was studied in chapter 3

Ferroresonance arises because of inductor saturation. At Meru, non-saturable inductors were used, as well as a ferroresonance-filter (developed by 'Hydro-Quebéc'). Ferroresonance causes dangerous over-voltages and current spikes, which lead to SSR. SSR was experienced, but no excessive over-voltage or current spikes were observed.

University of Cape Town

These findings, in conjunction with those of Beukes et al. [18] show that ferroresonance was not the cause of SSR associated with the Meru-Petronet system.

Self-excitation is a result of the undamped propagation of natural currents within a capacitor-induction-motor circuit (Wagner [23]). Self-excitation results in SSR, at frequencies typical to those experienced in the Meru-Petronet system.

The initial literature study revealed that the nature of the current and voltage oscillations, with respect to their frequency, amplitude and the effect they had on the rotor speed of the induction machine, support the possibility that self-excitation is the cause of resonance and not ferroresonance. The hypothesis was therefore refined to state: "SSR associated with a CCS-IM system arises because of an interaction between the CCS and IM. The most significant cause of such SSR is self-excitation."

In chapter 4, a mathematical, dynamic-systems model in the form of a transfer function was developed to represent a CCS-IM system. It was shown to replicate the model of self-excitation developed by Wagner [23] accurately (see Figure 75). Useful insight into the dynamics of a CCS-IM system, and the methods that can be used to prevent SSR were found by analysing its transfer function, using Root-Locus.

Root-Locus analysis of the transfer function, which represents the CCS-IM system, showed that a passive controller could not suitably damp SSR, meaning that the system is uncontrollable by means of a passive filter. Therefore, in order to prevent SSR either the system configuration should be changed; or active control, using FACTS devices is required. These prevention techniques are required to supply energy to the CCS-IM system during the rotor speed range where it is susceptible to SSR. Therefore, a relatively simple starting sequence could be used to start an IM using a CCS where the IM is required to run at close to rated speed. However, in the case where a speed control device, such as a VSD, is used to control the rotor to a speed falling within the region where self-excitation is likely to occur, such a starting sequence would prove ineffective. Instead, semi-permanent current injection would be required.

University of Cape Town

It was found that it might prove more economical not to compensate a CCS inductively. In this way, less energy will be consumed by shunt resistors. With compensation, shunt resistors use ~50% [18] of the power supplied to a CCS in order to damp self-excitation, but without compensation, resistors use less than 16% [23] of that power. In both cases, there is energy loss, which is bad practice in a time where energy is an increasingly scarce and precious commodity.

A 'steady-state' simulation of self-excitation was developed that did not predict transients well. However, it was useful for predicting speed and torque values that an induction-motor experiencing self-excitation would be likely to reach. This was because the simulation replicated voltage and current conditions as supplied by a CCS when experiencing SSR. The simulation was useful in designing and testing results of the UCT laboratory model. A physical model was built at UCT to replicate self-excitation. Results from this model were captured using a data logger that was developed for the project. Data was then analysed, and used in the study of self-excitation.

Although theoretical predictions did not exactly match the physical results obtained from the UCT, Stellenbosch or Meru systems, such differences were attributed to parameter and model inaccuracies, as well as the assumption that the voltage source was ideal, and therefore the transmission system was omitted from the model. Theoretical and predicted capacitances vs. frequency results for the UCT laboratory model were found to follow similar mathematical trends, thereby strengthening the validity of the model. The validity of the model was further strengthened by the way in which the UCT laboratory model reacted to changes in loading showed it to behave in a way that was expected of a system experiencing self-excitation.

Based on the preceding theoretical and empirical data and the relationships that were drawn from the data, there is strong evidence supporting the hypothesis that self-excitation is indeed the cause of SSR associated with a CCS-IM system.

University of Cape Town

9.2 Main findings

Special mention of the following must be made:

- After a preliminary research study, either ferroresonance or self-excitation was identified as the most likely causes of SSR.
- Ferroresonance arises as a result of inductor saturation.
- Over-voltages associated with ferroresonance were not observed at the Meru, Stellenbosch or UCT systems. With ferroresonance prevention systems in place at the Meru CCS, SSR was still experienced.
- Self-excitation is a result of the undamped propagation of natural currents within a capacitor-IM circuit (Wagner [23]).
- Self-excitation can result in SSR, at frequencies typical to those experienced in the Meru-Petronet system.
- Numerous authors suggest that self-excitation is the cause of SSR typical with CCS-IM scenarios.
- Wagner's [23] model of self-excitation was studied, and a dynamic-systems model developed that replicated his model. This model could easily be modified when required to represent similar systems.
- Laboratory results showed signs of self-excitation, evident in the resonance frequencies observed, rotor speeds reached; and the way in which the UCT laboratory model reacted to changes in load, and capacitance, which agreed with theoretical predictions.
- The dynamics of the transfer function that represent the CCS-IM system are ultimately controlled by open-loop pole positions, which means that the system is uncontrollable by means of a passive filter.
- To prevent self-excitation, either the system configuration must be adjusted; for example, by using a shunt resistor; or the system must be controlled actively using FACTS devices.
- It must also be noted that damping or current injection is only required to pull a CCS-IM system past the region in which SSR is likely to occur.

University of Cape Town

The following must also be mentioned:

- The possible return on investment is 1:14, provided a solution to the instability problem is found. Eskom will benefit in the future should the CCS technology be made successful. [16]
- A dynamic-systems approach to the CCS-induction machine system was valuable when investigating the likelihood of self-excitation and the effectiveness of various compensation techniques.
- Compensating inductance in a CCS cancels the reactive effects of the CCS, making the CCS an ideal source at supply frequency.
- A compensated CCS will not improve the power factor of the overall grid network to which it is connected, assuming that the overall grid is slightly inductive in nature.
- Compensating inductance significantly increases the power that is wasted through shunt resistors, if they are used to prevent self-excitation.
- The dynamic model did not take into account the influence of differences between induction machines, such as the various types of rotors; resulting in inaccuracies. The influence of the transmission network was also excluded to allow a greater emphasis to be placed on an analysis of the phenomenon of SSR.
  Such differences do not have a significant effect on the underlying structure of the model.
- The Stellenbosch motor was unloaded resulting in less power being required to damp any oscillations that did occur.
- Indications are that smaller (100 kVA to 170 kVA) capacitive coupled substations (CCS) have been built and used successfully in Canada, Mexico and South America. [16]
- The Meru CCS was tested successfully with resistive loads.
- With accurate equivalent circuit parameters, motor information, and possibly small model adjustments, the CCS-IM model can be used to predict the frequency at which SSR will occur and determine the size of the current injector or shunt resistance required to prevent SSR resulting form self-excitation, for systems such as Meru-Petronet setup.

University of Cape Town

10 RECOMMENDATIONS

Based on the conclusions that have been made, the following is recommended:

- Ferroresonance is not the cause of the SSR under investigation, and future CCS-IM work should not focus on this. However, the possibility of it occurring in such a system should not be overlooked.
- Research has shown that self-excitation is the cause of SSR associated with a capacitance connected in series with an induction motor. Techniques of damping self-excitation should therefore be developed further.
- A dynamic model was developed that replicated Wagner's [23] model of self-excitation. The model was adapted as required, and should be used when designing a CCS-IM system.
- The dynamics of the transfer function that represents the CCS-IM system are controlled by open-loop pole positions. Therefore, a passive filter is not an adequate solution to CCS-IM SSR prevention.
- To prevent self-excitation, either the system configuration must be adjusted, or FACTS must be used to damp SSR actively.
- Damping or current injection is only required to pull a CCS-IM system past the region in which SSR is likely to occur. Therefore, such a system should be sized with this in mind. Smaller injectors or dampers being required for IMs that run at approximately their synchronous speed, and larger systems for IM that are controlled to specific speeds.
- It is advisable not to use CCS technology to supply power to induction motors until self-excitation problems have been resolved. However, the technology can presently be used to supply power to remote communities that use predominantly resistive loads.

University of Cape Town

10.1 Future work:

- Adapt the dynamic model so that it takes into account the influence of the supply voltage and transmission system on resonant frequency predictions.
- Load the Stellenbosch motor so that the active filter can be tested for worst-case SSR conditions.
- Measure the equivalent circuit parameters, obtain data about the makeup of the Petronet induction-motor, and adjust the model accordingly. In this way, the CCS-IM model can be used accurately to assist in the design of a method to prevent self-excitation and therefore SSR of the Meru-Petronet System.
- It may be more economical not to compensate a CCS inductively. In this way, significantly less power will be required by shunt-resistors to prevent self-excitation. Such a technique could be incorporated as a short-term starting sequence. In addition, as most electricity networks have a slightly inductive nature, the overall grid-power-factor will be improved by the capacitive effect of a CCS. More work should to be done to investigate the suitability of these proposals.

University of Cape Town

References:

[1] H.G. Sarmiento, R.de la Rosa, V. Carrillo, J. Vilar, '*Solving Electric Energy Supply to Rural Areas, The Capacitive Voltage Divider.*' IEEE. Morelos, Mexico., 1989.

[2] J. W. Butler, C. Concordia, '*Analysis of Series Capacitor Application Problems.*' AIEE. Transactions, vol. 56, pp. 975–988, August 1937.

[3] L. Stubbs, '*Tapping power from high voltage transmission lines using insulated lightning shield-wires and series compensation.*' MSc. Thesis, Witwatersrand University, Johannesburg, South Africa, 1994.

[4] N. Knudsen, '*Technical problems arising from the use of series capacitors.*' ASEA Journal, ASEA reg. 7234. 733, 1950.

[5] R. Wilde, '*Customer service direct from transmission lines.*' Saskatchewan Power Corporation, Regina, Saskatchewan. 1980.

[6] M. Sanaye-Pasand, R Aghazadeh '*CCS Ferroresonance Prevention Using Power Electronic Devices*' University of Tehran, Iran, 2003.

[7] '*Laboratory session 8. Squirrel cage induction motor characteristics.*' Milwaukee School of Engineering. [Online] Available: http://people.msoe.edu/~saadat/EE-340Exp8.pdf, 10 October 2005.

[8] P.C.Sen '*Principles of Electric Machines and Power Electronics, Second Edition.*'. John Wiley and Sons. Ontario, Canada. 1997.

[9] K. Reeves '*The Design and Implementation of a 6kW Wind Turbine Simulator.*' BSc. Thesis, University of Cape Town, South Africa. Oct 2004.

University of Cape Town

[10] J. de Kock, '*Industrial Power System Stability*' MSc. Thesis, University of Stellenbosch, South Africa. Oct. 1987.

[11] M. Braae, lecture notes: '*Control Engineering 1, Second Edition*' University of Cape Town, South Africa. 2001.

[12] Mohan, Underland, Robins, '*Power Electronics: Converters, Applications and Design Third Edition.*' USA. John Wiley and Sons. 2003.

[13] A. Langsdorf, '*Theory of Alternating Current Machinery, Second Edition.*' Tokyo, Japan. McGraw-Hill Book Company, inc. 1937.

[14] L. Bolduc, B. Bouchard, G. Beaulieu, '*Capacitive Divider Substation*' Quebec, Canada. IEEE Transactions on Power Delivery. Vol. 12. No 3. pp. 1202-1209 July 1997.

[15] M.B. Nene, R.M. Naidoo, "Harmonic penetration from capacitor coupled sub-stations.", procured from the South African Universities Power Engineering Conferecne (SAUPEC). South Africa, 2004.

[16] M. Scholder, A.C. Britten, M.E. Mathebula '*Evaluation of a 275KV TO 22KV Capacitor Coupled Substation.*' Eskom Resources and Strategy Research Division, South Africa, 09 OCT 2003.

[17] Transpower, '*Definition of Hunting*' [Online] Available: http://www.transpower.co.nz/?id=1641, 14 Nov. 2005.

[18] J. Beukes, R. Lategan, A. Molepo. '*Captap Series Resonance Compensation.*' Eskom Holdings Limited. 2003.

University of Cape Town

[19] R Constable, '*Capacitive coupling substation SCC-3,*' High Voltage Technology Southern Africa (Pty) Ltd. South Africa, 2001.

[20] R. Aghazadeh, M. Sanaye-Pasand, '*Damping of capacitive voltage substations ferroresonance using a suitable RLC filter.*' IEEE Proceedings - Generation, Transmission and Distribution, Vol. 151, No. 6, Nov. 2004.

[21] M. Sanaye-Pasand, R. Aghazadeh, '*Capacitive Voltage Substations Prevention Using Power Electronic Devices.*' International Conference on Power System Transients (IPST), New Orleans, USA, 2003.

[22] M. Schilder, E. Mathebula, '*Analysis of the commissioning test results*' Interim report, Eskom Resources and Strategy Research Division, Report no: RES/IR/02/19332, Project no: PRJ02-00388400-1596 South Africa, 24 Mar 2003.

[23] C.F.Wagner, '*Self-excitation of Induction Motors with Series Capacitors*' Fellow AIEE, Vol. 60, 1941.

[24] Askawa, '*AC Drives: Maintenance Free, Efficient, Accurate Control*' [Online] Available: http://www.yaskawa.com/site/Industries.nsf/reportFiles/AR4022?OpenDocument&fileFormat=B, 6 April 2005.

[25] J. Dixon, G. Venegas, L. Moran, '*A Series Active Power Filter Based on a Sinusoidal Current-Controlled Voltage-Source Inverter.*' IEEE Transactions on Industrial Electronics, Vol. 44, No. 5, Oct. 1997.

[26] J. Kassakian, M. Schlecht, G. Verghese, '*Principles of Power Electronics.*' Addison-Wesley publishing company, Massachusetts Institute of Technology, USA, 1991.

University of Cape Town

[27] Macnab, Lecture notes: ' *Control Systems 1'*, University of Calgary, USA. Lecture 20 – 21. [Online] Available: http://www.enel.ucalgary.ca/People/Macnab/enel441,10 October 2005.

[28] *'Tutorials for Matlab'* The University of Michigan. [Online] Available: http://www.engin.umich.edu/group/ctm/rlocus/rlocus.html, 10 October 2005.

[29] O. Ojo, '*Electro-mechanical sub-synchronous resonance of a series capacitive compensated line start induction motor drive.'* IEEE Industry Applications Society Annual Meeting, Vol.1, p. 238-247, 1989.

[30] M. Braae, K.A. Folly, C.T. Gaunt '*Analysis of Simulation Studies for the Eskom 275/22kV Capacitor Coupled Substation – CCS.*' UCT, South Africa. Copyright of Eskom Holdings Limited, 28 April 2004.

[31] E. Cheever, '*Symbolic Circuit Analysis in Matlab (SCAM)*', Swathmore Engineering. [Online] Available: http:www.swarthmore.eduNatSciecheeve1RefmnaMNA6.html#Downloading, 14 Nov. 2005.

[32] M. Braae, Lecture notes: '*Control Engineering 2, Second Edition*' University of Cape Town, South Africa. 1998.

[33] Dr. Johan Beukes et. Al., '*Shunt compensation of CCS Progress Report*', Stellenbosch, South Africa, June 2005.

[34] Wolfram Research '*Van der Pol Equation'*, [Online] Available: http://mathworld.wolfram.com/vanderPolEquation.html, 6 Dec 2005.

[35] D.Limebeer, R. Harley, '*Sub-synchronous resonance of single-cage induction motors*' IEEE Proc, Vol. 128, Pt. B, No. 1, Jan 1981.

University of Cape Town

Appendices

Appendix A:	Parameters of various models
Appendix B:	Voltage, current and associated DFFT plots for capacitor variation of the 3kW UCT Lab model
Appendix C:	Torque speed plots
Appendix D:	Motor logger code
Appendix E:	Resonant frequency predictions, and complete Meru-Petronet circuit analysis
Appendix F:	Digsilent simulation by M. Schilder
Appendix G:	Effects of ferroresonance filter on the Meru-Petronet system and the UCT Lab model. SCAM comparison
Appendix H:	Independent parameter-variation sensitivity analysis

University of Cape Town

Appendix A

University of Cape Town

Wagner's Parameter Values:

Table 1: Resistances used by Wagner [22]	
Component	Resistance (p.u.)
Xc	0.04
R_1	0.04
X_1	0.15
X_2	0.1
R_2	0.04
X_m	2

Parameter values used to plot Root-Locus graphs of Wagner's circuit:

Table 2: Component values used Wagner [22] Note: that component values calculated using 50Hz.	
C	0.08 F
R_1	0.04 Ω
L_1	0.48 mH
L_m	6.37 mH
L_2	0.32 mH
R_2	0.04 Ω

University of Cape Town

Stellenbosch Parameters:

Table 3: Parameters used for the Stellenbosch Mini-CCS induction machine	
Stator resistance, Rs	0.040Ω
Rotor resistance, Rr	0.022Ω
Stator inductance, Ls	0.39mH
Rotor inductance, Lr	0.39mH
Magnetising inductance, Lm	16.6mH

University of Cape Town

Meru Parameters:

At Meru, the following values are used for the passive filter:

Table 4: Component values of passive filter at the Meru Sub-station.	
Component	**Value**
Cf	13.2μF
Lf	0.7675H with Q = 300 (R = 0.803Ω)
Rf	500Ω

Meru CCS and estimated Petronet induction machine values.

Table 5: Values used at Meru and with Petronet Motor [15], [29], [Digsilent Simulation by Melanie Schilder (see appendix)].	
C_1	**0.56547 μF**
C_2	**6.2970μF**
L_{com}	**1.476F**
R_1	**0.096 Ω**
L_1	**2.44 mH**
L_m	**0.102 H**
L_2	**2.44 mH**
R_2	**0.12 Ω**

University of Cape Town

Typical Inertia Calculations for the Petronet IM

For the following inertia calculations, it is assumed that the rotor is a solid iron cylinder. The relationship between the moment of inertia and the inertia time constant is the ratio of the stored energy at rated speed to the power rating of the machine and is given by [p132,1]:

$$H = \frac{1}{2}\frac{J\omega_0^2}{S}$$

The rated speed is given by:

$$\omega_0 = \frac{2\pi \mathrm{RPM}}{f}$$

Resulting in the following simplification:

$$H = 7.9 \cdot 10^{-3} J \frac{(\mathrm{RPM})^2}{S}$$

Where J is the moment of inertia, S is the power rating of the machine (in VA) and RPM is the rated speed of the machine in revolutions per minute.

The moment of inertia of a solid cylinder is given by:

$$J = \frac{1}{2}MR^2$$

Where M is the mass of the cylinder and R is the radius, or the sum of the inner and outer radii if a hollow cylinder is considered.

The Petronet motor weighs 5600 kg. If it is assumed that this is the rotor mass and a rotor radius of 0.5 m is assumed, the following inertia constant is calculated:

$$TaG = \frac{2H}{pf}$$

$J = 0.5*5600*0.5\text{^}2 = 700$
$H = 7.9e(-3)*J*3000\text{^}2/1.5e(6) = 33.18$
$TaG = 2H/0.9 = 73.73$

[1] Kundur, P., "Power System Stability and Control", McGraw Hill, Inc., 1993.

University of Cape Town

Induction motor parameters from no-load and blocked-rotor tests

Note that all readings are rms phase-to-neutral readings, unless otherwise stated.

Average R_1 resistance/phase measured using a galvanometer = 6.225Ω.

No-Load Test:

	Phase A	Phase B	Phase C	Average
Voltage (V)	220	220	220	220
Current (A)	0.515	0.575	0.520	0.540
Power (W)	59	56	51	55.3

The no-load impedance: $Z_{nl} = R_1 + X_1 + X_m = \frac{V}{I} = \frac{220}{0.54} = 407.4\Omega$

The no-load resistance: $R_1 = \frac{P}{I^2} = \frac{55.3}{0.54^2} = 190\Omega.$

Therefore, $X_1 + X_m = 361\Omega.$

Blocked-Rotor Test:

The rotor was blocked, and the supply voltage increased until rated current flowed in the stator windings.

Rated current/phase = $\frac{P}{V} = \frac{3KW/3}{220} = 4.55A.$

	Phase A	Phase B	Phase C	Average
Voltage (V)	91.6	91.5	91.8	91.6
Current (A)	4.51	4.48	4.4	4.46
Power (W)	270	260	270	267

The blocked-rotor impedance: $Z_{br} = R_1 + R_2' + X_1 + X_2' = \frac{V}{I} = \frac{91.6}{4.46} = 20.5\Omega$

University of Cape Town

The blocked-rotor resistance: $R_1 + R_2^{'} = \frac{P}{I^2} = \frac{267}{4.46^2} = 13.4\Omega.$

Therefore, $R_2^{'} = 13.4 - R_1 = 7.18\Omega.$

And so $X_1 + X_2^{'} = \sqrt{(Z_{br}^2 - R_{br}^2)} = 15.6\Omega.$

Assuming that $X_1 = X'_2$, $X_1 = X_2^{'} = 7.78\Omega.$

$$L_1 = L_2^{'} = 24.4mH.$$

From the no-load test, it was found that $X_1 + X_m = 361\Omega.$

Therefore $X_m = 353\Omega.$

$$L_m = 1.12H.$$

University of Cape Town

Appendix B

University of Cape Town

Capacitor variation for the 3kW UCT Lab model:

Table 1: Summary of DFFT results collected from the UCT-Lab model		
Capacitance (μF)	**Average resonant frequency (Hz)**	**Speed reached by rotor**
62	31,30 ave = 30.5	1810
75	27,28, ave = 27.5	1700
100	24,23 ave = 23.5	1400
112	23,22.5 ave = 22.75	1360
125	22, 22 ave = 22	1350
150	21,21 ave = 21	1240
162	21,20 ave = 20	1230
200	20, 18.5, ave = 19.25	1220

University of Cape Town

Raw data:

Star:

200u:

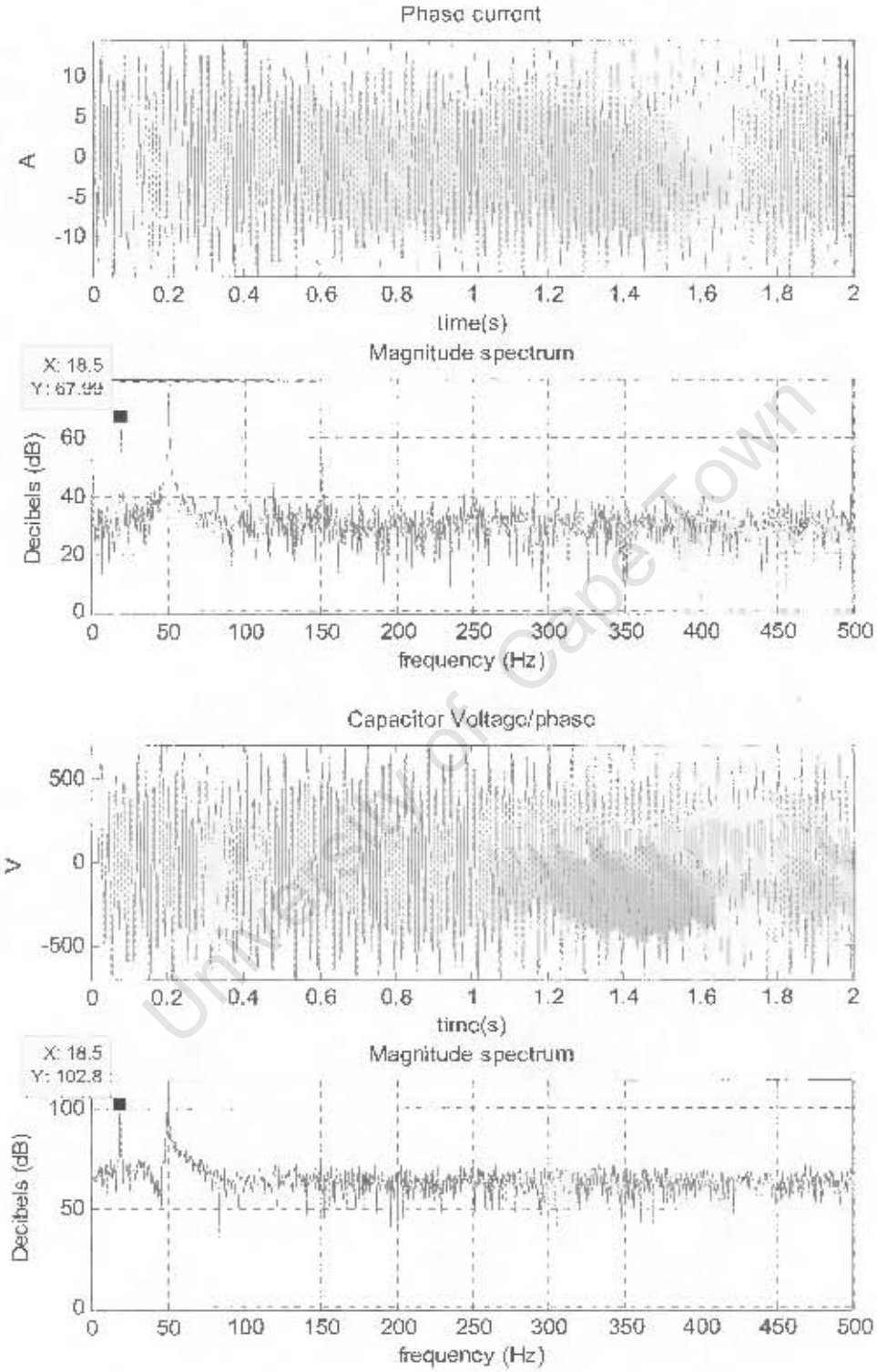

University of Cape Town

162u:

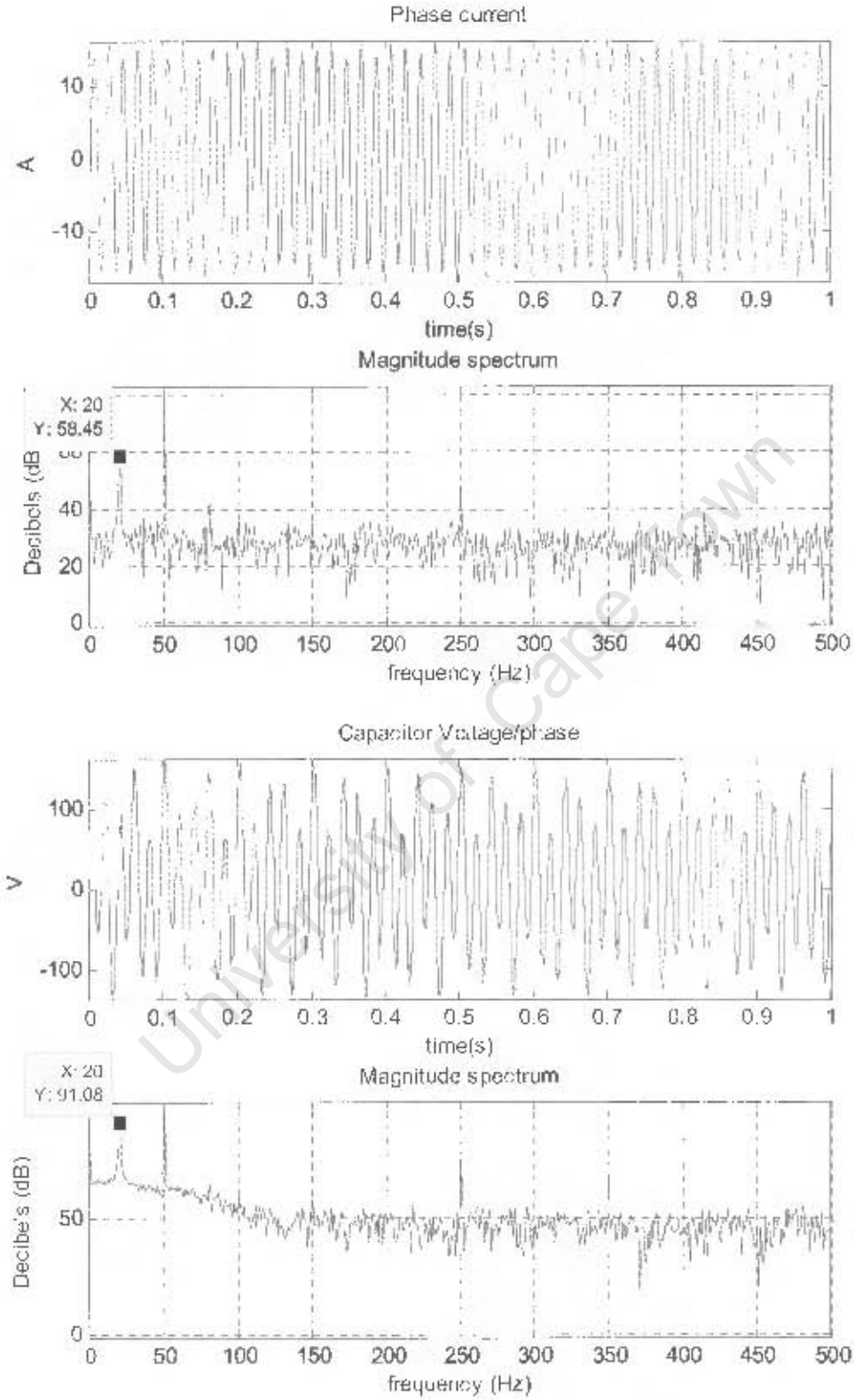

University of Cape Town

150u:

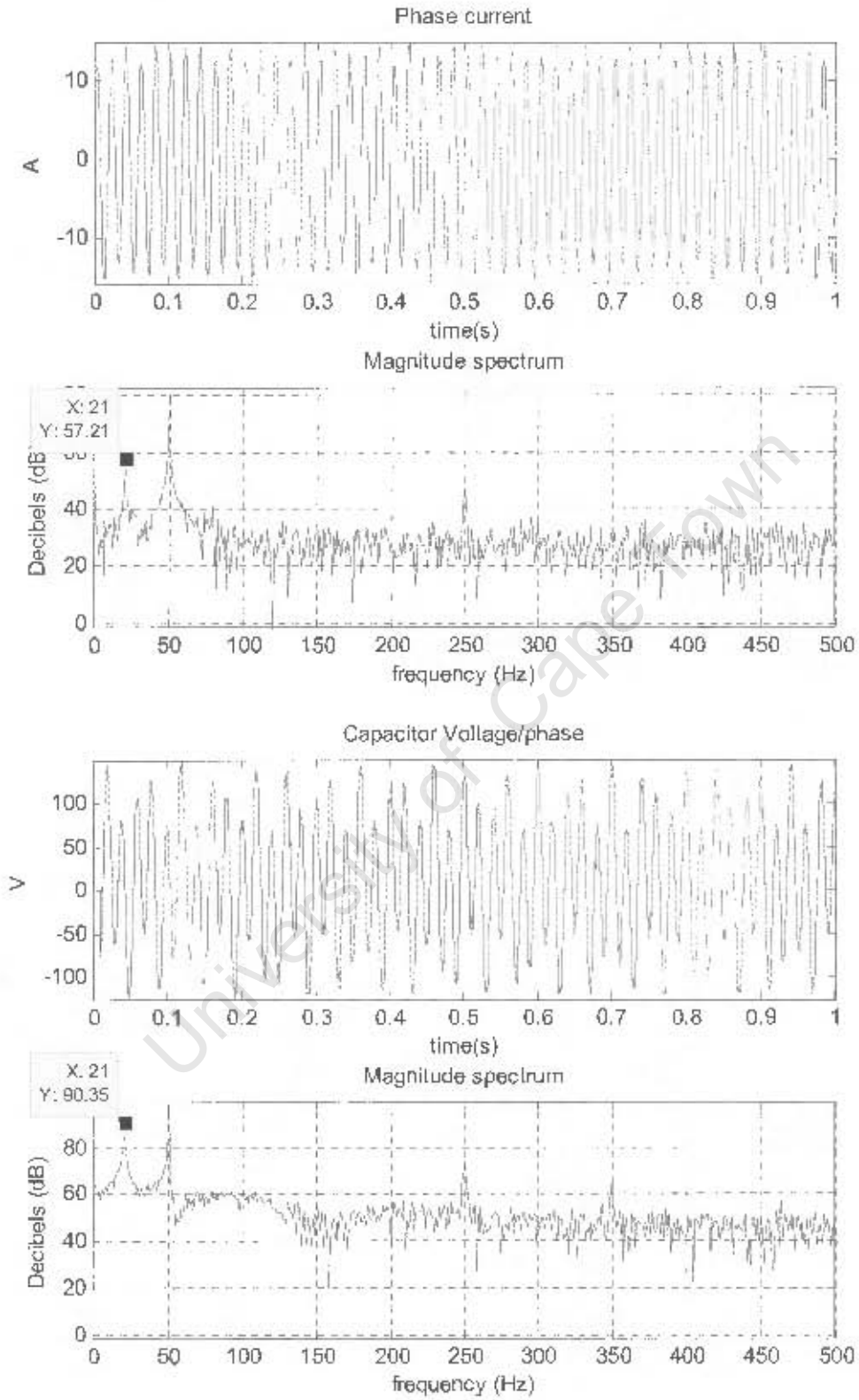

University of Cape Town

125u:

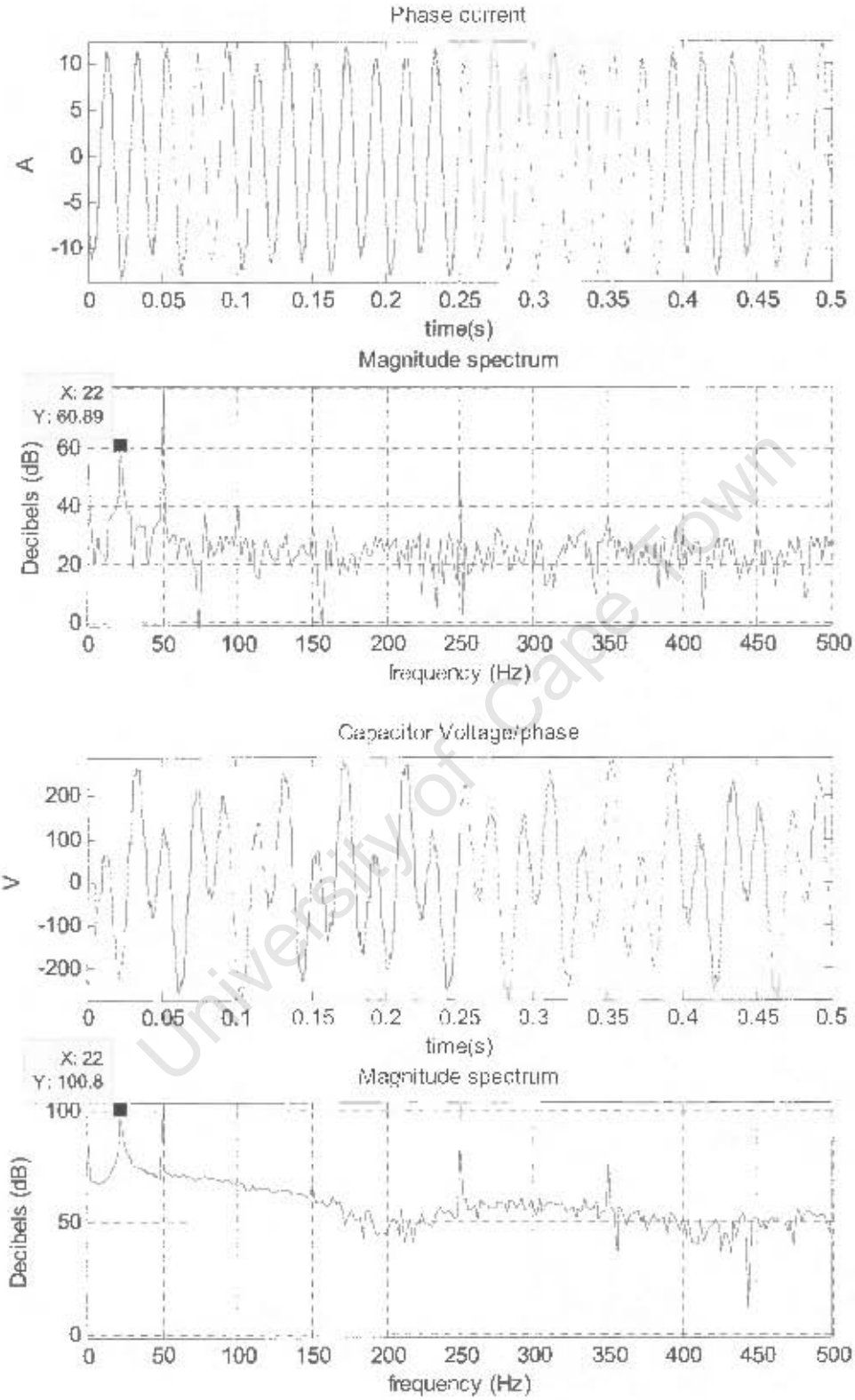

University of Cape Town

112u:

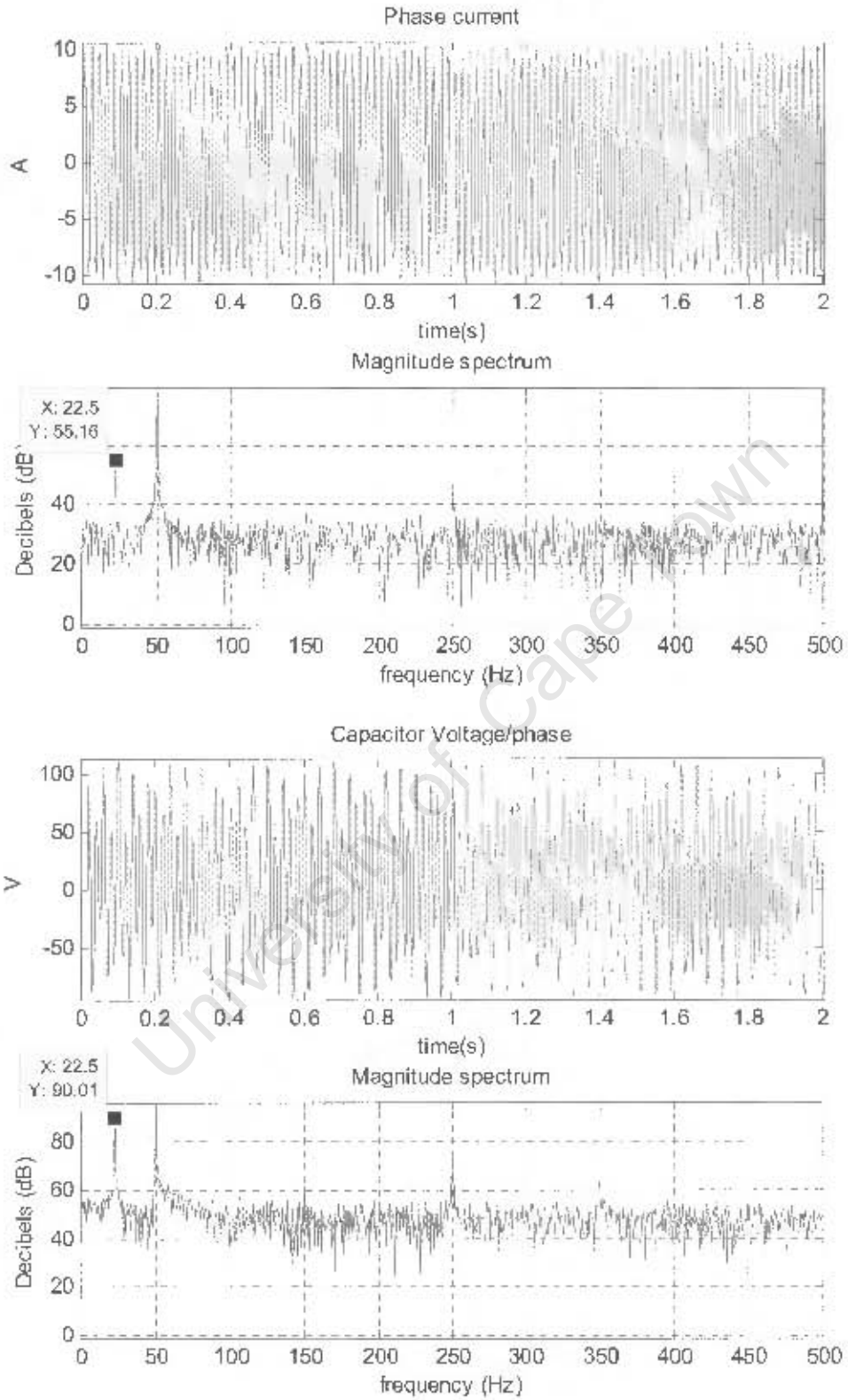

University of Cape Town

100u:

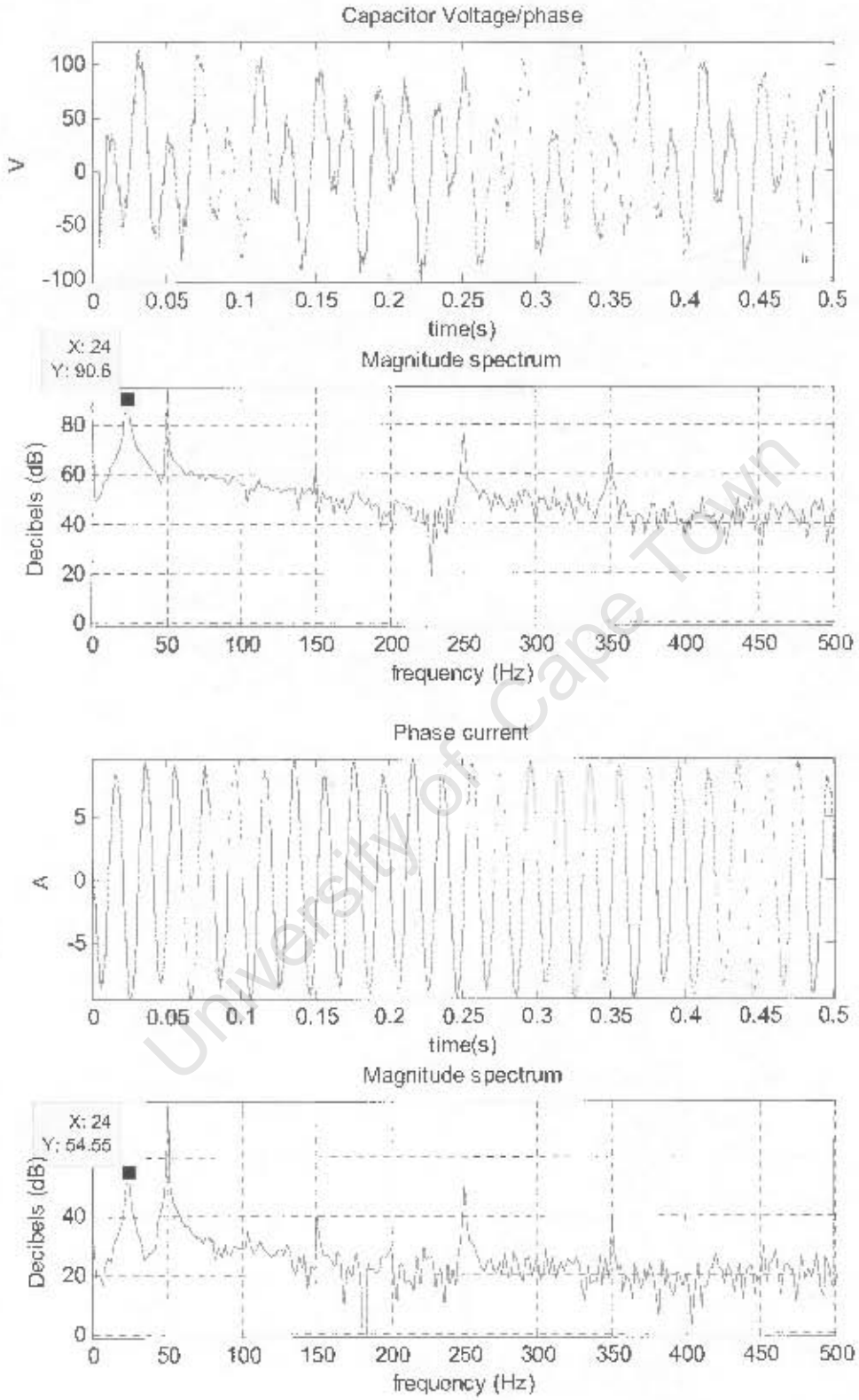

University of Cape Town

75uF:

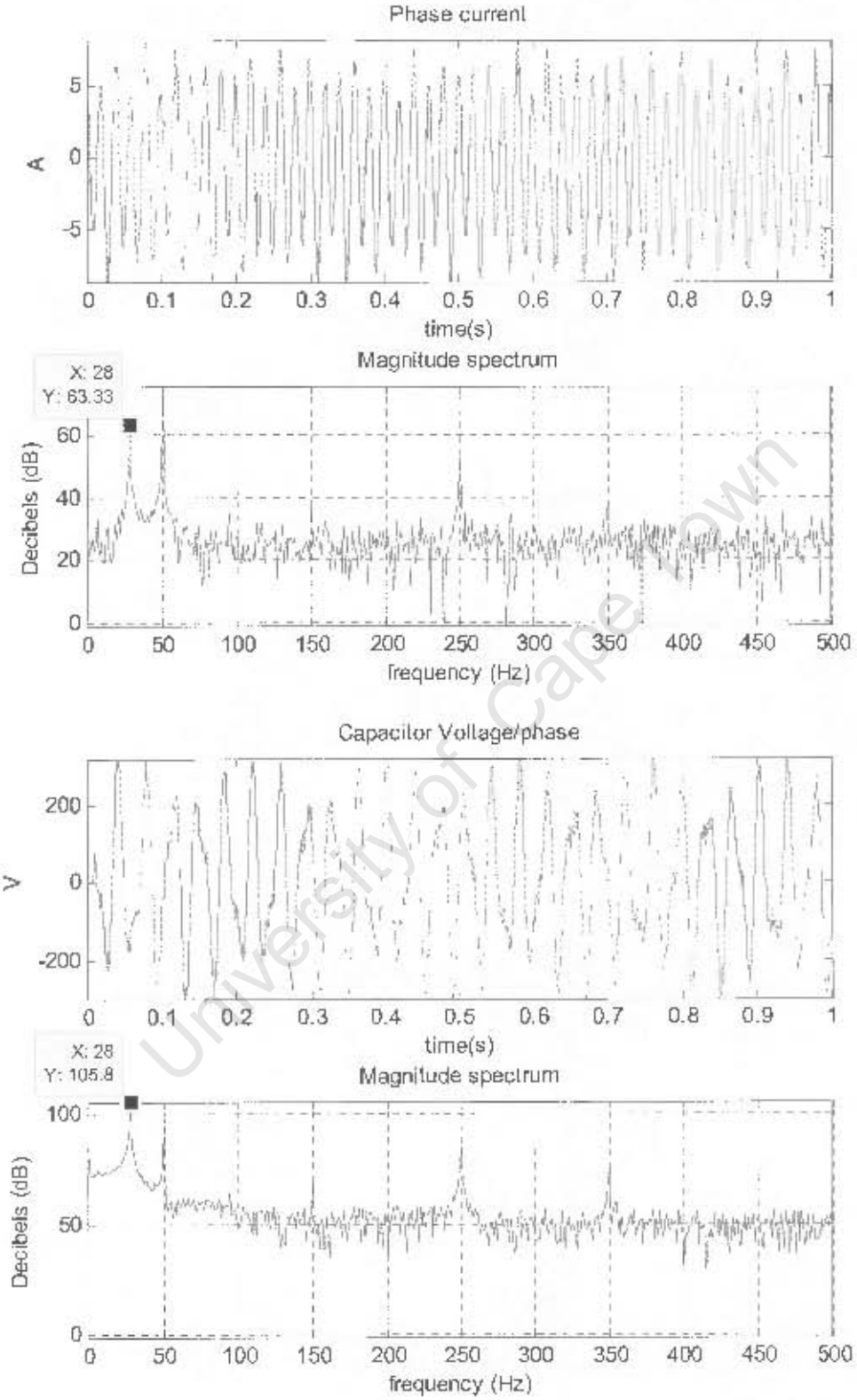

University of Cape Town

62u:

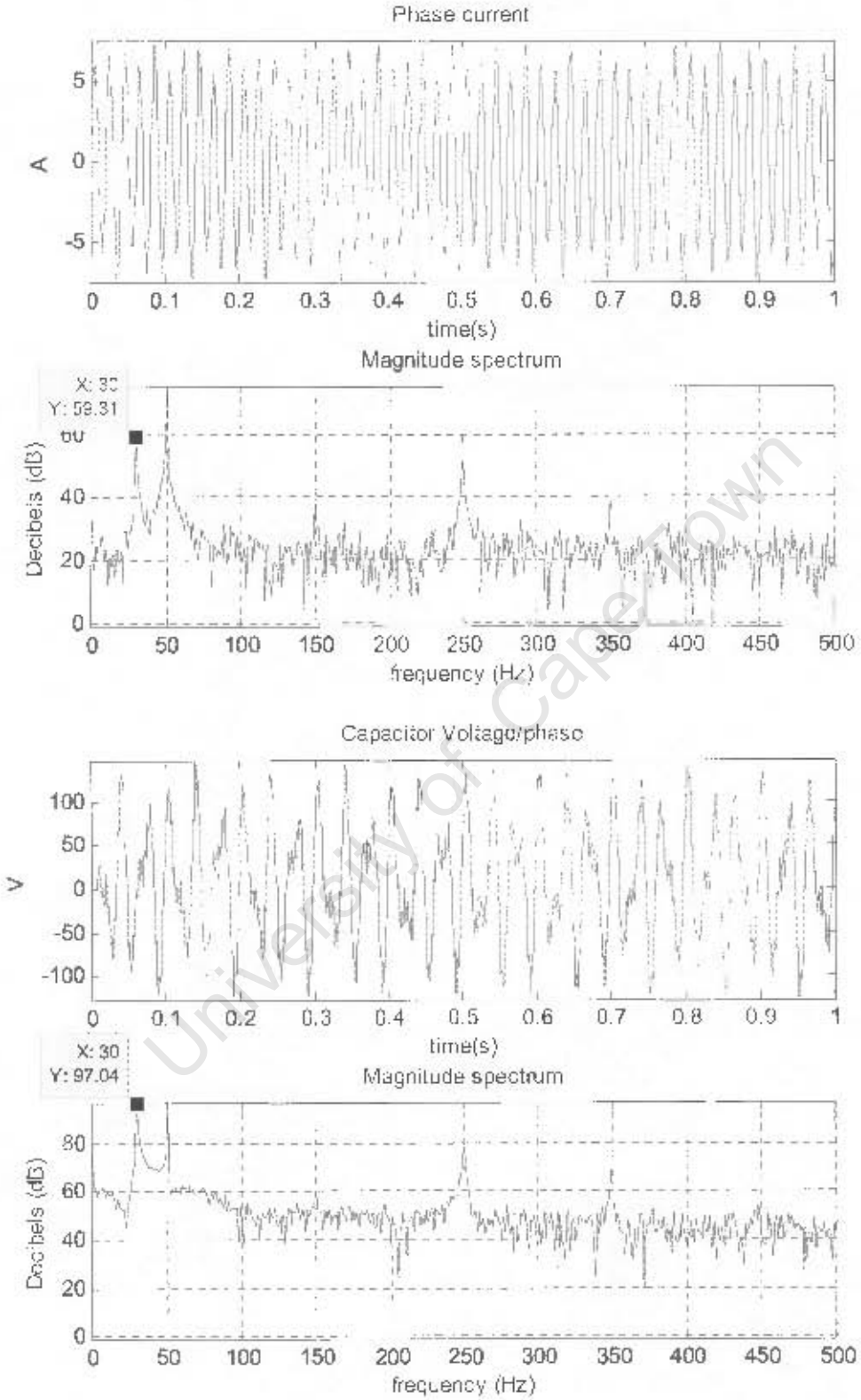

University of Cape Town

Appendix C

University of Cape Town

Torque speed plot with a 100μF capacitor:

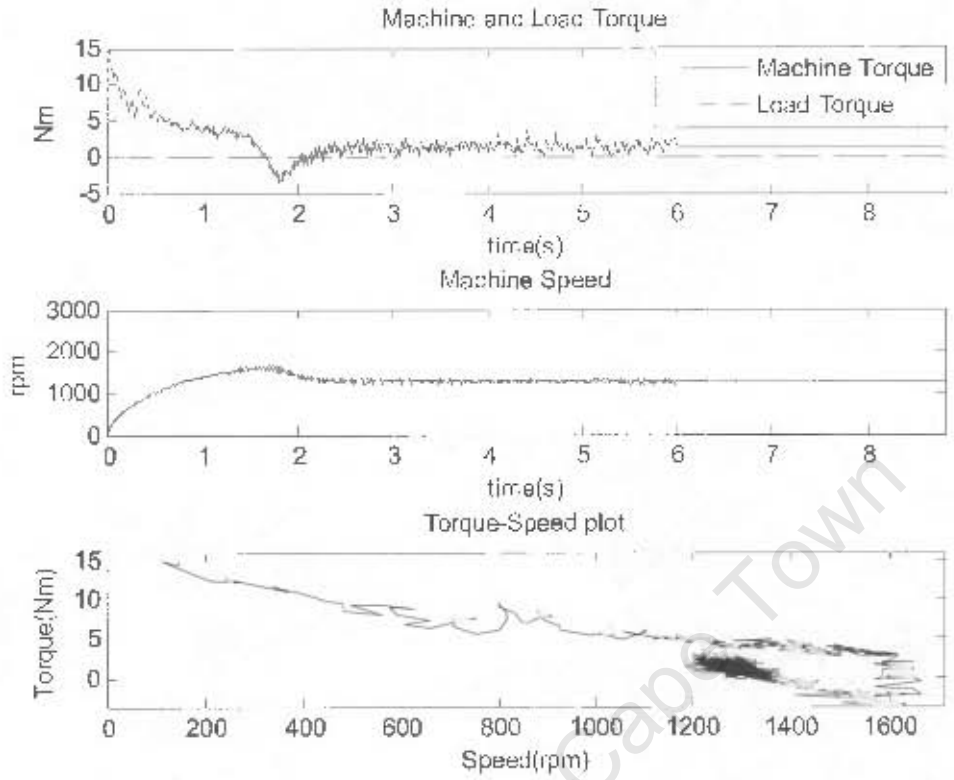

University of Cape Town

Torque speed plot with a 100μF capacitor:

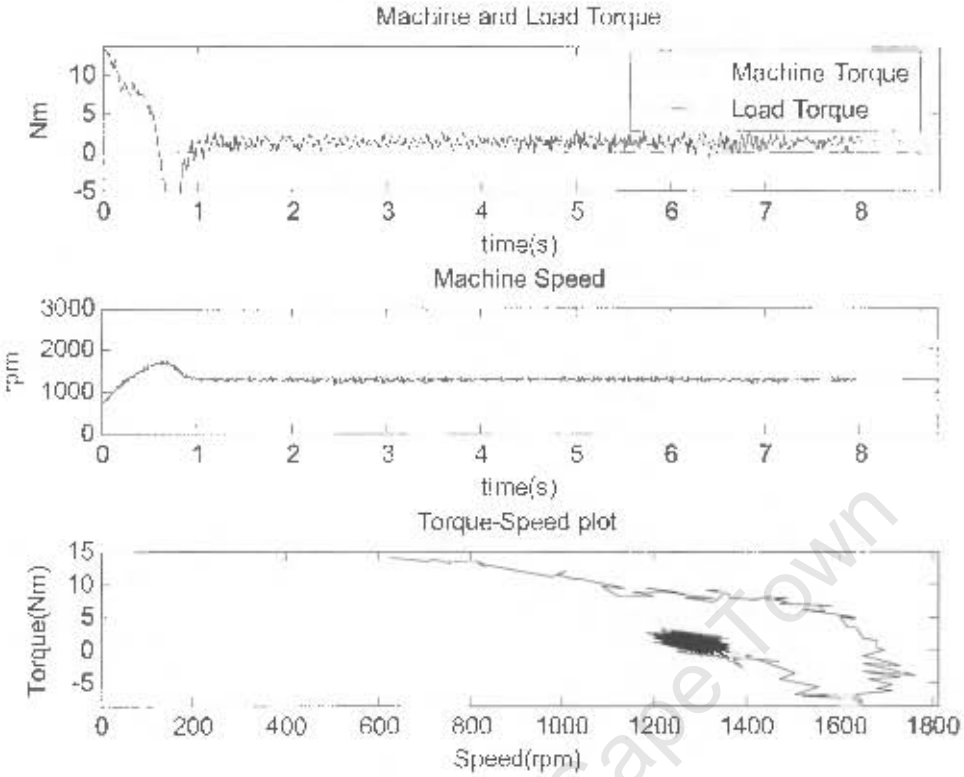

University of Cape Town

Torque speed plot with a 75μF capacitor:

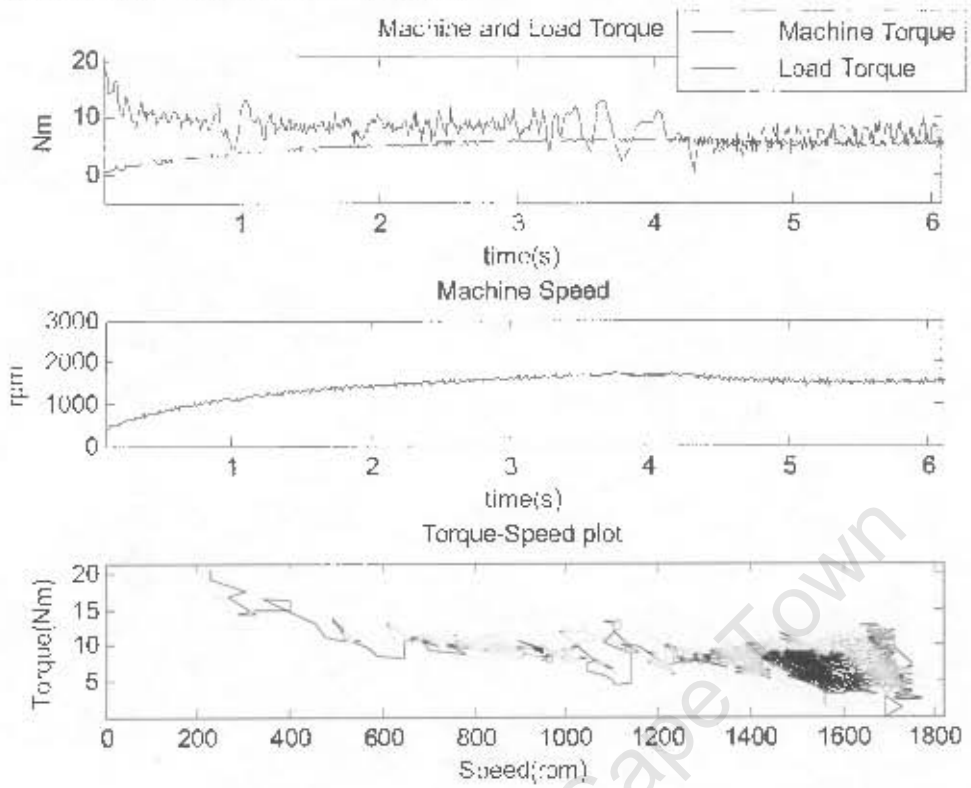

University of Cape Town

Torque speed plot with a 75μF capacitor:

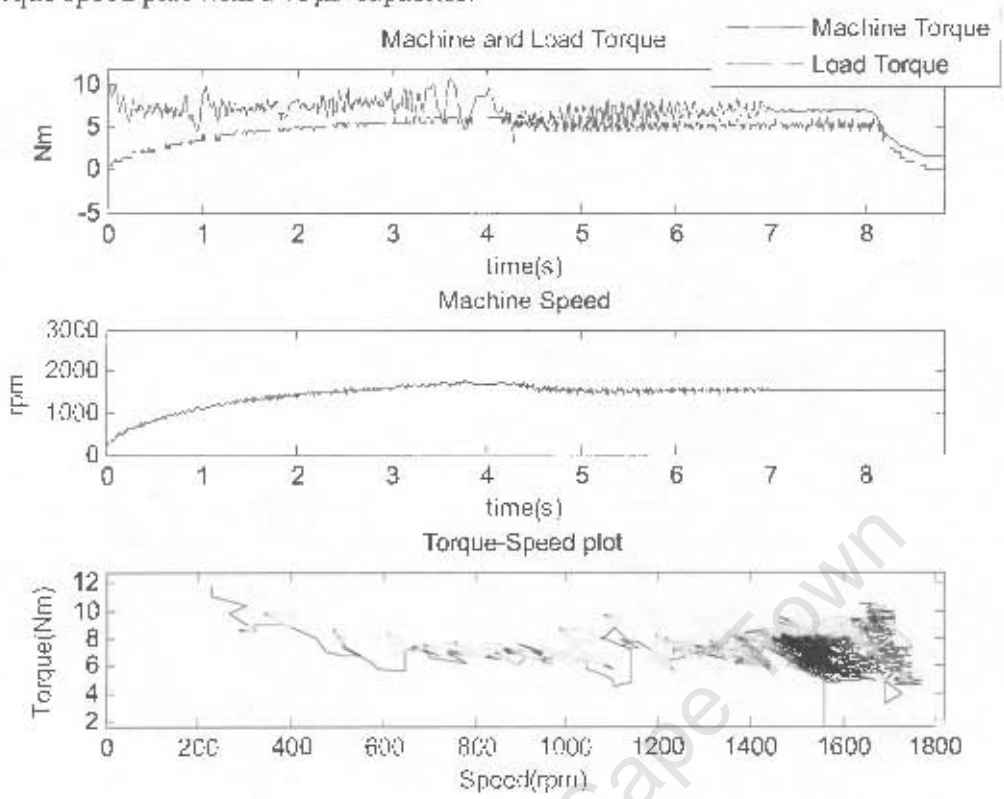

University of Cape Town

Appendix D

University of Cape Town

```
/*********************************************************************/
/*                          Data Logger                              */
/*   Code was adapted from a program written by C. Slabbert          */
/*  -1 Sept 2005
   measure: Vbc, Ib
         Vac, Ia to work out the input power using P1+P2.
         Vout, Iout (DC) for output power (P = IV).
         Speed measured to translate to torque.
/*  -8 Sept 2005 (Torque_reader_2)
   -Changed speed input to dc input and 1/(12.5) scale (from 1/40)
   -Changed dc_I input to 1/4 (was 1/10)

   -11 Sept (Torque_reader_5)
   - modify Pv Grid tie code to get serial communications working
   - change baud rate to 28800 (from 9600) to increase resolution of data recording
   - modify code so that adc is interrupt based. (Torque_reader_6)

   -14 Sept
   -Change ADC sample period to 1kHz (from 5)

   -15 Sept
   -Share arrays: an integer is 2 bytes long,
    so, for instance use 1 byte for Torque(MSB) and the other for Voltage(LSB).

/*********************************************************************/
#include "LF2407.h"   /* the dsp2407a registersb are here */

/* init Keypad + Display */
int rcvd,screen,Data_rd,charcount;
int Send,programfinish,Value;
char Send_flag,error;
char StackLengthDone,Hbyte,Lbyte;
long int m;

/*dac test*/
int i,k, saw_tooth;

/*clinton's variables*/
int DAC1,DAC2,DAC3,DAC4,DAC5,DAC6,DAC7,DAC8,rcvd;

/*tacho variables*/

/*raw voltage and currents*/
int V_dc1, dc_I1, I_B1, I_A1, V_bc1, V_ac1, speed1;
int V_dc2, dc_I2, I_B2, I_A2, V_bc2, V_ac2, speed2;
int V_dc, dc_I, I_B, I_A, V_bc, V_ac, speed;

/*voltage and currents refined*/
int V_dc_real, dc_I_real, I_B_real, I_A_real, V_bc_real, V_ac_real, speed_real;
int speed_radians;

/*p and t*/
long int power_a, power_b, power_in, torque_in;
int power_out, torque_out;

/*Arrays*/ /*Need Torque_out, Torque_in, Speed, V_ac, I_A */
```

University of Cape Town

```
int Speed_and_I_A_arr[900], Load_T_and_V_ac_arr[900]; /*Torque_arr[600]*/
int log_count,j, Log_done, printed_once, log_start, init_delay, start_speed;
int torque_log, speed_log, load_log, V_ac_log, I_A_log;

/*Torque averaging */
long int torque_sum;
int torque_count, torque_ave;

/*Sequence for interrupt:
   Test1
   GPT1_underflow
   Test3
   Test4
   Test5
   Xint2
*/
interrupt void Test1(void)
{
}

interrupt void GPT1_underflow(void)
{
/*ADC mux selection (there are 2 adc's that are multiplexed)      */

/*                                                    J8          */
/*                                                   ADC3         */
/*                                                   V_dc         */
/*                  INTERFACE BOARD                               */
/*                                                                */
/*                                                    J6          */
/*                                                   ADC2         */
/*                                                   dc_I         */
/*                                                                */
/*                                                                */
/*    J2       J3         J5          J7          J1(1/10)    J4  */
/* ADC8    ADC9     ADCA(10)   ADCB(11)    ADC0      ADC1 */
/*   I_a      V_ac       V_bc        speed         I_b             */
/*                                                                */
/*

/*Sample everything twice, starting with V_dc and going round, clockwise.*/

        *PADATDIR &= 0xFFBF; /*needed for dacs? */

        DAC8 = 250;
        DAC8 = DAC8<<4;
        DAC8 &= 0x0FFF;
        DAC8 |= 0xE000;
        *SPITXBUF = DAC8;
        for (i=0; i<4; i++) {}
        *PCDATDIR &= 0x0FFDF;
        *PCDATDIR |= 0x0020;

        *CHSELSEQ1 = 0x2233;
        *CHSELSEQ2 = 0x0011;
        *CHSELSEQ3 = 0xAABB;
```

University of Cape Town

```
*CHSELSEQ4 = 0x0099;

*ADCTRL2 |= 0x2000;
while(ADCTRL2 && 0x0200 == 0x0000) {};
*ADCTRL2 |= 0x0200;

V_dc1 = *RESULT0;
V_dc1 = V_dc1>>6;
V_dc1 &= 0x03FF;

V_dc2 = *RESULT1;
V_dc2 = V_dc2>>6;
V_dc2 &= 0x03FF;


dc_I1 = *RESULT2;
dc_I1 = dc_I1>>6;
dc_I1 &= 0x03FF;

dc_I2 = *RESULT3;
dc_I2 = dc_I2>>6;
dc_I2 &= 0x03FF;


I_B1 = *RESULT4;
I_B1 = I_B1>>6;
I_B1 &= 0x03FF;

I_B2 = *RESULT5;
I_B2 = I_B2>>6;
I_B2 &= 0x03FF;


speed1 = *RESULT6;
speed1 = speed1>>6;
speed1 &= 0x03FF;

speed2 = *RESULT7;
speed2 = speed2>>6;
speed2 &= 0x03FF;


V_bc1 = *RESULT8;
V_bc1 = V_bc1>>6;
V_bc1 &= 0x03FF;

V_bc2 = *RESULT9;
V_bc2 = V_bc2>>6;
V_bc2 &= 0x03FF;


V_ac1 = *RESULT10;
V_ac1 = V_ac1>>6;
V_ac1 &= 0x03FF;

V_ac2 = *RESULT11;
```

University of Cape Town

```
        V_ac2 = V_ac2>>6;
        V_ac2 &= 0x03FF;


        I_A1 = *RESULT12;
        I_A1 = I_A1>>6;
        I_A1 &= 0x03FF;

        I_A2 = *RESULT13;
        I_A2 = I_A2>>6;
        I_A2 &= 0x03FF;

        /*average the adc inputs*/
        V_dc = (V_dc1 + V_dc2)/2;
        dc_I = ((dc_I1 + dc_I2)/2);
        I_B = ((I_B1 + I_B2)/2)-512;
        speed = ((speed1 + speed2)/2);
        V_bc = ((V_bc1 + V_bc2)/2)-512;
        V_ac = ((V_ac1 + V_ac2)/2)-512;
        I_A = ((I_A1 + I_A2)/2)-512;

        /*conversion to real values*/

        /* __0 d.p.___|____1 d.p._____*/
        /* V_dc_real | dc_I_real   */
        /* V_ac_real | I_A_real    */
        /* V_bc_real | I_B_real    */
        /* speed_radi | power_out   */
        /*          | torque_in   */
        /*          | torque_out  */
        /*          | power_in    */
        /*          |             */

        V_dc_real = V_dc*5/16;          /*real/100 so 320V = 1024 || 320/1024 = 5/16*/
dc_I_real = dc_I*10/80;          /*real/4 so (3.2*4)A = 1024 || 12.8/1024 = 1/80*/
I_B_real =  I_B*10/32;           /*real/10 so (3.2*10)A = 1024 || 32/1024 = 1/32*/
I_A_real =  I_A*10/32;           /*real/10 so (3.2*10)A = 1024 || 32/1024 = 1/32*/
V_bc_real = V_bc*5/4;            /*real/400 so (320*4)V = 1024 || 1280/1024 = 5/4*/
V_ac_real = V_ac*5/4;            /*real/400 so (320*4)V = 1024 || 1280/1024 = 5/4*/
speed_real =speed*3;             /*real/(10*77) so (3.2*12.5*76.8)rpm = 1024 || 3072/1024 = 1/3*/
        /*Tacho measures the speed. rpm = (dc_tacho_V)*76.8 +0.7 -- remember that J1 is 1/40 */

/*Interface card scaling*/
V_dc_real = V_dc_real*37/32;
speed_real = ((long int)(speed_real*34))/32;

speed_radians = ((long int)(speed_real*107))/1024;   /*2*pi/60 = 6.283/60 = 107/1024*/
        if (speed_radians <= 5) speed_radians = 5;          /*prevents divide by 0*/ /*50 rpm*/

/*Power and torque*/

        /*2-Wattmeter method for finding the power input (PC Sen)*/
        power_a = ((long int)I_A_real)*((long int)V_ac_real);
        power_b = ((long int)I_B_real)*((long int)V_bc_real);

        power_in = power_a + power_b;
```

University of Cape Town

```
   torque_in = power_in/((long int)speed_radians); /*1 dp*/

    /* Load power */
          power_out = dc_I_real*V_dc_real;        /*1 dp */
   torque_out = power_out/speed_radians;    /*1 dp*/

   /*Power scaling*/
   power_out = ((long int)(power_out*33))/32;

   /*Torque averaging*/
   torque_sum +=torque_in;
   if (torque_count == 5)
   {    torque_ave = ((int)(torque_sum/5));
       torque_sum = 0;
       torque_count = 0;
   }
   torque_count++;

 if (init_delay >= 1000)  init_delay =1000;
 if ((speed_real>=start_speed)&&(init_delay >= 1000))  log_start = 1;
 if ((log_start == 1) && (Log_done == 0))
 {
      /*max is 255 so only have to send one byte*/
      torque_log = ((int)torque_ave)/8+10; if (torque_log > 255) torque_log = 255; if (torque_log < 0)
torque_log = 0;/*max torque is 30000/50 (P to 1dp)/(min speed) = 600*/
      speed_log  = speed_real/16; if (speed_log > 255) speed_log = 255; if (speed_log < 0) speed_log = 0;
      load_log   = torque_out; if (load_log > 128) load_log = 128; if (load_log < 0) load_log = 0; /*Always
positive, so we are ok*/
      V_ac_log   = (V_ac_real)/16+64; if (V_ac_log > 127) V_ac_log = 127; if (V_ac_log < 0) V_ac_log =
0;/*V_ac = 380rms so max pk 2 pk is 1103 so to fit in 128, divide by 9 and add 64*/
      I_A_log    = I_A_real/16+64; if (I_A_log > 127) I_A_log = 127; if (I_A_log < 1) I_A_log = 1; /*max
I_A is 5Arms therefore max pk 2 pk is 141 so to fit in 128 add 64*/

      /*Torque_arr[log_count] = torque_log;          /*works*/
      Speed_and_I_A_arr[log_count] = (I_A_log*256) + speed_log;    /*Max msb number is
127*256*//*I_A is MSB*/
      Load_T_and_V_ac_arr[log_count] = (load_log*256) + torque_log;       /*Max msb number is
127*256*//*V_ac is MSB*/ /*works*/

      if (log_count >= 900) {log_count = 900;  Log_done = 1;}
      log_count++;
}

          DAC1 = torque_ave;
          DAC1 = DAC1<<4;
          DAC1 &= 0x0FFF;
          DAC1 |= 0x0000;
          *SPITXBUF = DAC1;
          for (i=0; i<4; i++) {}
          *PCDATDIR &= 0x0FFDF;
          *PCDATDIR |= 0x0020;

          DAC2 = torque_count;
          DAC2 = DAC2<<4;
          DAC2 &= 0x0FFF;
```

University of Cape Town

```
DAC2 |= 0x2000;
*SPITXBUF = DAC2;
for (i=0; i<4; i++) {}
*PCDATDIR &= 0x0FFDF;
*PCDATDIR |= 0x0020;

DAC3 = torque_sum/16;
DAC3 = DAC3<<4;
DAC3 &= 0x0FFF;
DAC3 |= 0x4000;
*SPITXBUF = DAC3;
for (i=0; i<4; i++) {}
*PCDATDIR &= 0x0FFDF;
*PCDATDIR |= 0x0020;

DAC4 = torque_in/32+10;
DAC4 = DAC4<<4;
DAC4 &= 0x0FFF;
DAC4 |= 0x6000;
*SPITXBUF = DAC4;
for (i=0; i<4; i++) {}
*PCDATDIR &= 0x0FFDF;
*PCDATDIR |= 0x0020;

DAC5 = speed_radians/2;
DAC5 = DAC5<<4;
DAC5 &= 0x0FFF;
DAC5 |= 0x8000;
*SPITXBUF = DAC5;
for (i=0; i<4; i++) {}
*PCDATDIR &= 0x0FFDF;
*PCDATDIR |= 0x0020;

DAC6 = torque_out;
DAC6 = DAC6<<4;
DAC6 &= 0x0FFF;
DAC6 |= 0xA000;
*SPITXBUF = DAC6;
for (i=0; i<4; i++) {}
*PCDATDIR &= 0x0FFDF;
*PCDATDIR |= 0x0020;

DAC7 = I_A_real/16+128;
DAC7 = DAC7<<4;
DAC7 &= 0x0FFF;
DAC7 |= 0xC000;
*SPITXBUF = DAC7;
for (i=0; i<4; i++) {}
*PCDATDIR &= 0x0FFDF;
*PCDATDIR |= 0x0020;

DAC8 = 0;
DAC8 = DAC8<<4;
DAC8 &= 0x0FFF;
DAC8 |= 0xE000;
*SPITXBUF = DAC8;
```

University of Cape Town

```
        for (i=0; i<4; i++) {}
        *PCDATDIR &= 0x0FFDF;
        *PCDATDIR |= 0x0020;

        init_delay++;
        *PFDATDIR |= 0x0004;
        *EVAIFRA |= 0x0200;   /*clears the interrupt flag*/
}

interrupt void Test3(void)
{
}

interrupt void Test4(void)
{
}

interrupt void Test5(void)
{
}

interrupt void XINT2(void)
{
}

void main(void)
        {
  *MCRA |= 0x0FC0;      /*added*/

        /* turning on clks */
        *SCSR1 = 0x00EC;    /*added*/
        *SCSR1 |= 0x0040;


        /* interrupt setup */

        *IMR = 0x0022;
        *IFR = 0xFFFF;
        *EVAIMRA = 0x0200;
        asm("     clrc INTM");

        /* SPI port setup for DAC coms */

        *SPICCR &= 0x0FF7F;
        *MCRB |= 0x001C;
        *SPICCR |= 0x000B;
        *SPICTL = 0x0006;
        *SPIBRR |= 0x0003;
        *SPICCR |= 0x0080;

        *PCDATDIR |= 0x2020;

        /* registers for IOPF2 code-timer */

        *MCRC &= 0xFDFF;
        *PFDATDIR |= 0x0404;
```

University of Cape Town

```
/* registers for ADC */
        *ADCTRL1 = 0x0FD0;
        *ADCTRL2 = 0x0000;
        *MAXCONV = 0x000D;

        *COMCONA = 0x0307; /*added*/
        *COMCONA = 0x8307;  /*added*/
/*-------------------------------------------------------------------------------------------------------------------------------
        Setting up Serial port communication
-------------------------------------------------------------------------------------------------------------------------------*/

        *MCRA |= 0x0003;  /* IOPA0 = SCITXD & IOPA1 = SCIRXD  */
        *SCICCR = 0x0007;  /*  1 stop bit, no parity, 8 bit char length, loopback enabled  */
        *SCICTL1 = 0x0003;
        *SCIHBAUD = 0x0001;  /*  Baud rate set to 9600  */
        *SCILBAUD = 0x0FF;
        *SCICTL2 = 0x0002;  /*  enable RXRDY interrupt  */
        *SCICTL1 = 0x0023;  /* relinquish from reset  */

  /*set up of t1, which triggers interrupt T1_underflow*/
        *T1PR = 50000;  /* Period = 50_000*25nsec*2 = 20_msec : freq 400Hz */
        *T1CNT = 0x0;
        *T1CON = 0xAB02;   /* up/down continuous mode */
        *T1CON = 0xAB42;   /* start the clock */    /*Prescaler = 1*/

        /*Initialization of variables*/
        V_bc1 = 0;
        power_in = 0;
        power_out = 0;
        speed_radians = 50;
        Log_done = 0;
        printed_once = 0;
        log_start = 0;
        log_count = 0;
        init_delay =0;
        torque_sum=0;
        torque_ave = 0;
        torque_count=0;

        for(j=1;j<900;j++)
        {
                /*Torque_arr[j]=0;*/
                Speed_and_I_A_arr[j]=0;
                Load_T_and_V_ac_arr[j]=0;
        }
        *SCITXBUF = 84;
                for(;;)
                {
        rcvd = *SCIRXBUF;

        if ((rcvd == 56) && (Log_done == 0))  /*8*/
        {

                                Send = log_start;
                /*              Hbyte = Send>>8;*/
```

University of Cape Town

```
                                Lbyte = (char)Send;
                                *SCITXBUF = Lbyte;while((*SCICTL2 & 0x0080) == 0x0000) {};
                                for (m=0; m<10000; m++) {}
/*                              *SCITXBUF = Hbyte;while((*SCICTL2 & 0x0080) == 0x0000) {};*/
                                for (m=0; m<10000; m++) {}

   }

        if ((rcvd==116) && (Log_done == 1))  /*t*/
        {
                /*      *SCITXBUF = 84; while((*SCICTL2 & 0x0080) == 0x0000) {};  /*T*/
                /*      *SCITXBUF = 111;while((*SCICTL2 & 0x0080) == 0x0000) {}; /*o*/
                /*      *SCITXBUF = 114;while((*SCICTL2 & 0x0080) == 0x0000) {}; /*r*/
                /*      *SCITXBUF = 113;while((*SCICTL2 & 0x0080) == 0x0000) {}; /*q*/
                /*      *SCITXBUF = 117;while((*SCICTL2 & 0x0080) == 0x0000) {}; /*u*/
                /*      *SCITXBUF = 101;while((*SCICTL2 & 0x0080) == 0x0000) {}; /*e*/


                        for(j=1;j<900;j++)
                        {
                                /*Send = Torque_arr[j];*/
         /*Start sequence*/
/*         if (j < 10) Send = 10;          */

                                if(Send < 0) Send = 0;
                                if(Send > 65535) Send = 65535;
                                /*Hbyte = Send>>8;*/
                                Lbyte = (char)Send;
                                *SCITXBUF = Lbyte;while((*SCICTL2 & 0x0080) == 0x0000) {};
                                for (m=0; m<10000; m++)
                                {}
                                /**SCITXBUF = Hbyte;while((*SCICTL2 & 0x0080) == 0x0000)
{};*/
                                for (m=0; m<10000; m++)
                                {}
                        }
                        printed_once = 1;
   }/*torque if end*/

   if ((rcvd==118) && (Log_done == 1))  /*v*/
        {

                        for(j=1;j<900;j++)
                        {
         Send = Load_T_and_V_ac_arr[j];
         /*Start sequence*/
/*         if (j < 10) Send = 10;          */

                                if(Send > 65535) Send = 65535;
                                if(Send < 0) Send = 0;
                                Hbyte = Send>>8;
                                /*Lbyte = (char)Send;*/
                                /**SCITXBUF = Lbyte;while((*SCICTL2 & 0x0080) == 0x0000)
{};*/
                                for (m=0; m<10000; m++)
                                {}
```

University of Cape Town

```
                                        *SCITXBUF = Hbyte;while((*SCICTL2 & 0x0080) == 0x0000) {};
                                        for (m=0; m<10000; m++)
                                        {}
                                }
                                printed_once = 1;
    }/*load if end*/


    if ((rcvd==105) && (Log_done == 1))  /*i*/
            {

                                for(j=1;j<900;j++)
                                {
            Send = Speed_and_I_A_arr[j];
            /*Start sequence*/
/*              if (j < 10) Send = 10;              */

                                        if(Send > 65535) Send = 65535;
                                        if(Send < 0) Send = 0;
                                        Hbyte = Send>>8;
                                        /*Lbyte = (char)Send;*/
                                        /**SCITXBUF = Lbyte;while((*SCICTL2 & 0x0080) == 0x0000)
{};*/
                                        for (m=0; m<10000; m++)
                                        {}
                                        *SCITXBUF = Hbyte;while((*SCICTL2 & 0x0080) == 0x0000) {};
                                        for (m=0; m<10000; m++)
                                        {}
                                }
                                printed_once = 1;
    }/*speed if end*/

    if ((rcvd==115) && (Log_done == 1))  /*s*/
            {

                                for(j=1;j<900;j++)
                                {
            Send = Speed_and_I_A_arr[j];
            /*Start sequence*/

                                        if(Send > 65535) Send = 65535;
                                        if(Send < 0) Send = 0;
                                        /*Hbyte = (char)Send>>8;*/
/*              if (j < 10) Hbyte = 10;                 */
                                        Lbyte = (char)Send;
                                        *SCITXBUF = Lbyte;while((*SCICTL2 & 0x0080) == 0x0000) {};
                                        for (m=0; m<10000; m++)
                                        {}
                                        /**SCITXBUF = Hbyte;while((*SCICTL2 & 0x0080) == 0x0000)
{};*/
                                        for (m=0; m<10000; m++)
                                        {}
                                }
                                printed_once = 1;
    }/*V_ac if end*/
```

University of Cape Town

```
    if ((rcvd==111) && (Log_done == 1))  /*o*/
          {

                                for(j=1;j<900;j++)
                                {
           Send = Load_T_and_V_ac_arr[j];
           /*Start sequence*/

                                        if(Send > 65535) Send = 65535;
                                        if(Send < 0) Send = 0;
                                        /*Hbyte = (char)Send>>8;*/
                                        Lbyte = (char)Send;
/*              if (j < 10) Hbyte = 10;             */
                                        *SCITXBUF = Lbyte;while((*SCICTL2 & 0x0080) == 0x0000) {};
                                        for (m=0; m<10000; m++)
                                        {}
                                        /**SCITXBUF = Hbyte;while((*SCICTL2 & 0x0080) == 0x0000)
{};*/
                                        for (m=0; m<10000; m++)
                                        {}
                                }
                                printed_once = 1;
    }/*I_A if end*/

    /*Prescaler*/
          if (rcvd==49)  /*2*/
          {
          *T1PR = 20000;  /* Period = 20_000*25nsec*2 = 1_msec : freq 1000Hz */
          *T1CON = 0xA802;   /* up/down continuous mode */
          *T1CON = 0xA842;   /* start the clock */     /*Prescaler = 1*/
          start_speed = 1500;
          }
          if (rcvd==50)  /*2*/
          {
          *T1PR = 20000;  /* Period = 20_000*25nsec*2*2 = 2_msec : freq 500Hz */
          *T1CON = 0xA902;   /* up/down continuous mode */
          *T1CON = 0xA942;   /* start the clock */     /*Prescaler = 1*/
          start_speed = 1000;
          }
          if (rcvd==51) /*3*/
          {
          *T1PR = 50000;  /* Period = 50_000*25nsec*2*4 = 10_msec : freq 100Hz */
          *T1CON = 0xAA02;   /* up/down continuous mode */
          *T1CON = 0xAA42;   /* start the clock */     /*Prescaler = 1*/
          start_speed = 50;
          }
          if (rcvd==52)  /*4*/
          {
          *T1PR = 50000;  /* Period = 50_000*25nsec*2*8 = 20_msec : freq 50Hz */
          *T1CON = 0xAB02;   /* up/down continuous mode */
          *T1CON = 0xAB42;   /* start the clock */     /*Prescaler = 1*/
          start_speed = 50;
          }
  }/*forever loop end*/
}/*void main end*/
```

University of Cape Town

Appendix E

University of Cape Town

1.1. Stellenbosch Mini-CCS resonant frequency predictions

Wagner's resonant frequency prediction method:

Using the method developed by Wagner, the following frequency vs. stator resistance graph was formed:

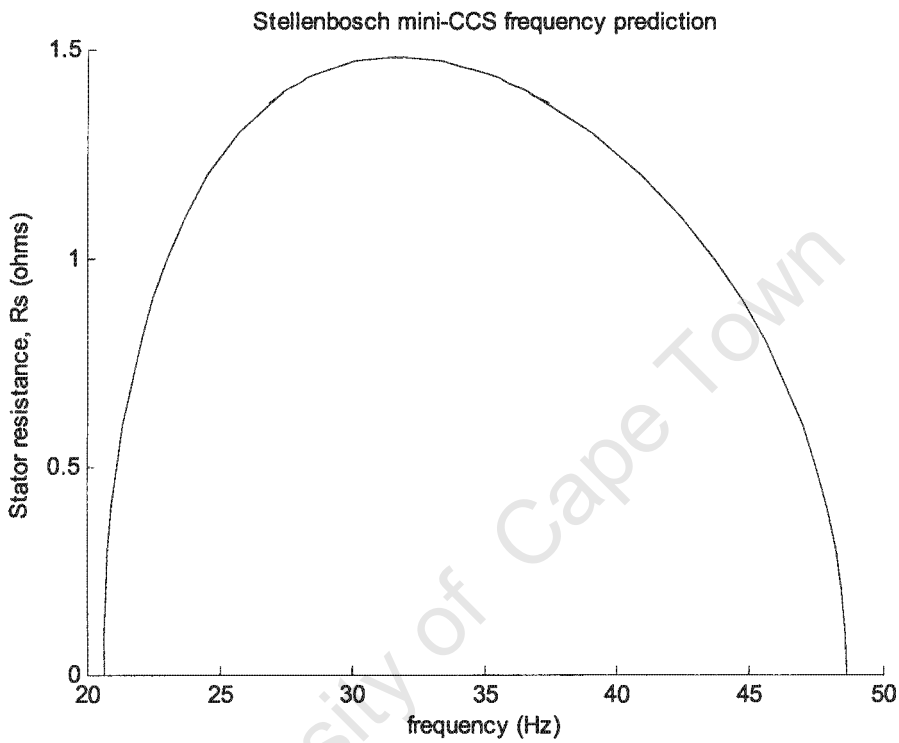

University of Cape Town

Figure 1: Prediction of resonant frequency using Wagner's method.

When the stator resistance is 0.04 ohms, the lower and upper resonant frequencies are 21Hz and 48Hz; which correspond to resonant circuit slips of -0.001 and -0.5 respectively.

Root-locus method:

When a transfer function was constructed for the resonant circuit used by Wagner, and the same parameters used, the following Root-Locus is plotted:

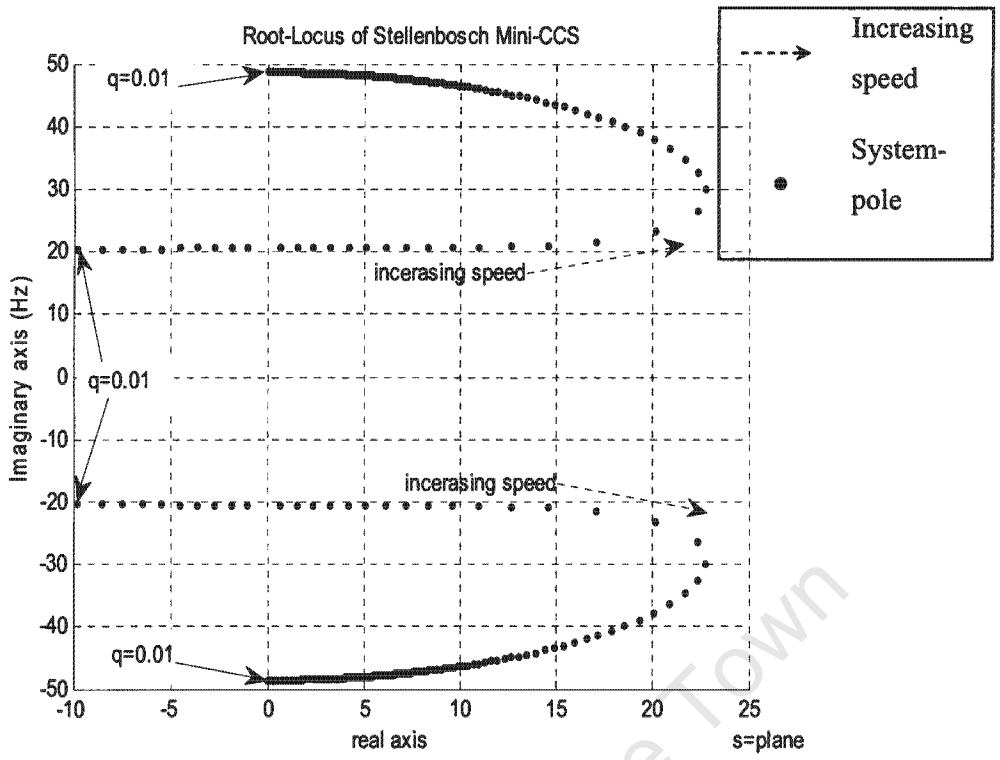

Figure 2: Root-Locus plot of Stellenbosch Mini-CCS.

Each dot in Figure 2 shows the system-pole positions for a particular slip. Starting at 0.01, the slip is decreased in steps of 0.001 until it is equal to -0.5.

The Root-Locus predicts lower and upper resonant frequencies of approximately 21 and 48Hz respectively, the corresponding lower and upper slip values are approx. -0.01 and -0.5 respectively.

University of Cape Town

1.2. Meru-Petronet CCS-IM resonant frequency predictions

Wagner's resonant frequency prediction method:

Using the method developed by Wagner, the following frequency vs. stator resistance graph was formed:

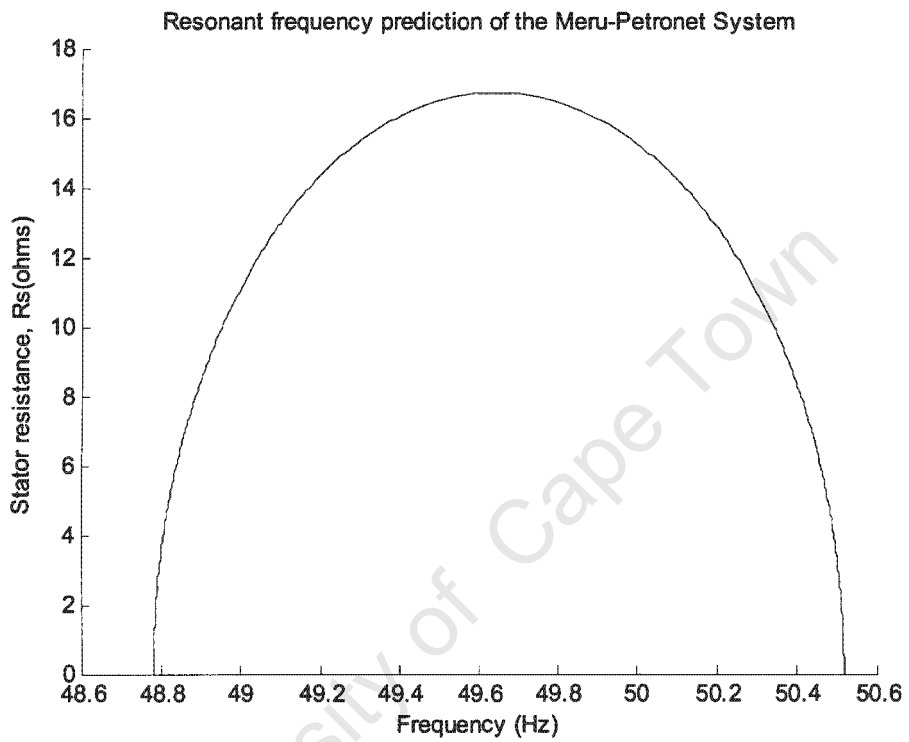

University of Cape Town

Figure 3: Prediction of resonant frequency using Wagner's method.

When the stator resistance is 0.11 ohms, the lower and upper resonant frequencies are 48.8Hz and 50.5Hz; which correspond to resonant circuit slips of -0.001 and -1.3 respectively.

Root-locus method:

When a transfer function was constructed for the resonant circuit used by Wagner, and the same parameters used, the following Root-Locus is

plotted:

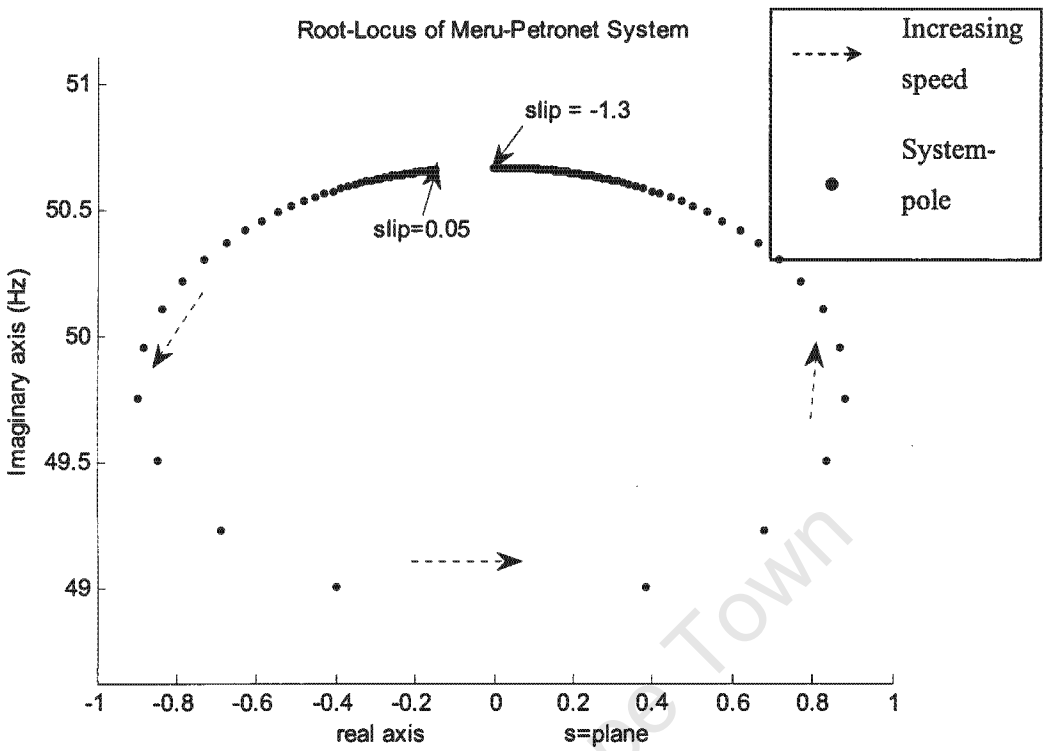

Figure 4: Top half of the Root-Locus plot for the Meru-Petronet system.

Each dot in Figure 4 shows the system-pole positions for a particular slip. Starting at 0.05, the slip is decreased in steps of 0.001 until it is equal to -1.3.

The Root-Locus predicts lower and upper resonant frequencies of approximately 51Hz and 49Hz respectively, the corresponding lower and upper slip values are approx. -0.01 and -1.3 respectively.

University of Cape Town

1.3. Root-Locus analysis of the Meru-Petronet system with the CCS set up as-built

For the purpose of completion, the circuit of the Petronet-Meru system was analysed as it was built, with the aid of SCAM. Similar results were obtained to those of the analysis of the Thevenin Equivalent CCS, with the filter-bank omitted. The only difference between the two Root-Locus plots is that this one has stable system-poles, which can be seen in Figure 5:

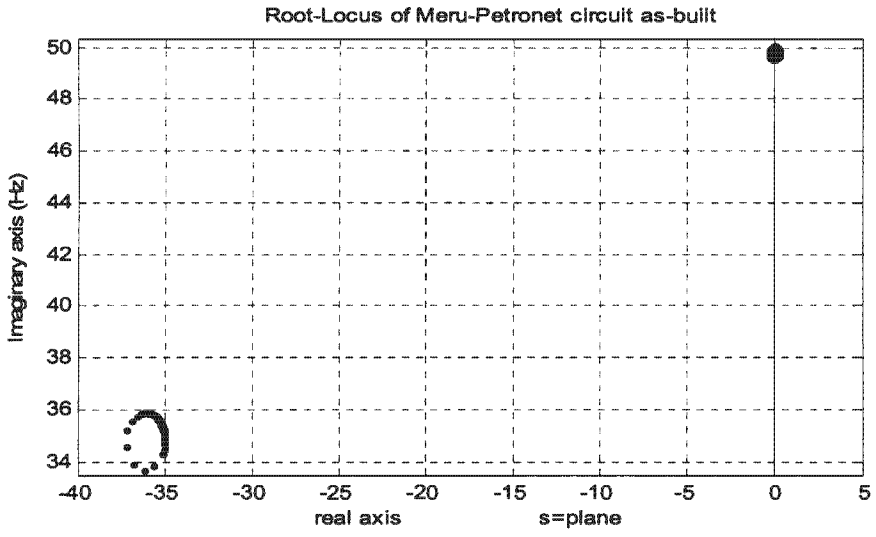

Figure 5: Root-Locus plot for the complete Petronet-Meru system

System-poles that arise as a result of the filter-bank can be see in the bottom-left corner of Figure 5. By zooming in on the top-right corner of this figure, Figure 6 is obtained.

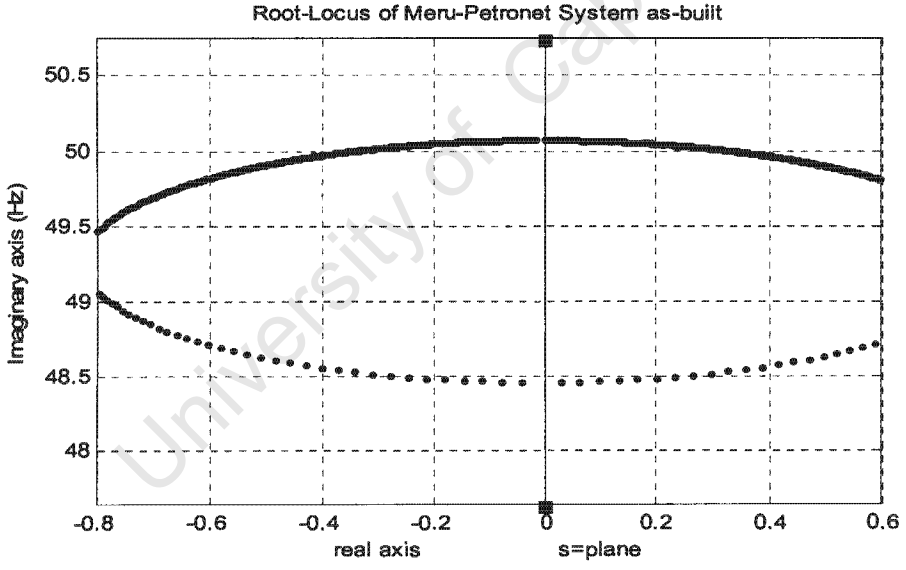

Figure 6: Zoomed-in region of Figure 5

Results of Figure 6 are very similar to those of Figure 4, therefore validating the use of the Thevenin Equivalent CCS, and no filter-bank to analyse the Meru-Petronet system.

University of Cape Town

Appendix F

University of Cape Town

Digsilent Simulation by Melanie Schilder

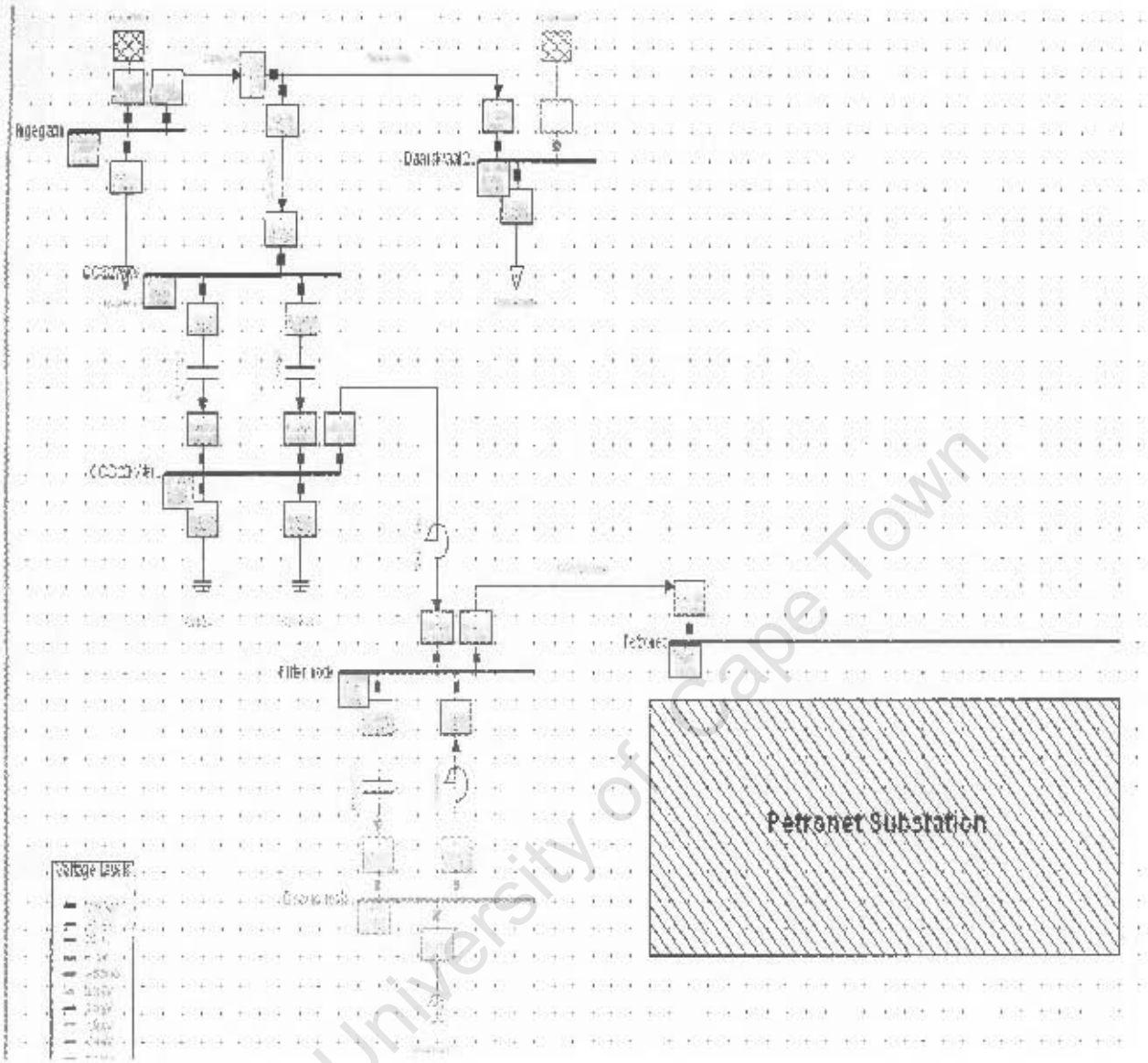

Figure 1: Simulation of Meru Grid

University of Cape Town

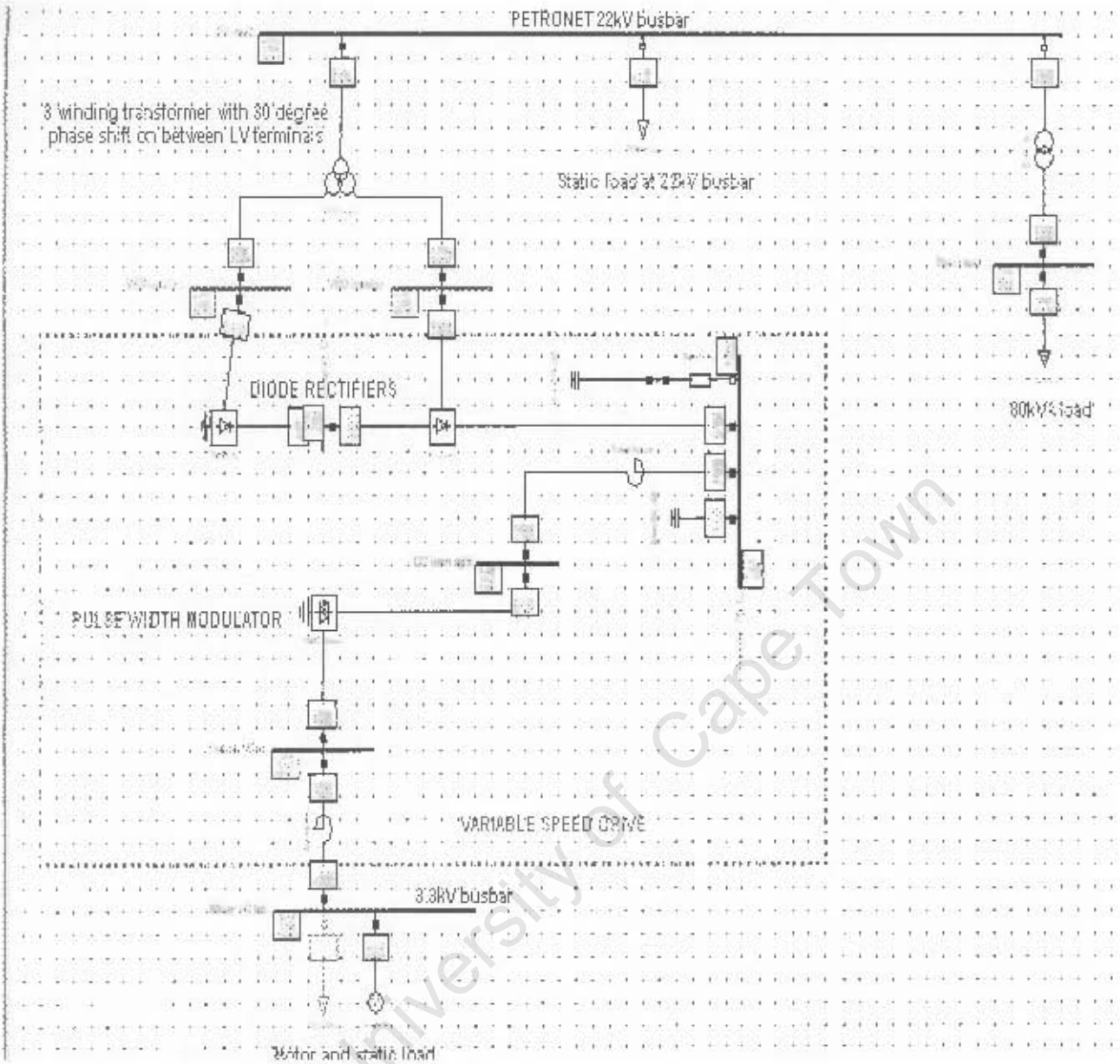

Figure 2: Simulation of Meru Substation

University of Cape Town

Parameters of the induction motor that is connected to the 3.3kV busbar of Figure 2 are:

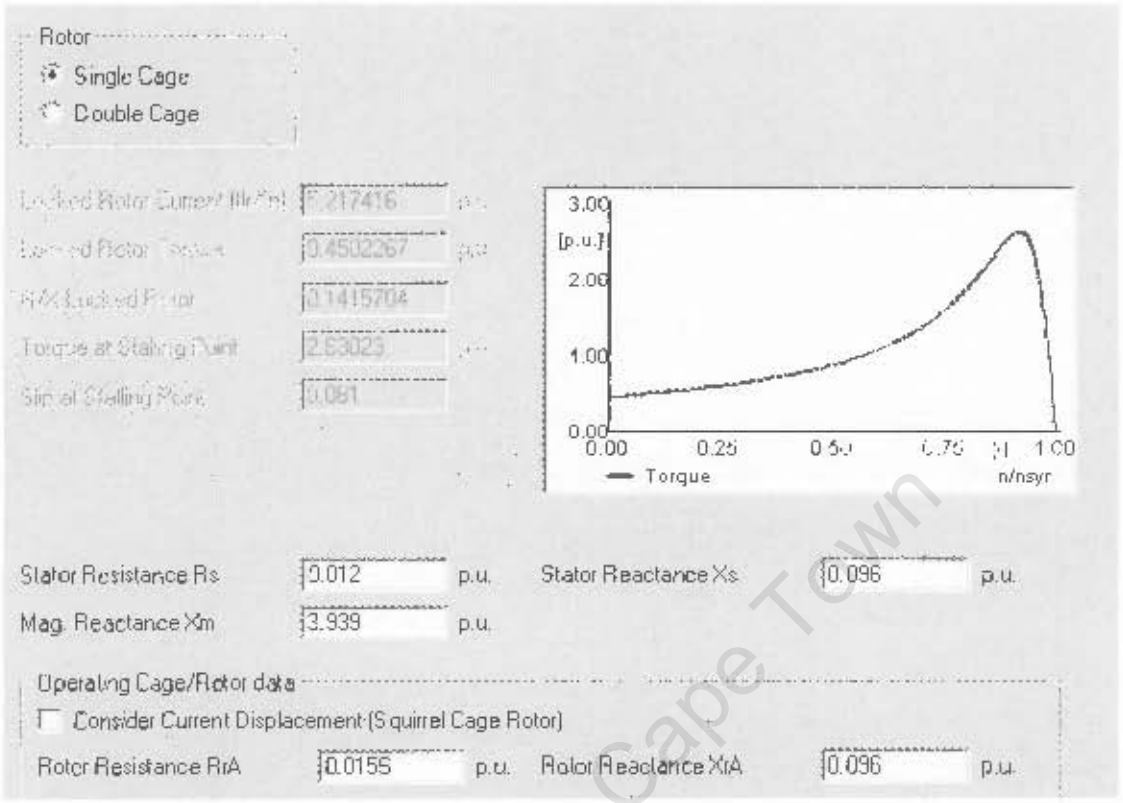

Figure 3: Parameters of the induction motor connected to the 3.3kV busbar

University of Cape Town

Appendix G

University of Cape Town

1. Effects of ferroresonance filter on the UCT Laboratory model and Meru-Petronet system

The effect of the passive filter on the UCT-Lab Model and the Petronet-Meru system is shown:

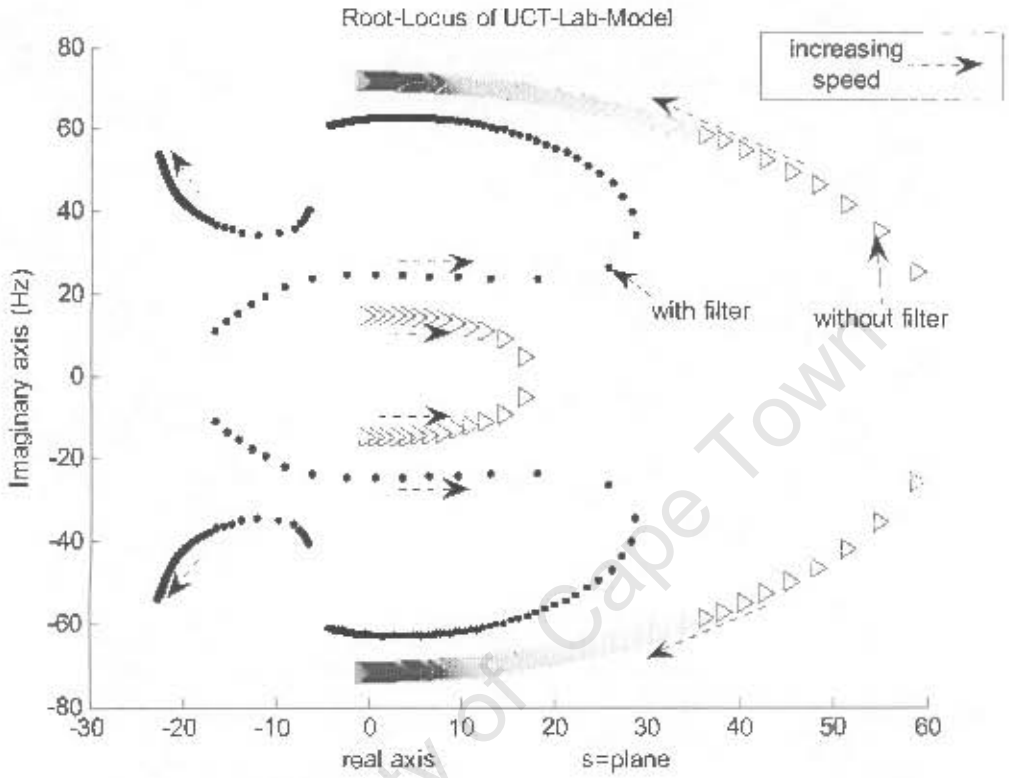

Figure 1: Effects of passive filter on UCT-Lab model

University of Cape Town

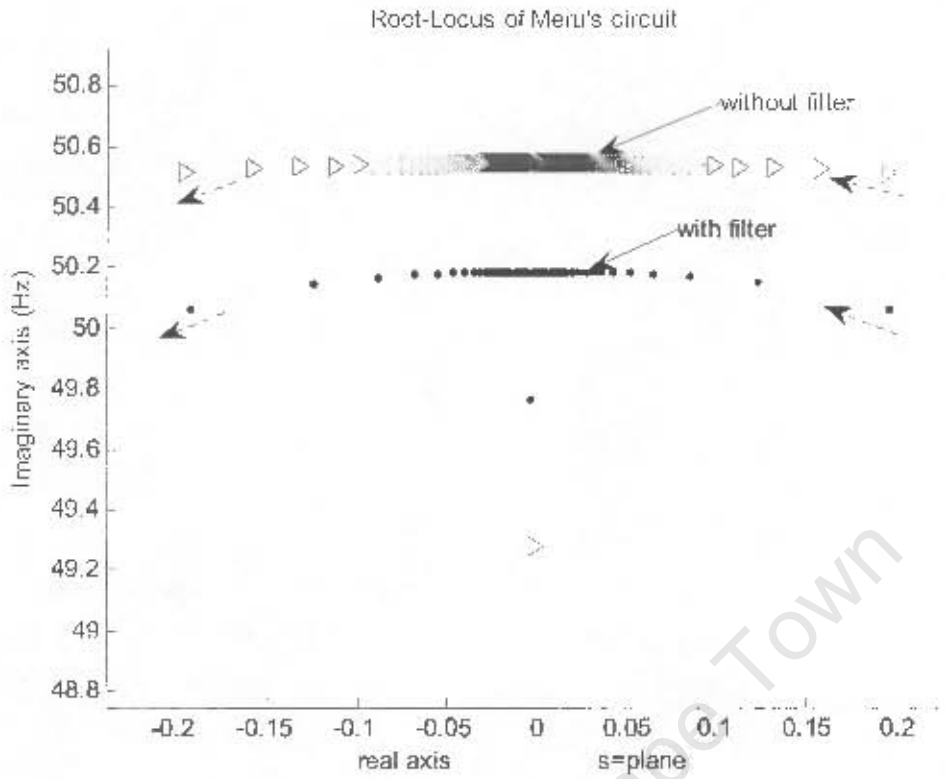

Figure 2: Effects of passive filter on Meru-Petronet system

University of Cape Town

2. SCAM comparison

In order to prove that SCAM could accurately produce a transfer-function for a system, Root-Locus plots were compared for a transfer function of Wagner's circuit that was calculated by the author (in chapter 4 see equation 4.2) and for the a transfer function of the same system produced using SCAM.

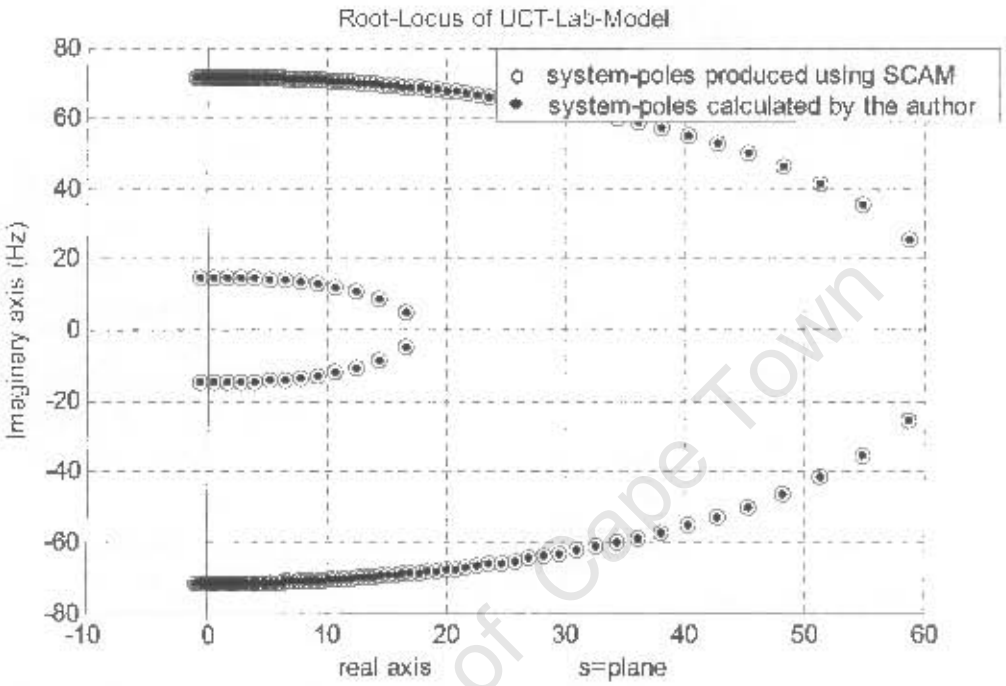

Figure 3: Comparison of SCAM with manual calculation used to determine a system transfer function, and construct the corresponding Root-Locus plot

It can be seen that SCAM produces identical results to those calculated by the author.

University of Cape Town

Appendix H

University of Cape Town

Sensitivity analysis by individually varying all parameters

Parameters were firstly varied by ±20% of their measured value. Figure 1 was obtained.

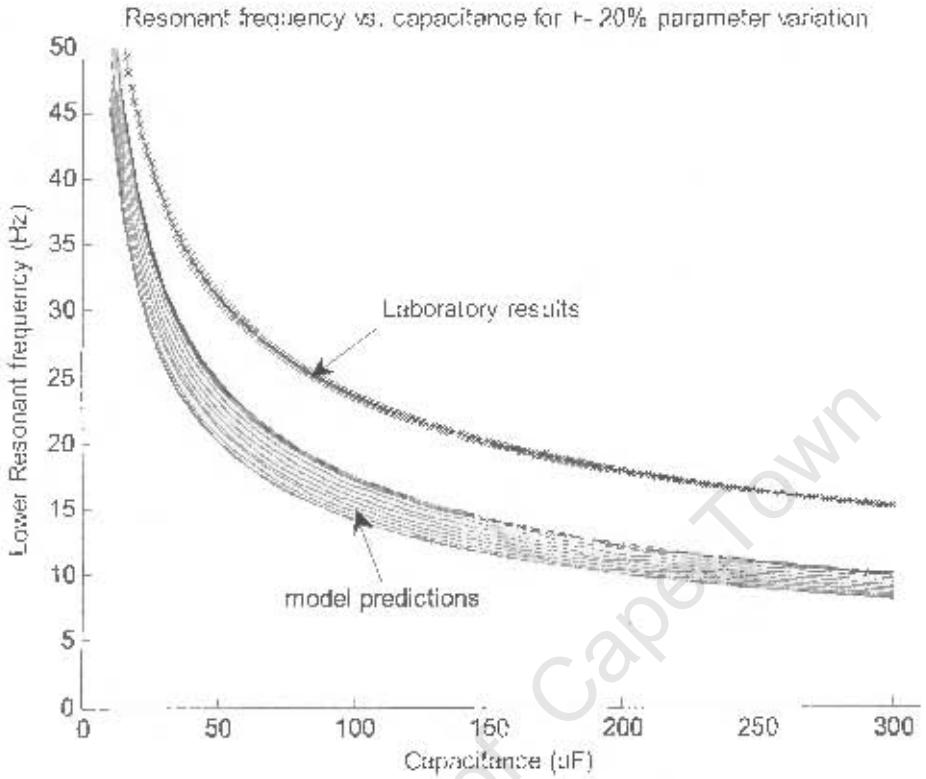

Figure 1: Sensitivity plot of lower resonant frequency vs. capacitance for UCT-Lab model for ±20% parameter variation

Parameters were then varied by ±50% of their measured value. Figure 2was obtained.

University of Cape Town

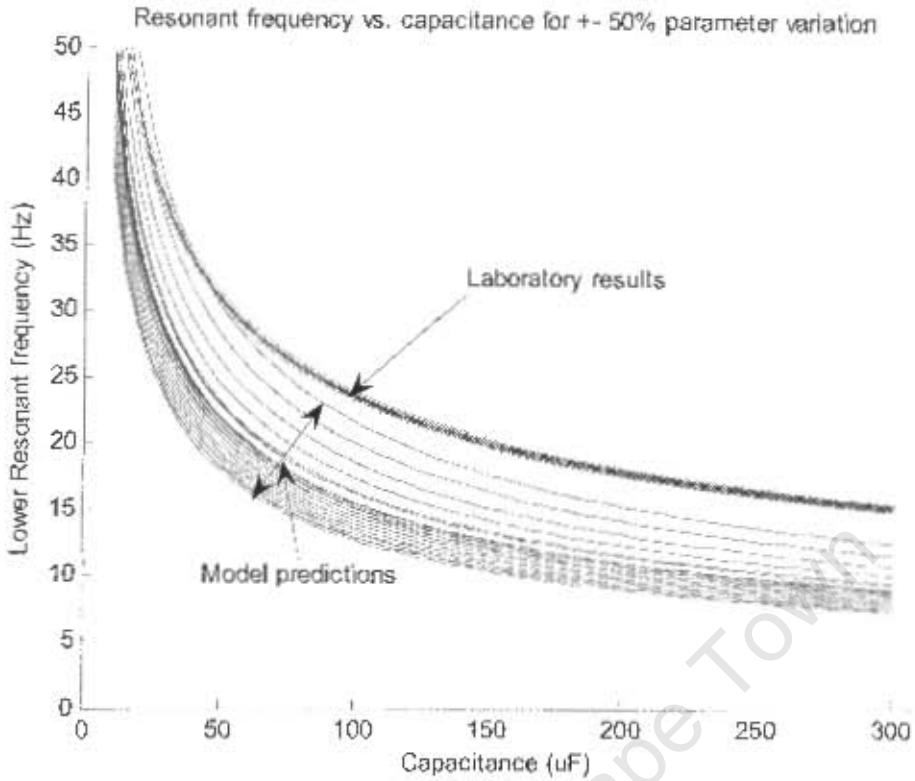

Figure 2: Sensitivity plot of lower resonant frequency vs. capacitance for UCT-Lab model for ±50% parameter variation

University of Cape Town